Analysis of Heating Rates and Forces on Bodies Subject to Rocket Exhaust Plume Impingement

A. W. Ratliff · M. L. Blackledge
H. W. Butler · D. E. Kooker

March 1968 · HREC-1150-1 · LMSC/HREC A791230
Contract NAS8-21150

Editorial guide

The original report is reproduced in source order. Prose is re-typeset at 12 points after comparison with the scan. Technical material that has not been confidently reconstructed is retained as clearly labeled source facsimiles, rather than guessed. Original scientific claims, units and numbering are not updated.

Original page boundaries are retained for cross-reference; a source page may span more than one reading-edition page. Running headers identify both the printed original page and its position in the supplied PDF. “Continued” marks a layout continuation, not an omission.

Re-typeset text is searchable. Source-facsimile interiors, including equations, graphs, handwriting and some symbol definitions, remain image-only. Editorial labels and navigation are new and are not part of the 1968 report.

Modern navigation

Click a heading to go to its source-page boundary. Original contents and their printed references follow in their original position.

General Disclaimer

Archival cover

Report title

Foreword

Summary

Contents

Contents (Continued)

1 Introduction

2 Technical Discussion

Figure 2-1

3 Impingement Analysis

Nomenclature for Section 3

4 Convective Heating

4.2 Noncontinuum Convective Heat Transfer

5 Radiative Heating

6 Methods and Procedures for Obtaining Test Data

7 Data Correlation

8 Conclusions

References

Appendix A — Low Density Stagnation Region Blunt Body Solution

Appendix A — Nomenclature

Appendix B — Free Molecular Heating

B.1 General Discussion

Appendix B — Nomenclature

Appendix B — Reference

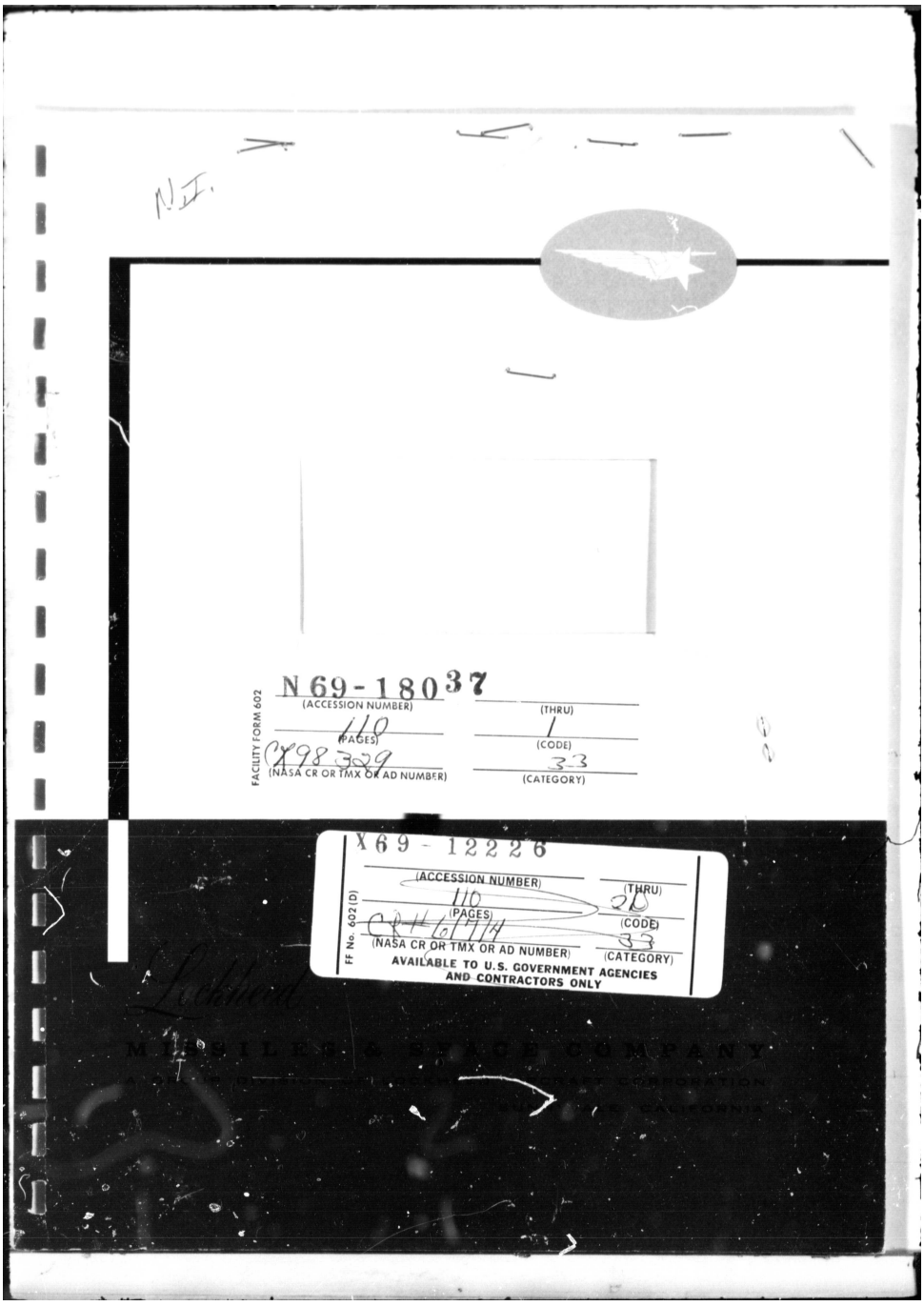
General Disclaimer

One or more of the Following Statements may affect this Document

- This document has been reproduced from the best copy furnished by the organizational source. It is being released in the interest of making available as much information as possible.
- This document may contain data, which exceeds the sheet parameters. It was furnished in this condition by the organizational source and is the best copy available.
- This document may contain tone-on-tone or color graphs, charts and/or pictures, which have been reproduced in black and white.
- This document is paginated as submitted by the original source.
- Portions of this document are not fully legible due to the historical nature of some of the material. However, it is the best reproduction available from the original submission.

Produced by the NASA Center for Aerospace Information (CASI)

Archival cover



SOURCE FACSIMILE — Archival cover, including accession labels and handwritten marks. Full-page source facsimile.

Report title

HREC-1150-1
LMSC/HREC A791230

Lockheed Missiles & Space Company

Huntsville Research & Engineering Center
Huntsville Research Park
4800 Bradford Blvd., Huntsville, Alabama

Analysis of Heating Rates and Forces on Bodies Subject to Rocket Exhaust Plume Impingement

March 1968
Contract NAS8-21150

by
A. W. Ratliff
M. L. Blackledge
H. W. Butler
D. E. Kooker

APPROVED BY: for J. S. Farrior
Resident Director

SOURCE FACSIMILE — Original approval/signature block. Source facsimile.

Editorial note: the author block is blemished in the scan. Full initials above use the supplied author information, in original author order.

Foreword

This document presents the results of work performed by personnel of the Lockheed Missiles & Space Company, Huntsville Research & Engineering Center. This work was sponsored by the Propulsion and Vehicle Engineering Laboratory of Marshall Space Flight Center under Contract NAS8-21150. The technical monitor for this study was Mr. James Moses of R-P&VE-PT. This report constitutes Volume I of a two-part final report for the investigation completed under this contract.

Acknowledgments

The contribution of Mr. S. J. Robertson, of Lockheed Missiles & Space Company, to this study is appreciated. In addition, the continuing technical guidance of Mr. James Moses of the Propulsion and Vehicle Engineering Laboratory is acknowledged.

Summary

Study effort was directed toward the development of engineering methods and computer programs for predicting convective heat flux and pressures in free molecular, transition and continuum flow regimes, for rocket exhaust plume impingement problems. The scope of this effort encompassed both solid and liquid rocket motors. Noncontinuum plume prediction techniques were investigated and a method was implemented into the plume flow field program. Radiant heating from both gaseous plumes and plumes with solid particles was treated with existing computer programs.

This study produced and/or improved a set of computer programs and engineering methods for the prediction of heating rates and forces in jet plume impingement problems. This set comprises the following:

- Flow field program for plume predictions by real gas method of characteristics and free molecular theory
- Thermochemical program
- General impingement program
- Set of programs for solid particle impingement and radiation
- Gaseous radiation program

This comprehensive group of programs can be used to calculate heating rates and forces for a wide variety of plume impingement problems.

Contents

Original contents and original page references. Modern navigation is provided separately.

Section	Title	Page
	Foreword	ii
	Acknowledgments	ii
	Summary	iii
1	Introduction	1
2	Technical Discussion	4
2.1	Flow Field Determination	4
2.2	Thermochemical Analysis	4
2.3	The Undisturbed Flow Field	5
3	Impingement Analysis	9
3.1	Body Location Detail	9
3.2	Description of Surfaces	12
3.3	Detection of Surface Shading	13
3.4	Pressures and Forces	14
4	Convective Heating	19
4.1	Continuum Convective Heating	19
4.2	Noncontinuum Convective Heat Transfer	38
4.3	Free Molecular Heating	51
5	Radiative Heating	53
6	Methods and Procedures for Obtaining Test Data	55
7	Data Correlation	57

Editorial note: the original contents places 3.2 on p.12; the heading itself begins on p.11. Original reference retained.

Contents (Continued)

Section	Title	Page
8	Conclusions	64
	References	67

Appendixes

Appendix	Title	Page
A	Low Density Stagnation Region Blunt Body Solution	A-1
B	Free Molecular Heating	B-1

1 Introduction

The flow of exhaust gases from rocket nozzles can cause a variety of complex design problems. Depending on vehicle altitude and the proximity of a rocket nozzle to adjacent surfaces, many problems can arise if the exhaust gases impinge on these surfaces. Such problems are especially acute in quasi-vacuum conditions which cause large billowing plumes. During separation of vehicle stages, rocket exhaust plume impingement may induce pressures and heat rates on the vehicle which must be evaluated. Attitude control rockets, as well as retrorocket and ullage motors, may cause direct impingement of exhaust gases on vehicle structure.

Because of the many problem areas associated with plume impingement, adequate engineering methods and computer programs are needed to predict heat flux and pressures in low density plume impingement areas. This study provided such methods and programs so that these problems can be adequately analyzed.

Effort during this study was expended in three primary areas. The first area involved the improvement of techniques for predicting noncontinuum exhaust plume flow fields, i.e., the slip flow, transition and free molecular regimes. The second area was concerned with the development of techniques to evaluate continuum heating due to plume impingement on bodies immersed in the flow field. The third major area of investigation was concerned with developing engineering methods for analyzing convective heating in the noncontinuum flow regimes.

A relatively minor area of effort was that of obtaining and learning to utilize existing programs for the prediction of radiant heating from gaseous and solid particle plumes. In addition, a cursory study was made of ways to obtain flight test data from existing Apollo program motors.

The complexities involved in determining heat flux and pressures, with resultant forces, on bodies subject to plume impingement; dictate that the approach to a realistic solution to this problem be divided into several subtasks. Lockheed/Huntsville therefore categorized the problem areas as follows:

- Flow Field Determination
- Impingement Analysis
  - body location
  - pressures and resulting forces
- Convective Heating
  - continuum
  - transitional
  - free molecular
- Radiative Heating

The basic output from this study is a set of experimentally verified computer programs for jet plume impingement heating rates and pressure predictions. The scope of this study covers continuum, transition and slip flow, as well as free molecular flow regimes.

The set of engineering methods and computer programs provided and/or developed under this study are as follows:

- A real gas method of characteristics program
- A program for determining thermochemical properties
- A general impingement program for the analysis of pressures, forces and heating rates
- A set of programs for the analysis of solid particle impingement and radiation
- A program for the analysis of gaseous radiation
- A program for the analysis of blunt body (probes) hemisphere heating rates in highly expanded plumes

- An engineering method for the analysis of plume impingement on a flat plate large with respect to the plume
- A specialized method for the highly accurate determination of pressures and heating rates on axisymmetric bodies whose axis of symmetry is coincident with the plume axis of symmetry.

2 Technical Discussion

2.1 Flow Field Determination

To initiate the analysis of any plume impingement problem, the rocket exhaust flow field must first be completely and accurately described. An accurate prediction of a rocket exhaust plume involves the treatment of several scientific disciplines. The salient features of such a calculation are:

- Description of the thermochemical behavior of the propellant system
- Prediction of the undisturbed exhaust plume properties via gas dynamic and thermochemical methods
- Determination of flow regimes (continuum, transitional or free molecular) within the plume.

The thermochemical properties determination is made using the NASA/Lewis Thermochemical Program (Reference 1) and the flow field is described by the Lockheed/Huntsville Method-of-Characteristics Program (Reference 2). The determination of the flow regime is based on an exhaustive literature search which has been reported by Robertson in Reference 3.

2.2 Thermochemical Analysis

The capability for analyzing reacting gas flows (real gases) is provided by thermochemical property data from the NASA/Lewis Thermochemical Program. This program has been specially modified to generate a binary tape containing all the pertinent parameters needed for flow field and heat transfer analysis including the mole fractions of each constituent. This method reduces much of the tedious time consuming effort normally necessary to prepare input for a single flow field calculation.

After the thermochemical program output has been examined and verification made that the calculations were successfully completed, the master tape generator program is executed. The master tape is updated by adding the newly generated case to information already on the tape. Thus, a library of thermochemical calculations is accumulated. This library currently contains about 100 different propellant systems.

Each system on the tape represents a complete Mollier diagram of the gas under consideration. Various entropy levels were included in order to remove the dependency of the thermochemical calculations on combustion pressure, thereby facilitating the analysis of “off-design” chamber pressure conditions.

2.3 The Undisturbed Flow Field

The Lockheed/Huntsville Method-of-Characteristics Program is provided for analysis of exhaust plume flow fields. This program is a flexible, user-oriented research and engineering tool capable of solving many types of complex supersonic flow problems. This program has been used extensively, and has been successfully correlated with a wide variety of test data.

Utilizing the Lockheed Method-of-Characteristics Program, the exhaust plume for any arbitrary nozzle and exhaust gas (ideal or reacting) system can be analyzed. At finite back pressures the program can generate the plume by continuum analysis. As the back pressure is lowered, the outer regions of the plume become progressively more rarefied until eventually the flow becomes free molecular. The Method-of-Characteristics Program was modified to allow for the transfer of the calculations from a continuum analysis to a free molecular analysis across a “freeze” front in the flow field.

Analytical Predictions of Low Density Plumes: The expansion of an inviscid axisymmetric exhaust plume into a vacuum or quasi-vacuum is essentially

a Prandtl-Meyer expansion complicated by distending effects as the flow progresses away from the axis of symmetry. Since no analytical solution to the equations of motion exists, it is necessary to resort to numerical techniques. The method-of-characteristics is a commonly used technique to apply to this problem and LMSC/HREC has developed a state-of-the-art computer solution to perform the necessary calculations. However, method-of-characteristics solutions are not always practical in describing flow fields at high altitudes where the flow becomes hypersonic. A numerical problem arises because the characteristic lines make such a small angle (arc sin 1/M) with the streamlines when the Mach number is high. In the numerical procedure the calculation will eventually diverge unless the mesh size is continually refined.

In light of the problems involved in the method-of-characteristic solution at high Mach numbers, a scheme was devised wherein the calculations for the low density plume are continued by free molecular theory once the flow has become sufficiently rarefied. The method of approach is based on the “freezing” of the various energy modes of the gas molecules. Since a large number of intermolecular collisions are necessary to maintain vibrational equilibrium and because the number of collisions steadily decreases with increasing rarefication, vibrational equilibrium eventually can no longer be maintained. In a similar manner the rotational, and eventually, the translational energy modes also “freeze” and at that time the flow is considered free molecular. The calculations are then continued along streamlines (considered straight because of the source-like nature of the flow at high altitude) with the temperature and velocity held constant. The density of the flow field in the free molecular region is allowed to vary inversely as the cross sectional area of the streamtubes formed by the adjacent streamlines.

The method for determining the flow regimes is described in detail in Reference 3. In order to gain insight into the effects of the various parameters which determine the “freezing” criteria, an auxiliary study was carried out using a source flow model. The results of this study are shown in Figure 2-1.

Figure 2-1

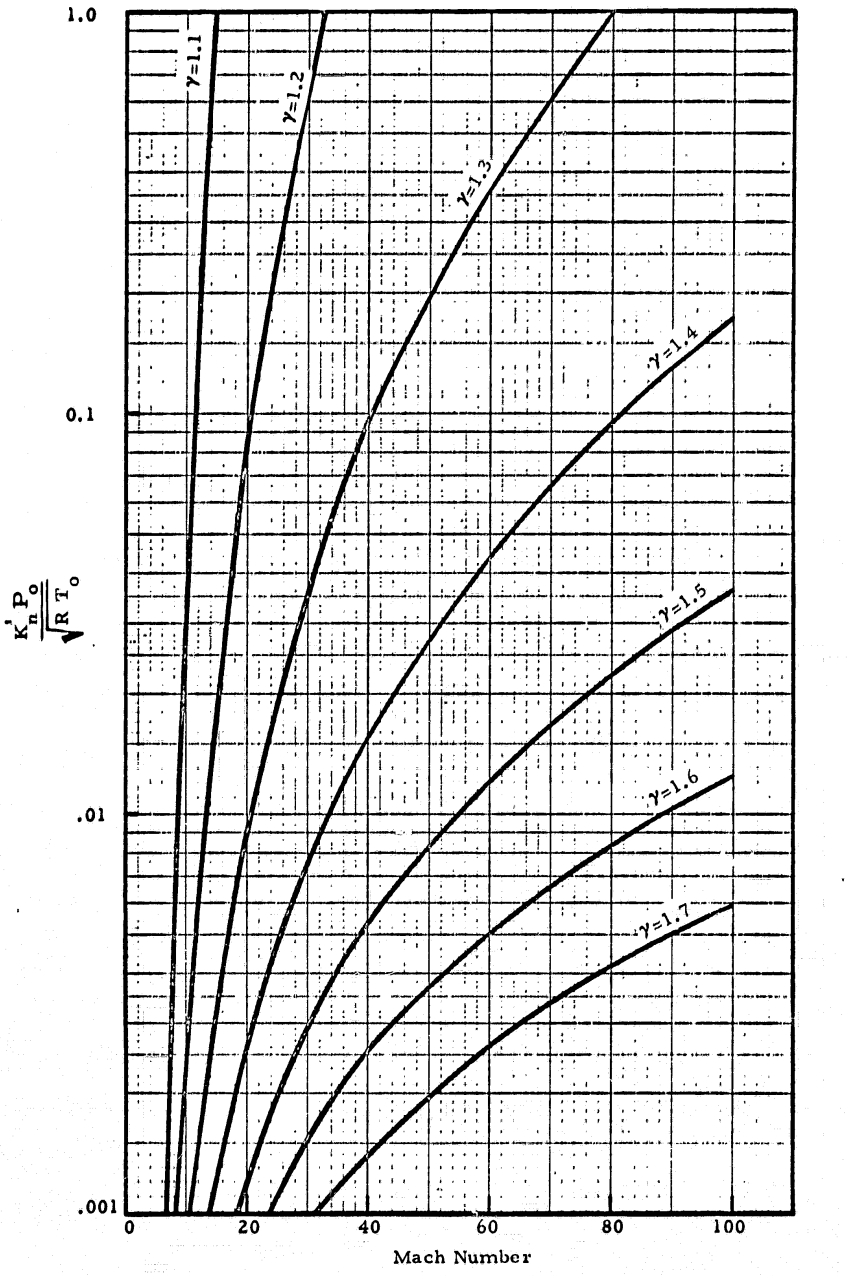


Figure 2-1 – Knudsen Number Parameter as a Function of Mach Number and Ratio of Specific Heats

SOURCE FACSIMILE — Figure 2-1 — Knudsen Number Parameter as a Function of Mach Number and Ratio of Specific Heats. Source facsimile; image-only axes and curves.

Utilizing this figure and choosing an arbitrarily large Mach number (i.e., say Mach 50) one can determine if his particular propellant system can be analyzed with the techniques developed in this study;

where

K_n' = Knudsen number

P_o = chamber pressure

T_o = chamber temperature

γ = ratio of specific heats

R = gas constant

SOURCE FACSIMILE — Parameter definitions, including original marked Knudsen-number symbol. Source facsimile.

Output from the Method-of-Characteristics Program in the form of flow field parameters at discrete locations is stored on binary tape for use with the impingement program which will determine the local pressures and heating rates.

3 Impingement Analysis

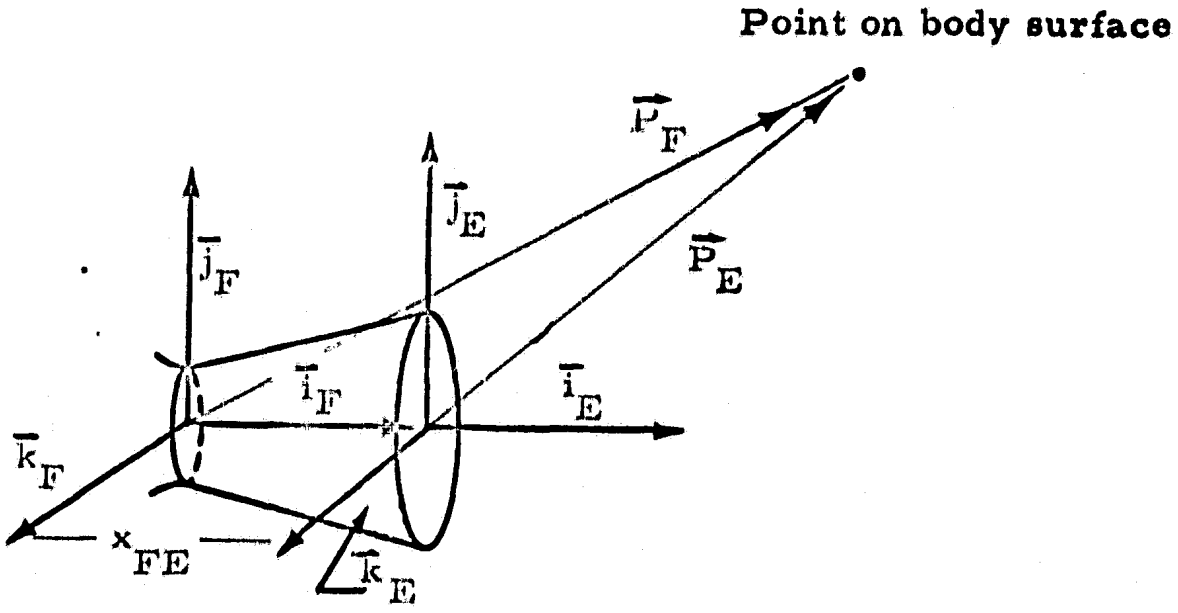
After the flow field is adequately described, the next step in the method of analysis is to locate the impinged body with respect to the flow field. A two-fold approach is taken depending on whether the body is large or small with respect to the flow field. For bodies large with respect to the flow field, Section 4.1.6 describes in detail the analysis procedure. For small bodies immersed in the plume a general impingement analysis program was developed which has the following features.

- Body geometry may be described by: (a) conic sections; (b) circular plates; or (c) rectangular plates. Any combination of the three basic shapes may be used to make up a composite body of up to 100 shapes
- Continuum, transitional or free molecular loads and heating are automatically calculated depending on the flow regime
- A printout of pressures and heating rates for each elemental area is provided.

A complete description of the impingement program and its use is contained in another volume of this final report package, Reference 4.

3.1 Body Location Detail

Before impingement analyses are performed, the rocket exhaust flow field will have been developed as discussed in Section 2.2. The flow field reference location, usually the rocket motor nozzle throat, may not always be convenient to use for the impingement analysis. An axial shift has been provided as an input quantity so that any axial station can be used as the impingement reference location as shown in the following sketch.



SOURCE FACSIMILE — Body-location geometry. Source facsimile.

$$\text{It can be seen that } \vec{P}_F = \vec{P}_E + x_{FE}\,\vec{i}_E. \qquad (3.1)$$

SOURCE FACSIMILE — Equation (3.1), including its lead-in. Source facsimile; vector marks retained.

It has been assumed that any complex structure to be analyzed may be described as a composite system of simple “subshapes.” These subshapes will be one of three types:

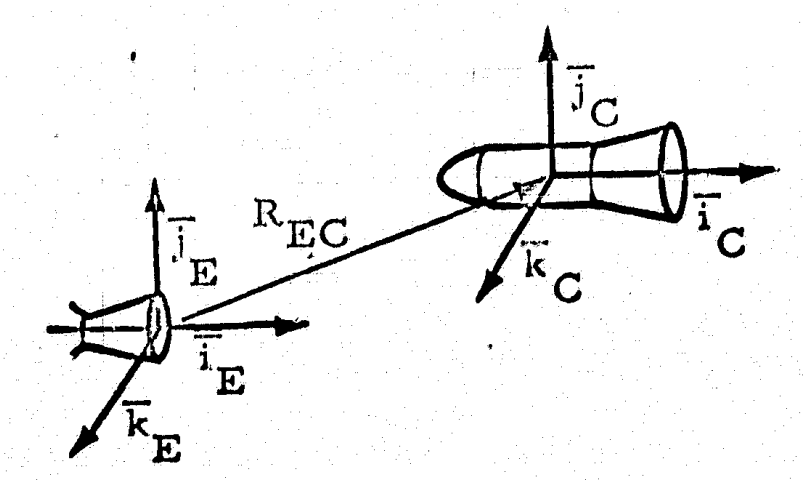
1. Conic surface of revolution (cylinders, spheres, cones, etc.).

2. Circular flat plate (any orientation).

3. Rectangular flat plate (any orientation).

Surface geometry is discussed in more detail later in Section 3.2.

Any point on the composite body may be used as the reference system, however, for illustrative purposes, the center of gravity of the composite structure in the sketch below has been chosen as the reference system. One axis of the right handed system is aligned along the principal axis of the body.



SOURCE FACSIMILE — Composite-structure reference frame sketch. Source facsimile.

From the sketch above, we have

$$\vec{R}_{EC} = x_{EC}\,\vec{i}_E + y_{EC}\,\vec{j}_E + z_{EC}\,\vec{k}_E$$

$$= [x\ y\ z]_{EC} \begin{bmatrix} \vec{i} \\ \vec{j} \\ \vec{k} \end{bmatrix}_E \qquad (3.2)$$

SOURCE FACSIMILE — Equation (3.2). Source facsimile; matrices and vector marks retained.

The unit vectors of the composite (“C”) system may be constructed as:

$$\begin{Bmatrix} i \\ j \\ k \end{Bmatrix}_C = [T_{EC}] \begin{Bmatrix} i \\ j \\ k \end{Bmatrix}_E \qquad (3.3)$$

SOURCE FACSIMILE — Equation (3.3). Source facsimile.

where T_{EC} is a 3 x 3 transfer matrix from the “E” system to the “C” system.

3.2 Description of Surfaces

The composite structure, as previously mentioned, will consist of one or more subshapes of either the conic, circular plates or rectangular plate type. (See sketch on following page.)

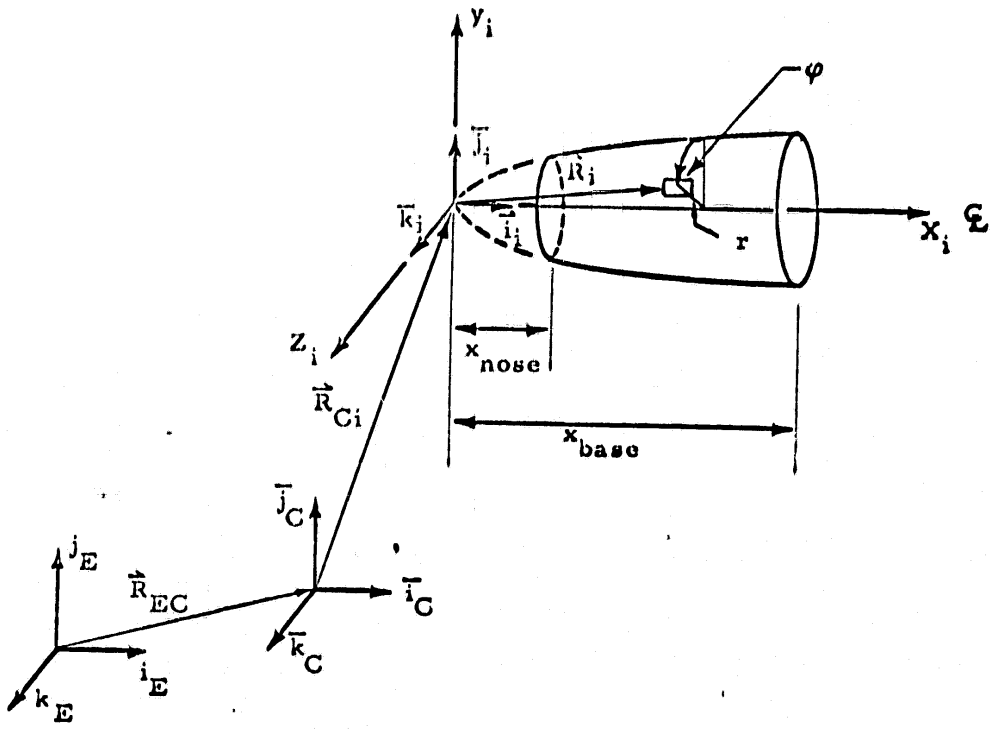
These subshapes are referenced to the composite axis in a similar manner to the composite/exit plane transfer; that is,

$$\vec{R}_{Ci} = \{x\ y\ z\}_{Ci} \begin{Bmatrix} \vec{i} \\ \vec{j} \\ \vec{k} \end{Bmatrix}_C$$

and

$$\begin{Bmatrix} \vec{i} \\ \vec{j} \\ \vec{k} \end{Bmatrix}_i = [T_{IC}] \begin{Bmatrix} \vec{i} \\ \vec{j} \\ \vec{k} \end{Bmatrix}_C . \qquad (3.4)$$

SOURCE FACSIMILE — Unnumbered vector representation and Equation (3.4), including “and.” Source facsimile.



SOURCE FACSIMILE — Subshape geometry. Source facsimile.

The conic surface shown in the sketch above is represented by the equation,

$$r = -a\left[\sqrt{b + cX_i + dX_i^2} + e\right] = 0, \quad X_N \leq X_i \leq X_b \qquad (3.5)$$

SOURCE FACSIMILE — Equation (3.5). Source facsimile.

where

$$y_i = v_i \cos\varphi$$

$$z_i = v_i \cos\varphi$$

SOURCE FACSIMILE — Coordinate definitions as printed. Source facsimile.

therefore, the vector representation of the point becomes

$$\vec{p}_i = x_i \vec{i}_i + y_i \vec{j}_i + z_i \vec{k}_i \qquad (3.6)$$

SOURCE FACSIMILE — Equation (3.6). Source facsimile.

It will be necessary to transfer any point on a subshape surface to the composite system in order to sum loads. This may be done as indicated below;

$$\vec{P}_C = \left\{\vec{R}_i\right\}\left[T_{iC}\right] + R_{Ci} \cdot \qquad (3.7)$$

SOURCE FACSIMILE — Equation (3.7). Source facsimile.

Ultimately, a point on the surface must be transferred to the flowfield or “E” system in order to determine flow properties at the point. This requires one more step as seen below

$$\vec{P}_E = \left[\left\{\vec{R}_i\right\}\left[T_{iC}\right] + R_{Ci}\right]\left[T_{CE}\right] + \vec{R}_{EC} \cdot \qquad (3.8)$$

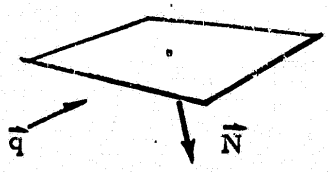
SOURCE FACSIMILE — Equation (3.8). Source facsimile.

The example presented is for a conic subshape; however, the circular and rectangular flat plate surfaces will be handled in a like manner, the only difference being in the representation of the surface in its own reference system.

3.3 Detection of Surface Shading

The composite structure may be a simple body of revolution or a complex combination of many subshapes. For either case, a scheme for detecting surface shading from the flow must be devised. Loads and heating for any flow regime require the knowledge of how much of the surface “sees” the approach flow. The method used for this study is described as follows.

The unit normal is calculated for each elemental area. A scalar product of the flow velocity ($\vec{q}$) and the unit normal ($\vec{N}$) is formed:



SOURCE FACSIMILE — Unit-normal/scalar-product statement and surface-normal sketch. Source facsimile; vector symbols retained.

If $\vec{q}$ dot N $\geq$ 0 the elemental area is "shaded," if $\vec{q}$ dot N $\leq$ 0 the elemental area "sees" the flow. For a composite structure which is a simple surface of revolution this test is all that is necessary.

SOURCE FACSIMILE — Surface-shading test, including original inequality signs. Source facsimile.

3.4 Pressures and Forces

A surface pressure integration for each subshape of the composite system is performed over the specified number of elemental areas. For each of these elemental areas a tape lookup determines the flow properties at that point. From the local flow properties and input reference lengths a local Knudsen number is calculated. A branch to a continuum, free molecular, or transitional pressure loads routine is then made, depending on pre-specified Knudsen number ranges. The three types of loads calculations are described in the following sections.

3.4.1 Continuum Flow Pressures

As discussed in Section 3.3, a test will already have been performed to determine if the elemental area “sees” the flow. Also available before the pressure calculation is made are the local flow properties which are obtained from the flow field tape. For the high Mach number application, a Newtonian flow calculation is made.

The angle θ between the velocity vector and the surface is calculated, and a Newtonian impact pressure is determined.

$$P = P_\infty \left\{ 1 + \gamma M_\infty^2 \sin^2\theta \right\}. \qquad (3.9)$$

where

P = local static pressure

P_∞ = freestream static pressure

γ = isentropic exponent

M_∞ = freestream Mach number

SOURCE FACSIMILE — Equation (3.9) and its complete parameter definitions. Source facsimile.

More elaborate techniques for determining impact pressure are needed if low Mach number gases are involved. For these cases, an oblique shock solution is employed to determine flow properties downstream of the shock. The normal component of the downstream velocity is stagnated isentropically, giving the surface pressure. For ideal gases at $M \rightarrow \infty$ this technique will approach modified Newtonian.

3.4.2 Transitional Flow Regime Pressures

When the Knudsen number calculated for an elemental area indicates that the flow regime is transitional, a weighted average of the continuum and free-molecular flow values is used. This weighted average is based on a curve fit of empirical data. The equation used is presented below.

$$P_{TRAN} = P_{CONT} + (P_{FM} - P_{CONT}) \sin^2\left[(\pi)\,(1/3 + 1/6 \log_{10} K_N)\right] \qquad (3.10)$$

where:
- P_{TRAN} - transitional impact pressure
- P_{FM} - free molecular impact pressure
- P_{CONT} - continuum impact pressure
- K_N - Knudsen number

SOURCE FACSIMILE — Equation (3.10) and complete parameter definitions. Source facsimile.

The above equation yields a smooth transition from free molecular to continuum flow, and is considered to be the best method presently available for estimating aerodynamic pressure over the entire transitional regime.

3.4.3 Free Molecular Flow Pressures

Making several assumptions as to the nature of the flow around a body, a straightforward calculation of the pressures on that body in free molecule flow may be made. Because of the length of the derivation, step-by-step presentation will not be made here, but only a summary that includes the assumptions made, a brief description of the method of solution, and the final results. If a detailed derivation is required, refer to Sentman (Reference 5) and, for a less detailed description, Patterson (Reference 6).

The following assumptions were made in the force equation derivation:

- The molecular velocity distribution ahead of the body is Maxwellian
- Diffuse reflection of the molecules from the body
- Non-concave surfaces

Making the above assumption and, of course, the free molecule assumption that the molecules do not collide with each other, then the pressure on an element of area can be computed. This is done by computing the pressure produced by the incident and reflected molecules using the kinetic theory of gases and then adding them together. The resulting equation is:

$$\frac{dF}{dA} = \frac{\rho}{2\beta}\left\{\frac{1}{\sqrt{\pi}}\,(k\epsilon + l\gamma + t\eta)\left[\gamma S^2\sqrt{\pi}(1 + \mathrm{erf}\gamma S) + Se^{-\gamma^2 S^2}\right]\right.$$

$$\left. + \frac{l}{2}\,(1 + \mathrm{erf}\gamma S) + \frac{l}{2}\sqrt{\frac{T_r}{T_i}}\,\left[\gamma S\sqrt{\pi}\,(1 + \mathrm{erf}\gamma S) + e^{-\gamma^2 S^2}\right]\right\} \qquad (3.11)$$

where

β	=	$1/2RT_i$ (dimensions of sec^2/ft^2)
R	=	gas constant
T_i	=	incident molecular temperature
T_r	=	reflected molecular temperature
S	=	molecular speed ratio
erfγS	=	the error function of γS
k, l, t	=	direction cosines between the local x, y and z axes and the desired force direction (x, y and z represent a natural coordinate system with y normal to the surface)
ϵ, γ, y	=	direction cosines between the local x, y and z axes and the velocity vector.

SOURCE FACSIMILE — Equation (3.11) and complete parameter definitions. Source facsimile; ambiguous Greek/direction-cosine symbols not guessed.

This equation is considered exact within the physical assumption of kinetic theory, free molecule flow, diffuse molecular re-emission, and non-concave surfaces.

For the three methods of determining pressures previously described, (continuum, transitional and free molecule) the final result is a surface or impact pressure. This surface pressure will vary from one elemental area to another and is integrated by finite difference methods over the entire body surface. This integration yields a distributed force which is summed over each subshape to give a total force and moment about the composite structure center of gravity.

Nomenclature for Section 3

T_{IC}	matrix to transform from individual to composite coordinate systems
dF/dA	force per unit area
dA	elemental area size
φ	angle of integration around conic shape
λ	scale factor used to determine whether an element is shaded or not
β	$1/2RT_i$ (dimensions of sec^2/ft^2)
ρ	molecular density
$\alpha_i, \beta_i, \gamma_i$	angles between the x_i axis and the x_i, y_i and z_i axes, respectively
$\alpha_i', \beta_i', \gamma_i'$	angles between the y_i axis and the x_c, y_c and z_c axes, respectively
ϵ, γ, η	direction cosines between the local x, y and z axes and the mass velocity vector
$\vec{R}_{EC}$	position vector from "E" to "C" reference frame
$\vec{T}_{EC}$	transfer matrix from "E" to "C" reference frame
$\vec{Q}_{FE}$	velocity of flow measure in "E" reference frame
$\vec{Q}_{RE}$	relative velocity of flow measure in "E" frame
$\dot{\vec{R}}_{EC}$	velocity of composite structure measure in "E" reference frame
IC JC KC	unit vectors of "C" frame measure in "E" reference frame
R_{CI}	position vector from "C" reference frame to "I"th subshapes
RI	position vector from "I"th subshape to elemental areas

SOURCE FACSIMILE — Complete Section 3 nomenclature. Source facsimile; vectors, primes, subscripts and printed wording retained.

4 Convective Heating

4.1 Continuum Convective Heating

4.1.1 Computer Program Development

The convective heating methods chosen for the low density plume impingement can be divided basically into the three following cases which will be analyzed by three distinct computer programs:

- Small plume – large surface
- Large plume – small body
- Master program – streamline divergence.

The first group of heat transfer problems include the effects of relatively small exhaust plumes impinging on large surfaces, such as during retro motor plume and staging interactions. In these cases, hypersonic assumptions cannot be applied to the calculation of the local flow properties over the large surfaces being analyzed; other methods must be used to obtain realistic heating rates to these surfaces. Lockheed/Huntsville has concluded a series of investigations using a modified method-of-characteristics program in conjunction with a normal shock computer program. These investigations provide a good analytic description of the flow field described above. This technique gives good data correlation for large surfaces parallel to the centerline of the exhaust plume.

The second grouping of convective heat transfer problems are those associated with relatively small bodies immersed in a large exhaust plume flow field. In these cases, a uniform approach flow may be assumed and rather

conventional means may be used to obtain heat transfer over these bodies. In this respect, a blunt-body program capability has been included in the low density plume impingement study. This program was used to correlate test data, and was modified for use in the low density plume real gas environment.

The final area of heat transfer problems were analyzed through use of the general impingement program in which the following heat transfer methods were programmed. The “streamline divergence” method will provide heating rates along streamlines as calculated over shapes immersed in a rocket exhaust plume. This method is the more general of the three separate methods described here and enables the analysis of a variety of plume body sizes. The most windward streamline heating rate calculation procedure has been checked out and is providing data for a variety of cases under investigation at Lockheed. Although not originally proposed, a method of tracing the different streamlines off the windward streamline has been programmed for providing more realistic heating rate distributions over the bodies. Besides the off-windward streamline calculation procedures, a real gas transport property subroutine is included in the main program. Also, an option for calculating the local flow properties at Newtonian pressures on the immersed bodies have been included in the main program.

4.1.2 General Impingement Program — Streamline Divergence

Since it is mandatory that the heat transfer prediction method be able to handle flat plates, spheres, cones, cylinders and cluster bodies in any arbitrary position and relative size in the exhaust plume, it is necessary to use a method which does not rely on a uniform flow field or constant properties of the flow medium. Lockheed/Huntsville has applied the Streamline Divergence Method of Vaglio-Laurin (References 7 and 8) to determine the impingement convective heating rates in the low density continuum regime by tracing streamlines over the body; and a simplified procedure, involving the local-to-windward streamline heating rate ratio, is used to determine the convective heating rates in the areas of separated flow.

The basic idea of the Streamline Divergence Method is relatively straightforward, and is a natural continuation of the zero angle-of-attack axisymmetric/flat plate transformation. As is known, axisymmetric bodies at zero degrees angle of attack have been analyzed successfully by two-dimensional methods with the introduction of various characteristic length transformations. In these transformations, the local normal radius of curvature of the body is the major contributing factor to the "stretched" characteristic length of the heating equations. This arises from the momentum change in the boundary layer as it moves around the axisymmetric body. When the axisymmetric body at an angle of attack is considered, the momentum change is no longer due only to a spreading effect, but also to cross flow effects. When the pressure distributions are known, these effects may be determined and the corresponding "stretching" parameter may then be calculated along the streamline as it passes over the body under consideration. The following paragraphs provide a description of the method.

The Streamline Divergence Method must provide a "new" characteristic length, which will modify the familiar zero pressure gradient (flat plate) heat rate equations into relationships which will handle flows with both circumferential and longitudinal pressure gradients. The method starts with the following equations for flat plate heating rates:

$$q_{fp_{Lam}} = .333(\rho_r \mu_r)^{1/2} (H_{aw} - H_w) Pr^{-2/3} \left(\frac{V_L}{X}\right)^{1/2} \text{(laminar)} \qquad (4.1)$$

$$q_{fp_{Turb}} = .0296\, Pr^{-2/3} (H_{aw} - H_w) \left(V_L \rho_r \mu_r^{1/4}\right)^{4/5} \frac{1}{X^{1/5}} \text{(turbulent)} \qquad (4.2)$$

where:

H_{aw} and H_w	=	the adiabatic wall and actual wall enthalpies, respectively
Pr	=	Prandtl number
ρ_r	=	density at reference conditions
μ_r	=	viscosity at reference conditions
V_L	=	velocity component in direction of streamline at edge of boundary layer

SOURCE FACSIMILE — Equations (4.1) and (4.2), including all original parameter definitions. Image-only mathematical notation.

These are the Blausius incompressible solutions modified for compressible flow by the introduction of reference condition fluid properties.

This approach also has been used to derive a relationship which predicts slip flow heating rates along the streamlines. The work of Reference 9 was extended to give the following relationship,

$$\dot{q}_{fp_{slip}} = \dot{q}_{fp_{lam}} \left[\frac{.13816}{J g} \left(\frac{\gamma T_w}{T_r} \right)^{1/2} \left(\frac{\mu_w}{\mu_r} \right)^{2.0} \left(\frac{M_L U_L^{2.0}}{x} \right) \right] \qquad (4.3)$$

where

μ_w, μ_r = wall and reference condition viscosity

T_w, T_r = wall and reference condition temperature

M_r = reference condition Mach number

γ = freestream isentropic exponent

$J g$ = energy conversion term.

SOURCE FACSIMILE — Equation (4.3) and all original parameter definitions. Image-only mathematical notation.

Considering only axisymmetric flows, for the moment, with pressure gradients, it has been shown that a transformation of the characteristic length, in which the momentum equation contains contributions from pressure gradients, may be written as

$$X_{Lam} = \frac{1}{\rho_r \mu_r V_L r^2} \int_0^{\ell} \rho_r \mu_r V_L r^2 \, d\ell \text{ (laminar)} \qquad (4.4)$$

SOURCE FACSIMILE — Equation (4.4), laminar characteristic length. Image-only mathematical notation.

$$X_{Tur} = \frac{1}{\rho_r \mu_r V_L r^{5/4}} \int_0^{\ell} \rho_r \mu_r V_L r^{5/4} \text{ (turbulent)} \qquad (4.5)$$

SOURCE FACSIMILE — Equation (4.5), turbulent characteristic length. Image-only mathematical notation.

where r is the local radial coordinate along a streamline of the body, and *l* is the length along that streamline. A zero momentum change across the streamline is assumed and thinning of the boundary layer, due to continuity considerations over the expanding surface area, is considered.

Considering the control volume element shown in Figure 4.1 (in which constant mass flow is assumed), heat transfer is influenced by, among other things, the thickness of the boundary layer.

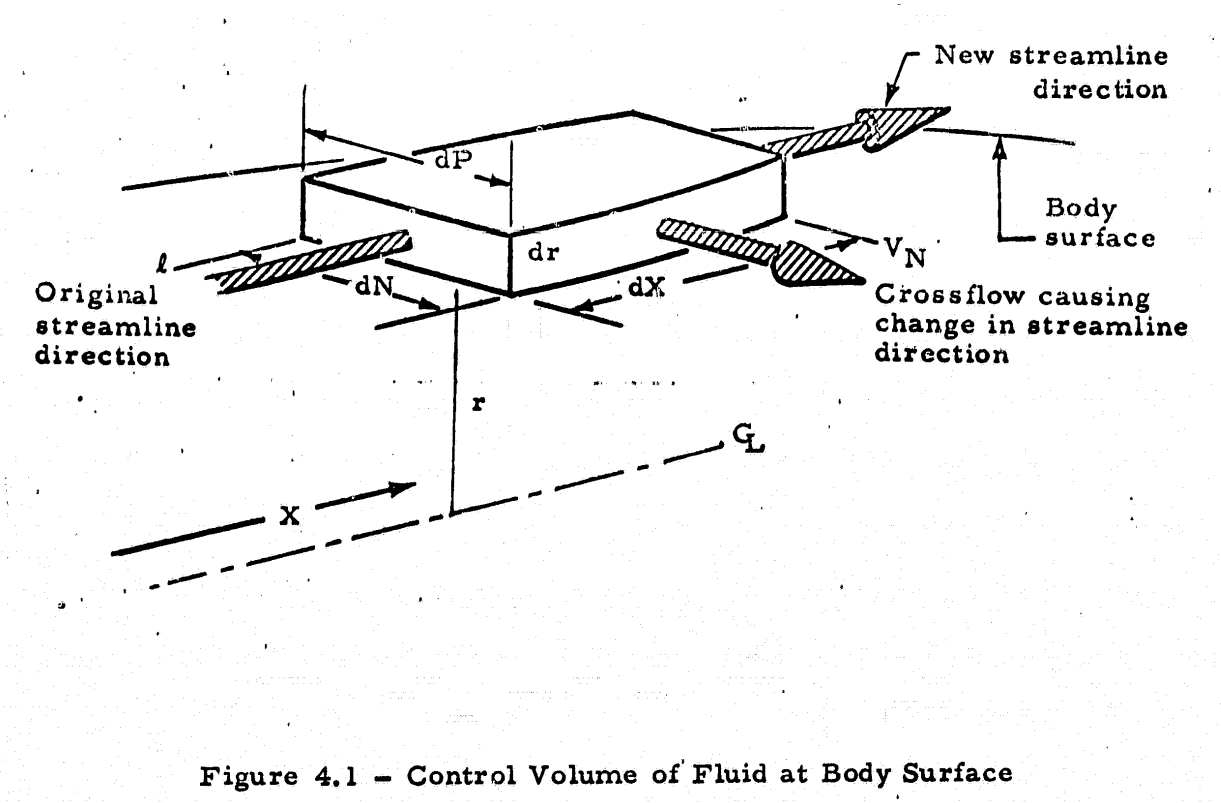


Figure 4.1 – Control Volume of Fluid at Body Surface

SOURCE FACSIMILE — Figure 4.1 — Control Volume of Fluid at Body Surface. Complete original diagram and caption; image-only labels.

This boundary layer is thinned by two effects, other than fluid density changes, as the flow expands about the surface. The first and most easily analyzed is boundary layer thinning due to changing of the surface area which the control volume of fluid must cover. This change in surface area is attributed to the radius of curvature (R) of the local streamline which for axisymmetric bodies at zero angle of attack lies in the plane containing the streamline (Figure 4.2)

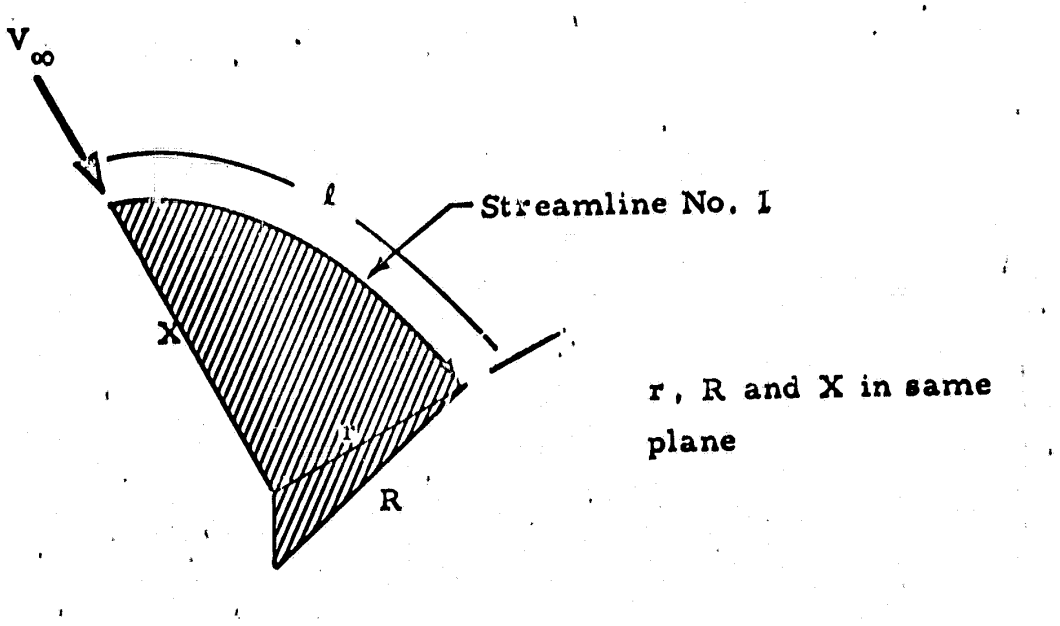


Figure 4.2 – Geometry of Streamline No. 1 for Axisymmetric Flow

SOURCE FACSIMILE — Figure 4.2 — Geometry of Streamline No. 1 for Axisymmetric Flow. Complete diagram and caption; image-only labels.

However, when a spanwise pressure gradient is present, i.e., body at angle of attack, a second thinning effect, that due to the component of cross flow, also exists. The effect of surface area undergoing change and the spanwise pressure gradients can be combined by making a transform to a pseudo-axisymmetric surface which would have the corresponding local flow conditions. This transformation coordinate, e, may be derived from the following differential equation

$$\frac{1}{e}\frac{\partial e}{\partial \ell} = \frac{1}{r}\frac{\partial r}{\partial \ell} + \frac{1}{V_N}\frac{\partial V_N}{\partial \ell} \qquad (4.6)$$

where V_N is the local cross flow velocity component. The first term on the right-hand side of Equation (4.6), $\frac{1}{r}\frac{\partial r}{\partial \ell}$ is a change in e due to the curvature

SOURCE FACSIMILE — Equation (4.6) and following original text containing inline notation; sentence continues on original p.25. Image-only technical content.

of the body's surface. The second term, $\frac{1}{V_N}\frac{\partial V_N}{\partial \ell}$ is a change in e along the streamline as the pressure gradient about the body changes, i.e., spanwise flow. By integrating Equation (4.6), e may be determined for application to the heating rate equation transformed variable. Thus, the characteristic lengths X_{Lam} and X_{Tur} can now be calculated as

$$X_{Lam} = \frac{1}{\rho_r \mu_r V_L e^2} \int_0^{\ell} \rho_r \mu_r V_L e^2 \, d\ell \quad \text{(laminar)} \tag{4.7}$$

$$X_{Tur} = \frac{1}{\rho_r \mu_r V_L e^{5/4}} \int_0^{\ell} \rho_r \mu_r V_L e^{5/4} \, d\ell \quad \text{(turbulent)} \tag{4.8}$$

SOURCE FACSIMILE — Continuation of the preceding original sentence, characteristic-length definitions and Equations (4.7)–(4.8). Image-only technical content.

Because these characteristic lengths are evaluated by integrating the changing parameters ρ_r, μ_r, V_L and e along the streamline, digital computer numerical techniques are most appropriate for evaluating the heating rates to a body by the Streamline Divergence Method. Using the local flow properties obtained from the Method of Characteristics Plume Program, the heating rate Equations (4.1) and (4.2) can be readily solved for points on the body streamline.

The streamlines are traced ring-by-ring over the body by assuming that they curve due to spanwise pressure gradients. The velocity component perpendicular to each streamline which arises as the streamlines move away from the stagnation point are vectorially added to the streamline at each ring. The accuracy of this method depends on the selection of subshape sizes when the initial problem is input to the computer.

Once the streamline has been analyzed, the streamline lengths and local pressure gradients are used to evaluate the characteristic length transforms as described above. Figure 4-3 shows a schematic of a body with subrings and streamlines distributed over the body. The local heating rates (laminar, turbulent and slip flow/transitional) are then printed out in the main program at equal increments around each ring.

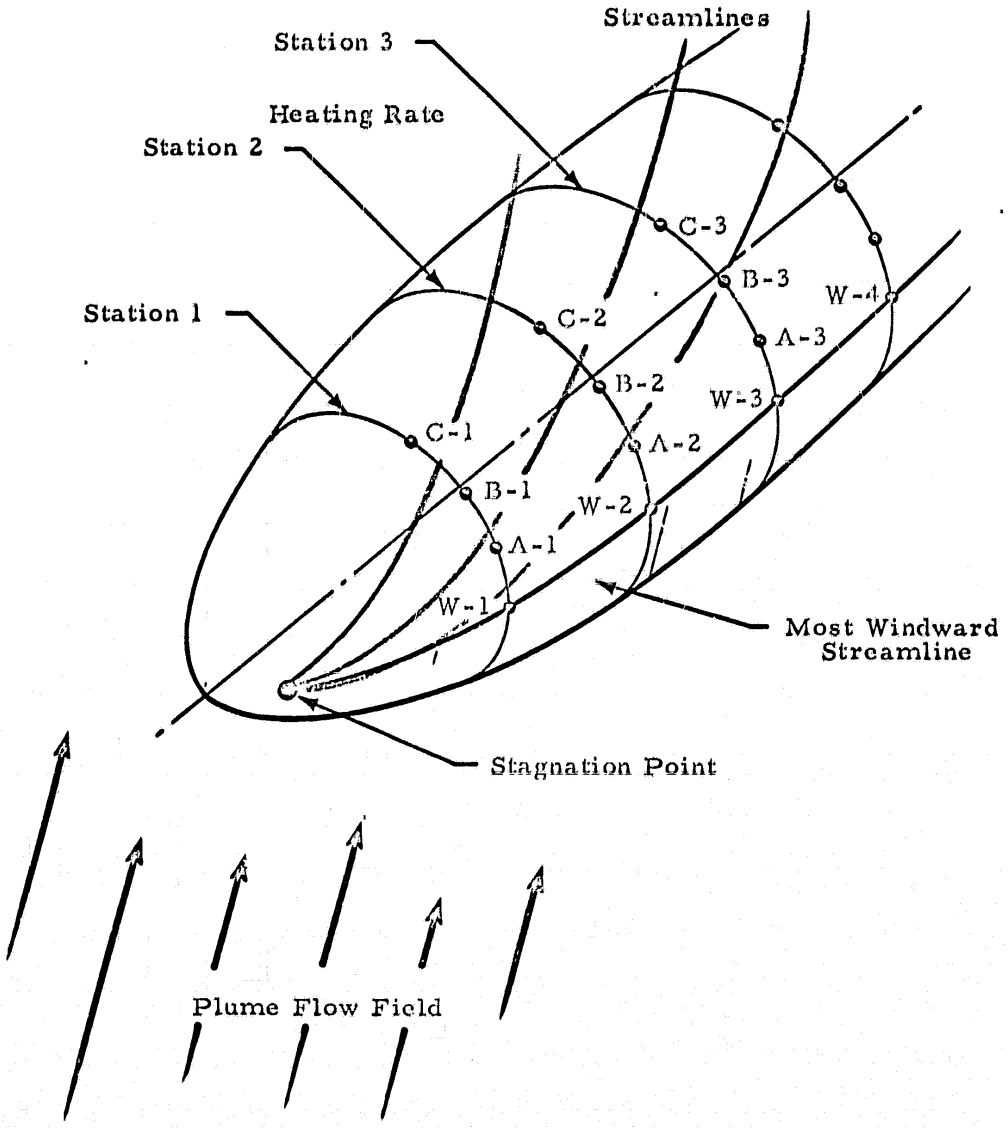


Figure 4-3 – Mapping Coordinates for Off-Centerline Heating Rate Distribution

SOURCE FACSIMILE — Figure 4-3 — Mapping Coordinates for Off-Centerline Heating Rate Distribution. Complete original figure and caption; image-only labels.

A transition Reynolds number based on momentum thickness is also output, so that the user can select the appropriate heating rate calculation i.e., turbulent or laminar.

4.1.3 Transition Criteria

Since the method evolved from this study includes analyses of both laminar and turbulent flow, a method of determining transition from one flow regime to another is required. Recent data correlations of the transition phenomena on various hypersonic vehicles show that a reasonable data reduction is possible if the parameters of local Mach number and local momentum thickness Reynolds numbers are incorporated into the analysis. These parameters are calculated for each step of the analysis of turbulent and laminar heating rate equations as described previously. This becomes merely the step of evaluating the following equation which is derived for pressure gradient flow fields about surfaces with changing curvature (Reference 10).

$$Re_\theta = \frac{.664\left[\int_0^\ell \rho_L \mu_L V_L e^2 \, d\ell\right]^{1/2}}{\mu_{Le}} \qquad (4.9)$$

SOURCE FACSIMILE — Equation (4.9), retaining the original integral and notation. Image-only mathematics.

As this parameter is determined, it is compared against a predetermined value for the transition occurrence and the nature of the flow will be evident, i.e., either laminar or turbulent. The generally accepted value at transition is $Re_\theta = 250$. Experimental data for blunted bodies are shown on Figure 4-4 as a function of Mach number and body diameter Reynolds number.

4.1.4 Separation Point Heating

Heat transfer rates in the separated flow regions are predicted using a data correlation approach. Experimental data such as that taken on the HL-10 and M2 vehicles, as well as from published reports have been correlated and empirical formulas developed and included in the computer program. The equation for heat transfer has the form,

$$q_L/q_{\text{prior to separation}} = \frac{1}{e^{\cdot 6(\Delta\delta)}} \left(\frac{x_{s_i}{}_{\text{prior to separation}}}{x_{s_i}{}_{\text{prior to separation}} + \ell} \right)^m \qquad (4.10)$$

where

ℓ = geometric shortest distance to local separation point

$\Delta\delta$ = difference between local flow angle and angle of surface

m = 1/2 for laminar flow prior to separation

= 1/5 for turbulent flow prior to separation

x_{s_i} = integrated characteristic length

SOURCE FACSIMILE — Equation (4.10) and all original parameter definitions. Image-only mathematical notation.

The local deflection angle of the section under consideration is a primary factor when considering separated flow, while the characteristic length based on the distance from the separation point, has secondary influence. Sufficient experimental data have been obtained to generate (Equation 4.10), for body configurations with separated flow orientations and various flow media. These data are presented in Figure 4-5.

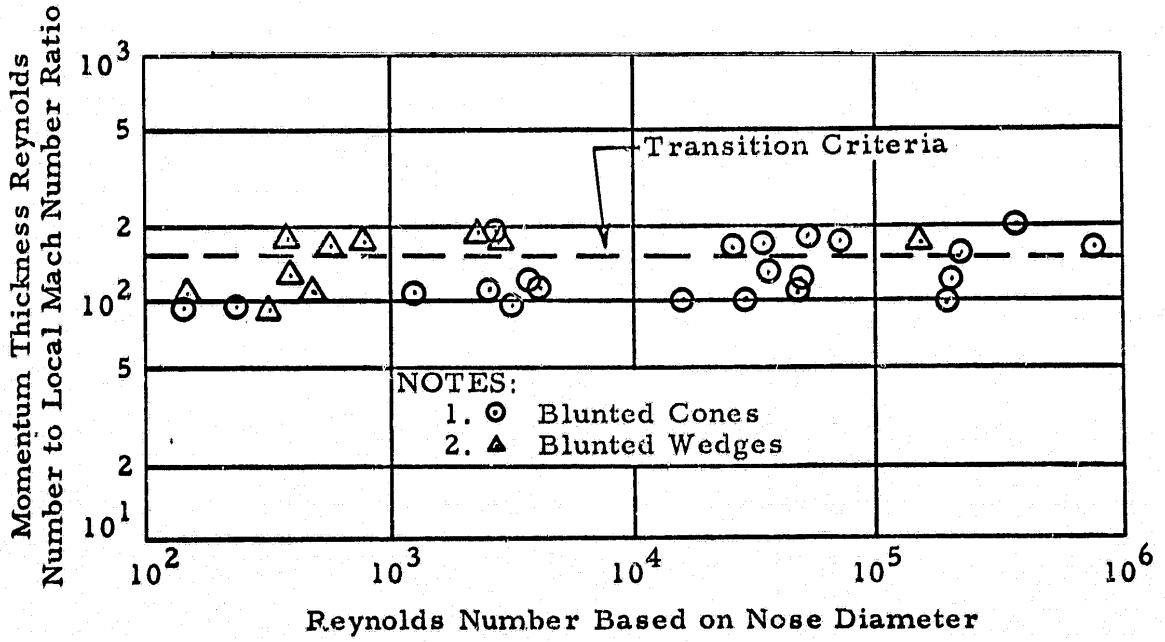


Figure 4-4 - Laminar to Turbulent Flow Transition Criteria

SOURCE FACSIMILE — Figure 4-4 — Laminar to Turbulent Flow Transition Criteria. All axes, plotted values, notes and caption retained; image-only labels.

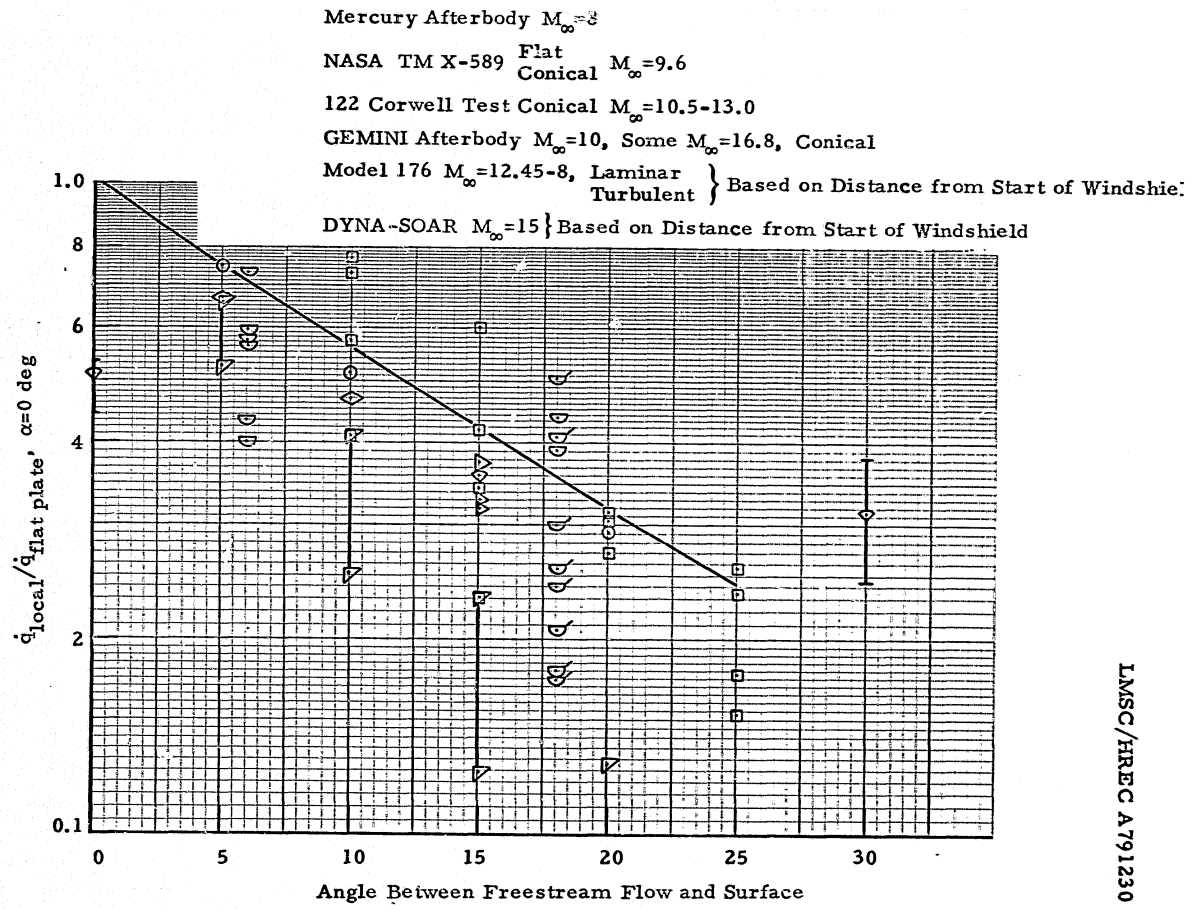


Figure 4-5 – Correlation of Leeward Heating Rates

SOURCE FACSIMILE — Figure 4-5 — Correlation of Leeward Heating Rates. Complete chart, legend, axes and caption, rotated for reading; image-only labels.

4.1.5 Stagnation Point Heating

The heating rates predicted by using the Streamline Divergence Method are not valid for the stagnation point and a small region around the stagnation point. For instance, for a hemisphere this region is usually considered to be ±15° from the stagnation axis. To obtain heating rates at the stagnation point, the following equation, taken from Reference 11, is used.

$$q_{sp} = \frac{Nu}{\sqrt{Re}} \sqrt{\rho_L \mu_L} \frac{1}{Pr} (H_{aw} - H_w) \sqrt{\frac{dV}{ds}} \qquad (4.11)$$

where

$$\frac{Nu}{\sqrt{Re}} = \left[\frac{Pr}{Pr_w} \sqrt{\frac{T_L}{T_w} \frac{\mu_w}{\mu}} \right]^{1.8} \left[1.0 - \frac{H_w}{H} \right]^{1.15} \qquad (4.12)$$

and

P_r = Prandtl number
μ = viscosity of gas
T = temperature of gas
Re = Reynolds number
H = enthalpy of gas
Nu = Nusselt number
ρ = density of gas
w = evaluated at wall conditions

SOURCE FACSIMILE — Equations (4.11) and (4.12), including all original parameter definitions. Image-only mathematical notation.

This equation has been empirically derived for arbitrary high enthalpy gas mixtures and has been shown to give excellent results as shown in Figure 4.6.

The real gas transport properties are generated by the Transport Property Program. A heating rate distribution away from the stagnation point such as Lees (Reference 12) is used in conjunction with the stagnation heating rate to predict heat transfer rates in the region around the stagnation point. Equation (4.11) requires a velocity gradient at the stagnation point, dV/ds, which is determined from pressure distributions from either test data or modified Newtonian theory for the various bodies.

SOURCE FACSIMILE — Original transport-property paragraph and stagnation-point velocity-gradient explanation; inline mathematical notation retained as an image.

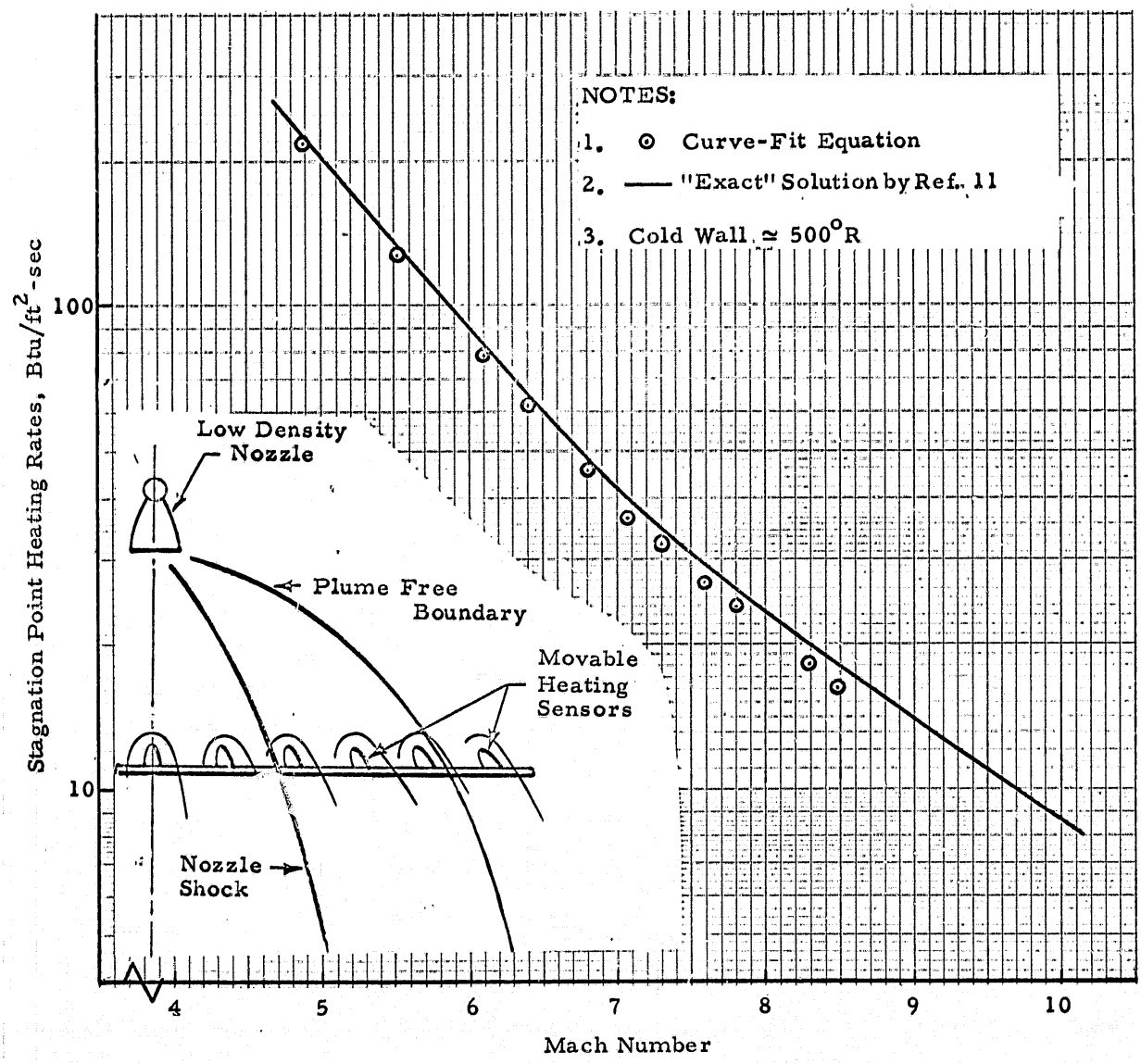


Figure 4.6 - Comparison of Stagnation Point Heating Rates versus Mach Number in a Typical Rocket Exhaust Plume

SOURCE FACSIMILE — Figure 4.6 — Comparison of Stagnation Point Heating Rates versus Mach Number in a Typical Rocket Exhaust Plume. Complete figure and caption; image-only labels.

4.1.6 Small Plume – Large Surface

For the special case of an exhaust plume impinging on a flat plate which is large with respect to the plume and position such that it is parallel to or angles away from the axis of symmetry of the rocket nozzle, Lockheed/Huntsville has a method of solution which uses the method of characteristics computer program to predict the impingement flow field.

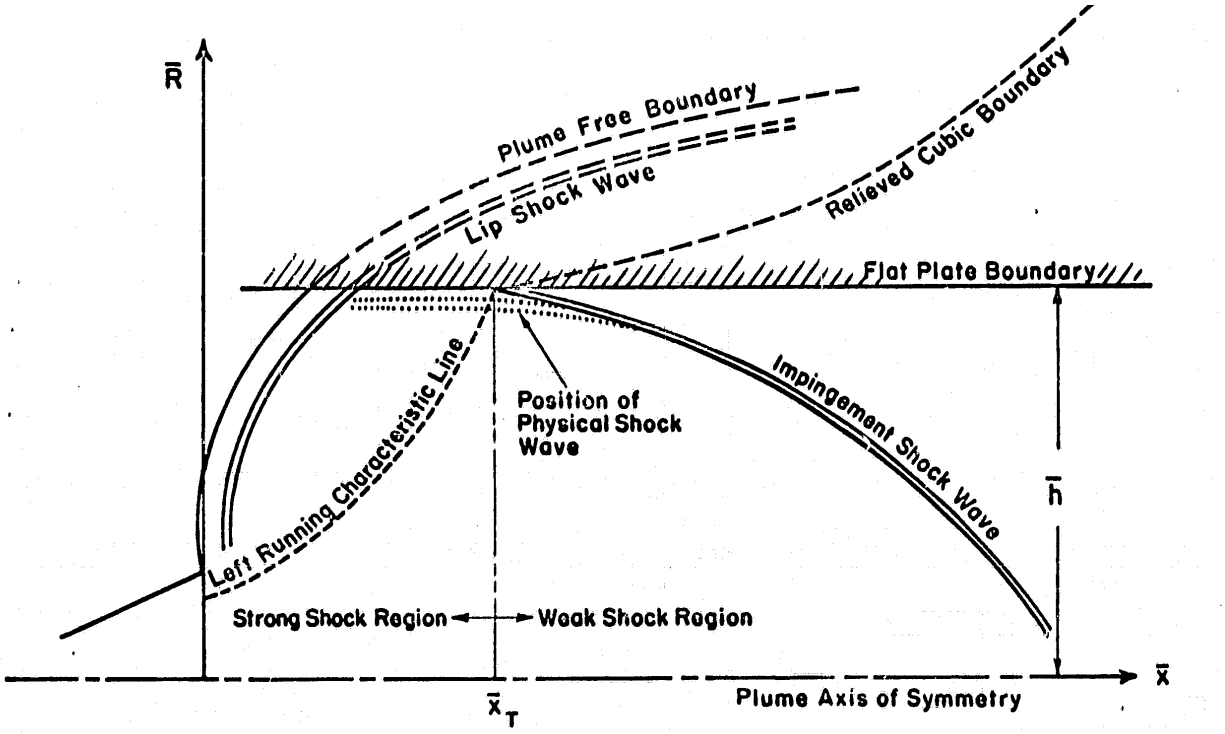


Figure 4-7 – Description of Flat Plate Impingement Problem (Not to Scale)

SOURCE FACSIMILE — Figure 4-7 — Description of Flat Plate Impingement Problem (Not to Scale). Complete diagram and caption; image-only labels.

The first step in this analysis is to run an axisymmetric method of characteristics description of the nozzle and plume flow field without the presence of the solid boundary (surface). The boundary is then superposed on the plume flow field as shown in Figure 4-7. Looking at each left running characteristic line as it intersects the boundary, a decision can be made whether the flow at that point could turn through an oblique shock and still remain supersonic. The point on the boundary closest to the nozzle exist plane which can meet this condition becomes the “turning point” and the left running characteristic line

passing through this point on the boundary becomes the start line to restart the impingement flow field. A weak oblique attached shock wave is artificially started at the turning point and is completely mapped out in the impingement flow field. The region on the upstream side of the start line is known as the strong shock region since the flow must pass through a strong shock and become subsonic to turn parallel to the wall. This region is difficult to analyze completely since some of the flow is reversed, but, in general, the region is small in comparison to the supersonic flow field over most of the flat plate. To find pressures in the strong shock region, Lockheed/Huntsville has an interpolation scheme (Reference 13) which uses the difference between the boundary and flow angle at each point as the turning angle required, (and then finds the shock angle between a normal shock and the shock for Mach 1.0 flow downstream), to turn the flow. The pressure on the other side of this shock is used as the pressure on the wall in this region. The pressures along the boundary in the weak shock region where the flow remains supersonic behind the shock are those pressures predicted by the method of characteristics solution at the wall.

To obtain heat transfer rates, the Lockheed/Huntsville Real Gas Boundary Layer Program (Reference 14) is used to calculate the growth of a boundary layer along the wall in the weak shock region beginning at the turning point. The program uses the local flow properties at the wall predicted by the method of characteristics as boundary layer edge conditions. In addition, accurate transport properties of the gas in the boundary layer at any temperature and pressure are found using the Transport Property Program. The results of the Transport Property Program, which is run for each propellant, are output on cards and become input for the Boundary Layer Program. Heat transfer predictions in the strong shock region have not been finalized and will need more development. The method used is a modification of the Fay and Riddell stagnation heating rate equation. The shock structure in the strong shock region approaches that of a normal shock and although the flow does not really stagnate, the velocity is low.

4.1.7 Transport Properties

To perform heat transfer studies involving gas mixtures, the viscosity, conductivity and heat capacity of the gas mixture as a function of temperature must be known. The method that is utilized for obtaining these properties for multi-component real gas mixtures is presented in the following paragraphs.

The theoretical method used for calculating viscosity and conductivity is based on the Lennard-Jones potential model, discussed in References 15 and 16. The Lennard-Jones method was selected because it has been successfully applied in practice (References 15 and 16). It is one of the most realistic models available, and the intermolecular force constants, which are used in the equations, can be estimated from physical properties when experimental data is not available. Many of these intermolecular force constants have been measured or estimated for about 200 gas species and are tabulated in Reference 15. The force constants are then used in the formulation of Hirschfelder (Reference 15) to obtain the viscosity and thermal conductivity of the individual gas species. The viscosity and thermal conductivity of gas mixtures is then calculated, using the method outlined in Reference 17.

A detailed knowledge of the chemical species and their concentrations present must be known in order to obtain accurate results. The chemical species and concentrations can be “specified” at some appropriate position in the flow field and the composition assumed to be frozen thereafter or they can be specified as a function of time or position in the flow field to simulate the quasi-equilibrium method.

Since the combination equations do not account for any chemical reactions occurring during recombination, it can be expected that the mixture

transport properties will have a lower value using this method than for the method where the chemical reactions upon recombining are not ignored. However, Butler and Brokaw (Reference 18), show that the ratio of thermal conductivity to heat capacity for reacting gas mixtures is about equal to the same ratio for non-reacting gas mixtures. Since most convective heat transfer equations use this ratio form, the differences due to neglecting the recombination reactions are small.

Viscosity

The coefficient of viscosity for a pure gas can be obtained for any degree of approximation. To a first approximation, the viscosity of a pure gas is given by the following relationship.

$$\eta = \frac{2.6693 \times 10^{-6} \sqrt{M T_k}}{\sigma^2 \Omega^{(2,2)*}(T^*)} \qquad (4.13)$$

SOURCE FACSIMILE — Equation (4.13). Image-only mathematical notation.

Values for the intermolecular force constant σ and T^*, along with molecular weights, are tabulated for about 200 gas species in Reference 15). The reduced collision integral $[\Omega^{(2,2)*}]$ is a function of the reduced temperature (T^*) and is tabulated for a large range of T^* in Reference 15. The reduced collision integral represents an averaging of the collision cross section over all orientations and the relative kinetic energies of collision molecules.

SOURCE FACSIMILE — Original definition and explanation of intermolecular force constants, reduced temperature and collision integral; technical symbols retained as an image.

Thermal Conductivity

The thermal conductivity of polyatomic gases is calculated by the equation (Reference 15) stated below.

$$\lambda = \frac{R\eta}{M}\left[\frac{15}{4} + f_{int}\left(\frac{C_p}{R} - \frac{5}{2}\right)\right] \qquad (4.14)$$

SOURCE FACSIMILE — Equation (4.14). Image-only mathematical notation.

The first term in the brackets represents the translational thermal conductivity and the second term the contribution of the internal degrees of freedom to the conductivity. The assumptions inherent in the above equation are that (1) the internal energy of the molecule is independent of the molecular velocity,

and (2) the exchange of internal and translational energy is sufficiently rapid, such that at each point, the distribution of molecules among the internal energy states is the molecule equilibrium distribution characteristic of the local temperature. The value of f_{int} for the Lennard-Jones potential over a large temperature range is approximately 1.32. This is the value for f_{int} that is used in the program.

Thermal conductivity calculated using Equation (4.14) above, is in error at temperatures below 500°K, therefore, experimentally obtained thermal conductivities should be used in preference to the calculated values at low temperatures. The effect of ionization is neglected in Equation (4.14), so care should be exercised when ionization of the gas mixture is expected to occur.

Specific Heat

The specific heat of the pure gas species is calculated from polynomial curve-fit coefficients derived from experimental data. The specific heat expressed in the polynomial form is

$$C_p = R(a_1 + a_2T + a_3T^2 + a_4T^3 + a_5T^4) \quad (4.15)$$

where a_1, a_2, a_3, a_4 and a_5 are the polynomial curve-fit coefficients.

To minimize the errors which result from representing the specific heat by a polynomial function, the five coefficients were calculated in Reference 15 for two temperature intervals. The polynomial curve-fit coefficients are tabulated in Reference 15 for 223 gas species.

Weighted Property Averaging

The preceding discussion describes the procedure for obtaining the values of viscosity, thermal conductivity and specific heat for the individual gas species of the real gas mixture under analysis. A weighted averaging method is used in the program to obtain the final transport properties of the gas mixture.

The viscosity, conductivity and specific heat of the gas mixture are calculated by the method of Wilke and Johnson. The equations of Wilke and Johnson are:

$$F = \frac{Fg_1}{1 + (MF_2/MF_1)\Phi_{12} + (MF_3/MF_1)\Phi_{13} + \ldots + (MF_n/MF_1)\Phi_{1n}}$$

$$+ \frac{Fg_2}{1 + (MF_1/MF_2)\Phi_{21} + (MF_3/MF_2)\Phi_{23} + \ldots + (MF_n/MF_2)\Phi_{2n}}$$

$$+ \frac{Fg_m}{1 + (MF_1/MF_m)\Phi_{m1} + (MF_2/MF_m)\Phi_{m2} + \ldots + (MF_n/MF_m)\Phi_{mn}} \qquad (4.16)$$

In this equation, $Fg_1, Fg_2, \ldots, Fg_m$ are the pure gas properties of species 1, 2, ..., m, and Φ_{mn} may be evaluated by Equation (4.17), where n is also the gas species 1, 2, ..., n.

$$\Phi_{mn} = \frac{\left[1 + (Fg_m/Fg_n)^{1/2}(MF_n/MF_m)^{1/4}\right]^2}{2\sqrt{2}\left[\frac{MF_n - MF_m}{MF_n}\right]^{1/2}} \qquad (4.17)$$

SOURCE FACSIMILE — Equations (4.16) and (4.17) and all intervening original definitions. Image-only mathematical notation, preserving the printed signs.

The molecular weight of the gas mixture is calculated by the equation:

$$M_{wt} = \sum_{i=1}^{i=m} MF_i \, M_{wt_i} \qquad (4.18)$$

SOURCE FACSIMILE — Equation (4.18). Image-only mathematical notation.

In the present program, the specific heat coefficients and the force coefficients for CO_2, H_2, H_2O, H, OH, CO, N_2, O_2 are prepared for the data tables in the property subroutine. Additional data may be prepared as needed by referring to Reference 19 for these coefficients.

4.2 Noncontinuum Convective Heat Transfer

A body of arbitrary size immersed in a high-altitude rocket exhaust plume may experience convective heating in one or all of the low density flow regimes, depending on the body's position in the exhaust plume and its relative size compared to that of the plume. The ability to analyze the flow conditions over a body of arbitrary size and shape is contained within the continuum Streamline Divergence Technique. To predict heating rates along streamlines on the body, the Streamline Divergence Technique needs both a method to determine the stagnation heat transfer value and a flat plate boundary layer equation which is then modified with an integrated characteristic length. It is assumed in the present low density, or noncontinuum heat transfer theory, that the basic framework of the Streamline Divergence Technique is still applicable for the overall heat transfer analysis if the stagnation point heat transfer theory and the flat plate boundary layer equation are correctly formulated for the low density environment.

4.2.1 Stagnation Region Heat Transfer Theory

Directly analogous with continuum heat transfer theory, the most severe heating rates will occur at the point where the low density flow stagnates on the body. Hence, considerable emphasis was placed on generating an accurate description of the low density stagnation region heat transfer problem. The low density blunt body solution chosen to describe this problem is due to H. K. Cheng, References 20 and 21. Cheng's stagnation region solution, based on the thin shock layer concept, is valid in the range from continuum flow to full transition flow, which includes the vorticity-interaction regime, the viscous shock layer regime, the incipient-merged-layer regime, and the fully merged layer regime as defined by Probstein, Reference 22.

The blunt body flow field, under the assumption of a uniform hypersonic low density approach flow, has been divided into two regions: (1) a shock transition zone which contains all the effects of the shock wave; and (2) a viscous

shock layer (see Figure A-1 in Appendix A). It is assumed that these two layers are thin with respect to the local nose radius and that gradients in the direction normal to the body surface are large in comparison to gradients along the body. The Navier-Stokes equations, with the above two assumptions, are applied to the shock transition zone and the viscous shock layer.

In the shock transition zone, the result of this application is a set of equations, denoted as modified Rankine-Hugoniot relations, which determine the value of flow properties on the downstream side of the shock wave. With the proper order of magnitude considerations consistent with the thin shock layer concept, the Navier-Stokes equations yield

$$\text{(a)} \qquad \rho_2 v_2 = \rho_1 v_1 \quad \text{(mass conservation)}$$

$$\text{(b)} \qquad p_2 = \rho_1 v_1^2 \quad \text{(normal momentum conservation)}$$

$$\text{(c)} \qquad \rho_1 v_1 (u_2 - u_1) = (\mu u_y)_2 \quad \text{(tangential momentum conservation)} \qquad (4.19)$$

$$\text{(d)} \qquad \rho_1 v_1 (H_2 - H_1) = \left\{ \frac{\mu}{Pr} \left[H + (Pr - 1) \frac{u^2}{2} \right]_y \right\}_2 \quad \text{(energy conservation)}$$

where

ρ = density

v = velocity component normal to shock wave (y-direction)

u = velocity component tangential to shock wave (x-direction)

μ = viscosity

Pr = Prandtl number

H = total enthalpy

SOURCE FACSIMILE — Equation (4.19), parts (a)–(d), conservation labels and original parameter definitions. Image-only mathematical notation.

$(\quad)_1$ = freestream value

$(\quad)_2$ = value at shock interface

$(\quad)_y$ = partial derivative with respect to y

SOURCE FACSIMILE — Continuation of parameter/subscript definitions for Equation (4.19). Image-only notation.

It can be seen that the modification of the usual Rankine-Hugoniot relations employed in gas dynamics is due to the presence of viscous effects in a low density shock wave. Equations (4.19c) and (4.19d) show that tangential momentum and total enthalpy are no longer conserved across the shock wave because of viscous forces. The relationships in Equation (4.19) define the boundary conditions which the viscous shock layer equations must satisfy at the shock interface (see Figure A-1 in Appendix A).

An analogous treatment of the Navier-Stokes equations in the viscous shock layer results in a set of partial differential equations which are valid in the entire shock layer around the blunt body. These equations are given by,

$$\text{(a)} \quad \frac{\partial}{\partial x}(\rho u Z) + \frac{\partial}{\partial y}(\rho v Z) = 0 \quad \text{(conservation of mass)}$$

$$\text{(b)} \quad \frac{\partial p}{\partial y} + K_c \rho u^2 = 0 \quad \text{(conservation of normal component of momentum)}$$

$$\text{(c)} \quad \frac{\partial p}{\partial x} + \rho \left(u \frac{\partial}{\partial x} + v \frac{\partial}{\partial y}\right) u = \frac{\partial}{\partial y}\left(\mu \frac{\partial u}{\partial y}\right) \quad \text{(4.20)}$$

(conservation of tangential component of momentum)

$$\text{(d)} \quad \rho \left(u \frac{\partial}{\partial x} + v \frac{\partial}{\partial y}\right) H = \frac{\partial}{\partial y}\left\{\frac{\mu}{Pr}\frac{\partial}{\partial y}\left[H + (Pr - 1)\frac{u^2}{2}\right]\right\}$$

(conservation of energy)

where

ρ = density

μ = viscosity

SOURCE FACSIMILE — Equation (4.20), parts (a)–(d), all conservation labels and initial parameter definitions. Image-only mathematical notation.

p = static pressure

Pr = Prandtl number

Z = coordinate defining shape of axisymmetric body

K_c = local curvature

v = velocity component normal to body (y-direction)

u = velocity component tangential to body (x-direction)

SOURCE FACSIMILE — Continuation of the complete parameter definitions for Equation (4.20). Image-only technical notation.

These equations are extremely difficult to solve in their present form. However, the solution required for the low density heat transfer theory is only that in the stagnation region, which affords some simplification to the task of solving the above equations. The method of solution, covered in greater detail in Appendix A, will be briefly described below.

The initial step is to transform the equations into von Mises coordinates (s,ψ) or streamline coordinates which means that the continuity equation is identically satisfied by the definition of a compressible stream function, $\psi(x, y)$. The three remaining equations and their boundary conditions are again transformed into normalized or "stretched" coordinates λ and ζ where

$$\lambda = \lambda(s)$$

$$\zeta = \zeta(\psi, s)$$

The equations are still partial differential equations in terms of λ and ζ. These equations may be simplified in the stagnation region by selecting λ as the independent variable and then setting up a coordinate perturbation problem. Thus, the solution is perturbed about $\lambda=0$, or the stagnation streamline. All of the flow variables are expanded in a geometric series in λ, e.g.,

$$u = u_0 + \lambda u_1 + \lambda^2 u_2 + \ldots$$

SOURCE FACSIMILE — Original von Mises/stretched-coordinate transformation explanation, unnumbered definitions and perturbation series. Greek-coordinate symbols retained without conjecture; image-only technical content.

By substituting these series expansions into the equations and equating like powers of λ, the partial differential equations for the various orders of the variables (u_0, u_1, etc.) become ordinary linear differential equations in the remaining independent variable ζ.

SOURCE FACSIMILE — Original explanation of the series substitution and remaining independent variable; image-only technical notation.

At this point, the low density flow regimes between continuum flow and transition flow are divided into two regions, denoted Regime I and Regime II, based on the order of magnitude of two important parameters

$$\epsilon = (\gamma-1)/2\gamma$$

$$K^2 = \epsilon \frac{\rho_\infty U_\infty a}{\mu_o} \left(\frac{T^* \mu_o}{T_o \mu^*} \right)$$

where

γ = ratio of freestream specific heats

ρ_∞ = freestream density

U_∞ = freestream velocity

μ = viscosity

T = static temperature

a = local nose radius

$( )_o$ = evaluated at freestream stagnation conditions

$( )^*$ = evaluated at reference temperature.

SOURCE FACSIMILE — The two unnumbered regime parameters and all their original definitions, including freestream and reference-condition subscripts. Image-only mathematical notation.

The parameter ε is a measure of the compression across the shock wave and K^2 is essentially a low density Reynolds number. The method of solution of the resultant perturbation equations is different for Regimes I and II, where these regimes are defined by the magnitude of the product of ε and K^2.

Regime I : $\quad O(1) \leq \epsilon K^2 < \infty$

Regime II: $\quad O(\epsilon) \leq \epsilon K^2 \leq O(1)$

SOURCE FACSIMILE — Original Regime I and Regime II inequalities. Image-only mathematical notation.

The solution to the equations in Regime I, which includes the vorticity interaction regime and part of the viscous-layer regime, is based on a local similarity solution familiar in boundary layer theory. The equations are

transformed into the variables f and η, where η is the integrated normal coordinate and f is a function whose first derivative with respect to η is proportional to the shock layer velocity. The equations become,

$$f''' + ff'' - 1/2\, f'^2 = -1/2 \left[\frac{T_w}{T_o} + \left(1 - \frac{T_w}{T_o}\right)\Theta\right] \left(\frac{\phi}{\phi_i}\right)$$

$$\Theta'' + Pr\, f \Theta' = 0$$

where

Θ = enthalpy function = $(H - H_w)/(H_\infty - H_w)$

H = total enthalpy

Pr = Prandtl number

$(\ )'$ = differentiation with respect to η

$(\ )_o$ = freestream stagnation conditions

$(\ )_w$ = body surface conditions

ϕ/ϕ_i = function representing the tangential pressure gradient

SOURCE FACSIMILE — Continuation of the coordinate-transformation description, unnumbered coupled equations and all original definitions. Image-only technical content.

These two coupled ordinary differential equations with the appropriate boundary conditions were solved with a numerical integration scheme. The iteration technique used in the numerical integration provides extremely rapid convergence.

The solution to the perturbation equations in Regime II, which includes part of the viscous layer regime, the incipient merged layer regime and the fully merged layer regime, is based on an analytical technique. Since the equations are linear, the principle of superposition can be used as a means of artificially uncoupling the momentum and energy equations. The flow variables are expanded in an order of magnitude series, e.g.,

$$u = u_{11} + u_{22} + u_{33} + \cdots$$

where it is assumed that u_{22} is an order of magnitude smaller than u_{11}, etc. Substituting a series of this type for each variable into the equations and evaluating terms based on their magnitude results in a set of equations for each of several orders of magnitude. The first order set, involving $(\ )_{11}$, contains two uncoupled ordinary differential equations which are fairly easy to solve. Then, this result is used to solve the next ordered set involving $(\ )_{11}$, $(\ )_{22}$ and $(\ )_{11} \times (\ )_{22}$ for the $(\ )_{22}$ variables. Each set is progressively more difficult to solve, but in the limit, the combined solution will be asymptotically close to the exact solution. For the present problem, sufficient accuracy was achieved by determining the $(\ )_{22}$ solution.

SOURCE FACSIMILE — Original order-of-magnitude series and its complete subscripted explanation. Image-only technical notation.

Some sample results from both Regime I and Regime II are shown in Figures 4-8, 4-9 and 4-10. Figure 4-8 shows how the velocity profile in the stagnation region shock layer varies as a function of the low density Reynolds number, K^2. Figure 4-9 shows how the enthalpy function profile in the stagnation region varies with K^2 for the same conditions as Figure 4-8. The profiles of both these quantities demonstrate the fact that as the freestream density decreases from a value close to continuum flow, the shock standoff distance becomes smaller and, at the same time, the shock layer flow field is dominated by viscous effects. Predictions of heat transfer coefficient in the stagnation region shock layer are compared with experimental data in Figure 4-10. This plot includes results from both methods of solution, Regime I and Regime II, as well as a comparison to the numerical solution of the full partial differential equations carried out by Cheng. However, the present results need only three

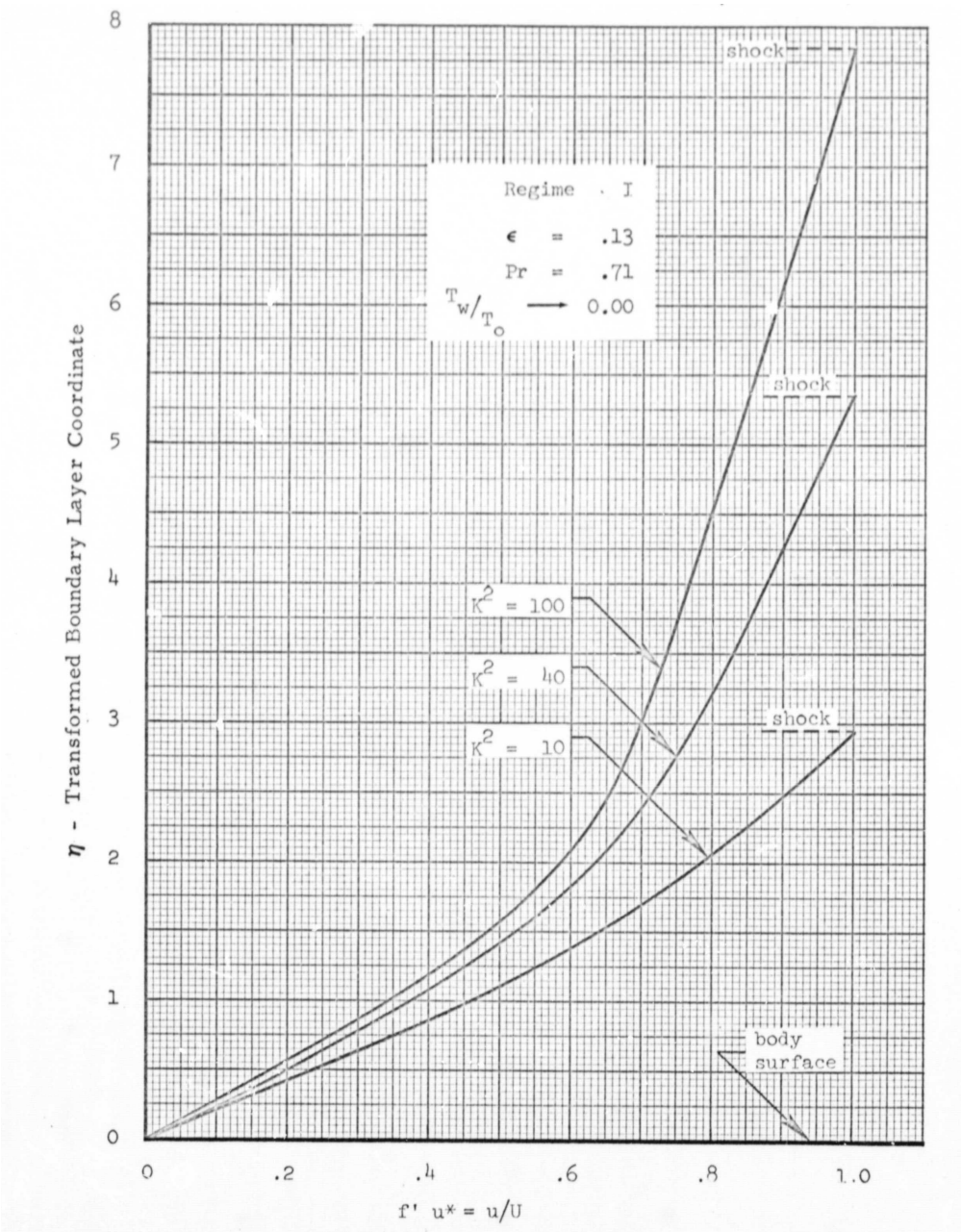


Figure 4-8 - Velocity Profiles in Shock Layer as a Function of Low Density Reynolds Number (K^2)

SOURCE FACSIMILE — Figure 4-8 — Velocity Profiles in Shock Layer as a Function of Low Density Reynolds Number (K^2). Complete original graph and caption; low-contrast original retained faithfully, with image-only labels.

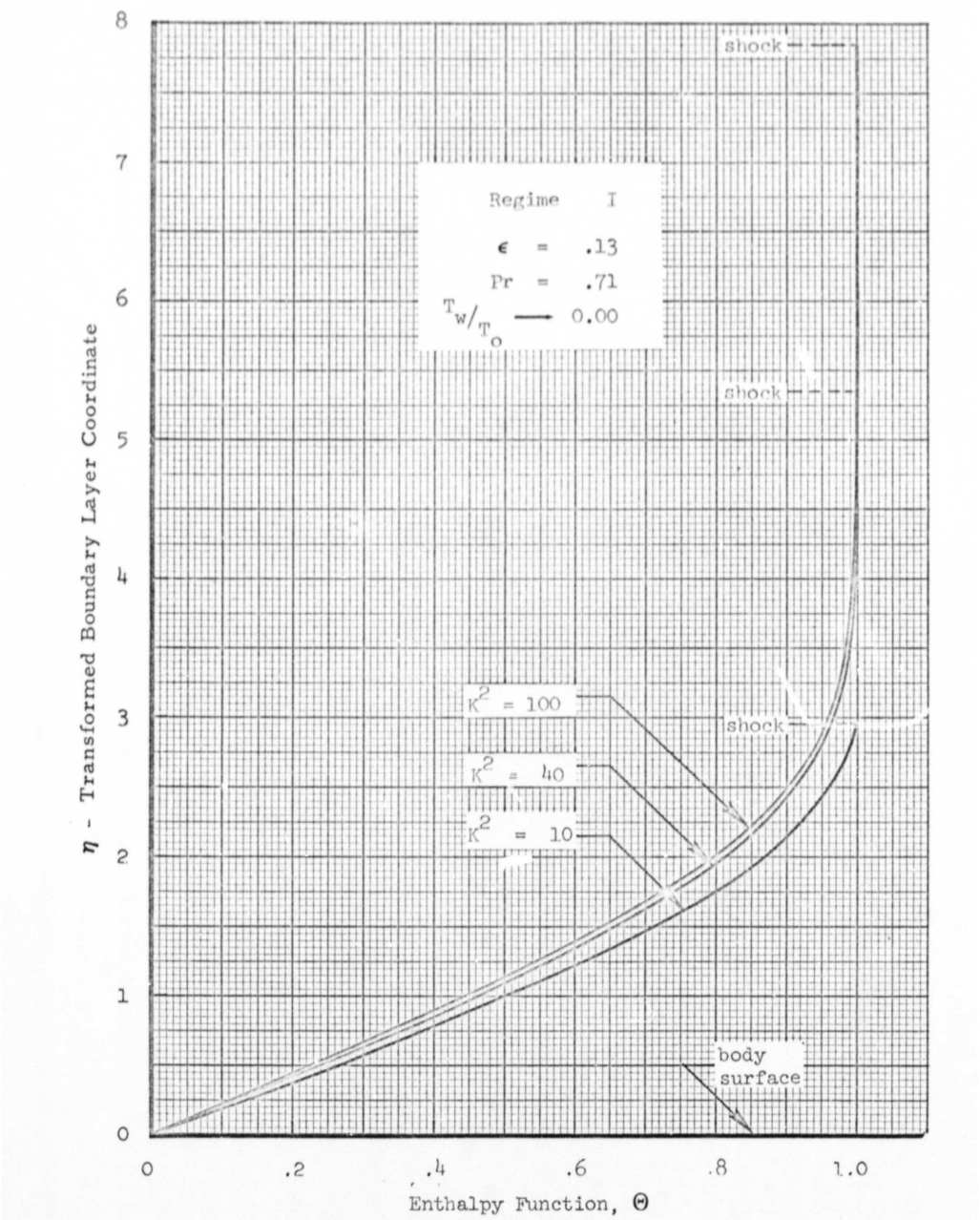


Figure 4-9 - Enthalpy Function Profiles in Shock Layer as a Function of Low Density Reynolds Number (K^2)

SOURCE FACSIMILE — Figure 4-9 — Enthalpy Function Profiles in Shock Layer as a Function of Low Density Reynolds Number (K^2). Complete original graph and caption; low-contrast original retained faithfully, with image-only labels.

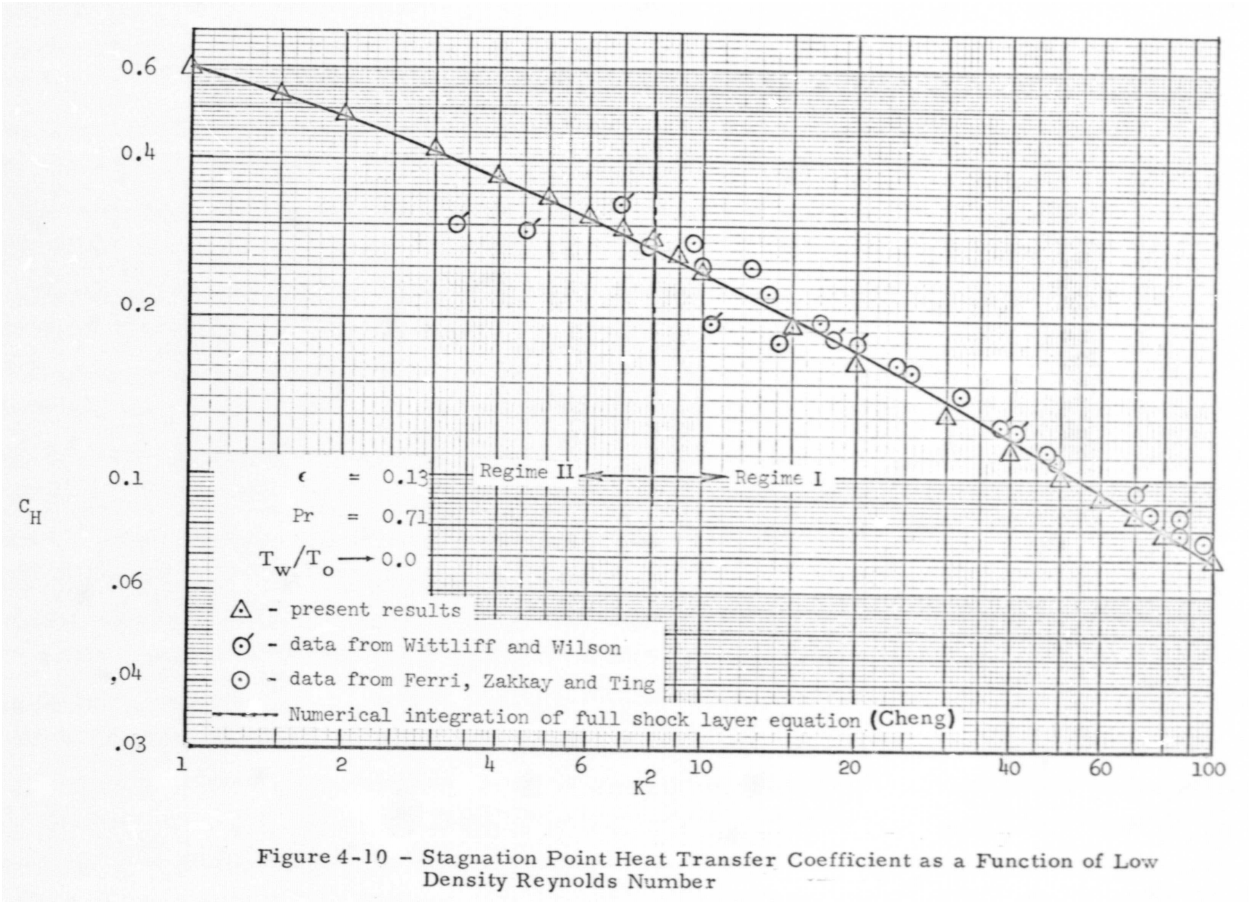


Figure 4-10 – Stagnation Point Heat Transfer Coefficient as a Function of Low Density Reynolds Number

SOURCE FACSIMILE — Figure 4-10 — Stagnation Point Heat Transfer Coefficient as a Function of Low Density Reynolds Number. Complete graph, legend and caption, rotated for reading; image-only labels.

seconds of Univac 1107 computing time per point as opposed to a lengthy numerical iteration procedure for the full shock layer equations. It can be seen that the present methods of obtaining low density stagnation region heat transfer rates are accurate and reliable. In addition, the objective of holding computation time to an absolute minimum was realized.

4.2.2 Low Density Flat Plate Boundary Layer Solution

To fulfill the requirement of the Streamline Divergence Technique for a flat plate boundary layer equation, it was decided to employ the solution originated by Maslen, Reference 10. Maslen's low density boundary layer solution predicts a correction term to the ordinary laminar boundary layer solution which accounts for the effects of a slip velocity and temperature jump at the surface.

The technique used to solve the laminar boundary layer equations including the low density effects is basically a parameter perturbation method, where the parameter involved is proportional to the Knudsen number. The laminar boundary layer equations are perturbed about their continuum value by expanding the flow variables in a geometric series in terms of ε_x,

$$\epsilon_x = \frac{M_e\sqrt{\gamma}}{\sqrt{Re_x}}$$

where

M_e = Mach number at edge of boundary layer

γ = ratio of specific heats

Re_x = Reynolds number based on edge conditions

SOURCE FACSIMILE — Original low-density expansion parameter and all its definitions. Image-only mathematical notation.

Hence, the series for each variable becomes,

$$u = u_0 + \varepsilon_x u_1 + \varepsilon_x^2 u_2 + \cdots$$

$$T = T_0 + \varepsilon_x T_1 + \varepsilon_x^2 T_2 + \cdots, \text{ etc.}$$

When these expansions are substituted into the conventional laminar boundary layer equations and the coefficients of the various powers of ε_x are equated to zero, a set of boundary layer equations results for each order of the expanded variable. Obviously, the set of equations governing the $(\,)_0$ order is simply the standard laminar boundary layer equations. These were solved by use of a similarity solution. The set of equations governing the $(\,)_1$ variables is very similar in nature to the $(\,)_0$ set, but the boundary conditions are significantly different due to the rarefied effects. After some manipulation, Maslen is able to solve this set for the $(\,)_1$ variables. The higher order solutions are considered to have a negligible influence on the overall solution. The combined solution, involving $(\,)_0$ and $(\,)_1$ variables, has a form such that $(\,)_1$ variables make a correction to the $(\,)_0$ order solution for non-negligible values of the parameter ε_x, or hence, the Knudsen number. In terms of the Nusselt number, the solution is

$$\frac{Nu_x}{\sqrt{Re_x}} = \left(\frac{Nu_x}{\sqrt{Re_x}}\right)_{\text{continuum}} + \epsilon_x \left(\frac{Nu_x}{\sqrt{Re_x}}\right)_1 \cdots$$

where $\left(\frac{Nu_x}{Re_x}\right)_1$ is given by an algebraic expression involving only continuum flow parameters. Hence, the full low density solution can be determined with knowledge of only the $(\,)_o$ order or continuum solution.

SOURCE FACSIMILE — Original Nusselt-number expansion and its complete following explanation, preserving the printed denominator forms. Image-only mathematical notation.

Employing the theory and assumptions used in the continuum laminar boundary layer part of the Streamline Divergence Technique, the following low density flat plate boundary layer expression was derived for heat transfer rate to the surface:

$$\dot{q}_w = \frac{0.332}{Pr^{2/3}} (H_{aw} - H_w) (\rho^* \mu^*)^{1/2} \left(\frac{u_e}{x_1}\right)^{1/2}$$

$$- \frac{0.13816}{J \cdot g} \sqrt{\frac{\gamma T_w}{T^*}} \frac{\mu_w^2}{\mu^*} \frac{M_e u_e^2}{x_1}$$

where

SOURCE FACSIMILE — Original unnumbered low-density flat-plate heat-transfer expression and “where” lead-in. Image-only mathematical notation.

ρ = density

μ = viscosity

H = total enthalpy

u = velocity

T = temperature

M = Mach number

γ = ratio of specific heats

x_1 = integrated characteristic length

Pr = Prandtl number

$(\ )_e$ = edge of boundary layer conditions

$(\ )_w$ = evaluated at surface temperature

$(\ )^*$ = evaluated at reference temperature

$(\ )_{aw}$ = evaluated at adiabatic wall conditions

SOURCE FACSIMILE — Complete original parameter and subscript definitions for the preceding heat-transfer expression. Image-only technical notation.

$$J = \text{mechanical equivalent of heat, } \frac{778 \text{ ft-lb}}{\text{Btu}}$$

$$g = 32.2 \ \frac{\text{ft-lbm}}{\text{lbf-sec}^2}$$

SOURCE FACSIMILE — Continuation of the preceding heat-transfer definitions: mechanical equivalent of heat and gravitational acceleration, with original units and numerical constants. Image-only notation.

This equation was incorporated into the Streamline Divergence Technique for use in the general impingement program.

4.3 Free Molecular Heating

When the density of a gas decreases beyond a point where the mean free path of the molecules is 10 times greater than a characteristic length of the body immersed in the gas, the mechanism of momentum and energy transfer to the body is governed by free molecular theory. Lockheed/Huntsville has developed a new method for predicting free molecular heat transfer which is capable of handling heating of bodies in high temperature gases of arbitrary composition. The conventional free molecular heating programs are based upon the assumption that a simple relationship exists between the ratio of specific heats and the number of degrees of freedom of the molecules, that is to say

$$\gamma = 1 + 2/j \quad (4.21)$$

γ = ratio of specific heats
j = number of degrees of freedom.

This is accurate only for, at most, diatomic molecules at relatively low temperatures. However, when the problem changes such that the gaseous medium is composed of a high temperature rocket nozzle exhaust, the conventional theory no longer applies. Lockheed/Huntsville's new theory makes use of real gas thermochemical data which are generated for any type of propellant used in a rocket nozzle. These data, in conjunction with Lockheed/Huntsville's method-of-characteristics solution of the exhaust plume, gives exact velocity and energy predictions for the given gas and plume configuration.

The free molecular heat transfer computer program treats both front and backside heating to a flat plate at any angle of attack to the freestream flow. Since the mechanism of energy transfer to an element of surface area on a body is not influenced by any preceding or adjacent phenomena, these flat plate heating rates can be treated as heating of a small differential area on a larger body. The total heating rate to the body is easily obtained by integrating these local heating rates over the surface of the body. If the particular surface element is shaded, then backside local heating rates apply and conversely, if the particular surface element “sees” the freestream flow, then frontside heating rates are used. A complete treatment of the free molecular heating development is contained in Appendix B.

5 Radiative Heating

A relatively minor amount of effect was expended during this study to obtain, check out and learn to utilize existing programs for the prediction of radiant heating from both gaseous plumes and those with solid particles entrained.

For gaseous radiation, the MSFC/Hayes Plume Radiation Program was obtained and checked out with a sample problem. Plume radiation from the LEM descent engine was calculated and compared with previous results obtained by TRW Systems in Houston, Texas. The two analyses agreed well. This program is documented in Reference 23.

A series of computer programs which calculate radiation from a particle-laden rocket exhaust plume was developed by Aeronutronics under contract to NASA/MSFC (Reference 24). The programs (Programs A, B and C) are used sequentially to solve a given problem.

Program A computes the centerline and limiting streamline trajectories for a given particle size. The calculation is started in the rocket combustion chamber where the particle velocity is assumed to be equal to the gas velocity, and proceeds through the nozzle and into the plume. The gas flow field in the nozzle and plume is calculated with the assumption that the effects of the particles can be uncoupled. A one-dimensional transonic solution is included in Program A as a subroutine, while the supersonic flow field can be calculated in advance by Lockheed's Method-of-Characteristics Computer Program, and the necessary flow field properties placed on a tape which is read by Program A. Program A punches out the particle velocity and temperature along the centerline and limiting streamlines for each particle size input. This punched output is used as input to Program B.

Program B computes the average radiative cross-sections, effective black body function, temperature, particle number density and particle thermal and kinetic energy fluxes at specified locations within the two-phase plume. Input required includes the punched output from Program A plus Mie scattering theory tables for particle sizes comparable to the wavelength of the radiation. The scattering tables presently incorporated in Program B are particularized for aluminum oxide particles of radii between 0.1 and 20.0 microns. The particles size distribution is also input to Program B in the form of a skew-symmetric formula. Output includes punched cards with the average scattering and absorption cross-section and back-scatter ratio, the effective spectral black body function, and the total particle number density throughout the plume. These cards are used as input to Program C.

Program C computes the radiation from the particle cloud to a target with arbitrary location along a specified line-of-sight. Multiple lines-of-sight may be selected to give the total hemispherical radiation to a given target. The radiative properties of the particle cloud are obtained from the punched output from Program B. The program prints out the radiative intensity to the target for each of a series of specified wavelengths.

Programs A, B and C have been fully checked out for a sample case based on the exhaust plume of an S-II ullage motor at an altitude of 120,000 feet. These programs and their available documentation (Reference 24) are supplied as a part of this study.

6 Methods and Procedures for Obtaining Test Data

There exists a definite need for plume impingement testing under orbital conditions. Vacuum chamber limitations of maximum expansion and testing duration leave much to be desired. Therefore, flight tests would be of great value in the determination of pressures and heating rates due to plume impingement in a vacuum. Different methods could be used to obtain orbital flight test data. Permanent sensors could be used; or temporary sensors, under the control of resident astronauts would permit greater flexibility of design and data collection.

Instrumentation of surfaces and regions adjacent to existing Apollo program motors would yield considerable data. Control motors located on the Command and Service Module could be used as well as the APS motors on the S-IVB Orbital Workshop. Ideally, the sensors should be located by hand during extravehicular activity of the astronauts; they could be located at off-surface positions and at several different locations in the plume if they are positioned by an astronaut. This would also avoid protection problems during ascent. Figure 6-1 depicts a typical AAP configuration showing locations of the various motors which could be used for plume impingement testing.

ARCHIVAL SOURCE NOTICE — “REPRODUCIBILITY OF THE ORIGINAL PAGE IS POOR.” The notice is present on this source page; labels are retained rather than reconstructed.

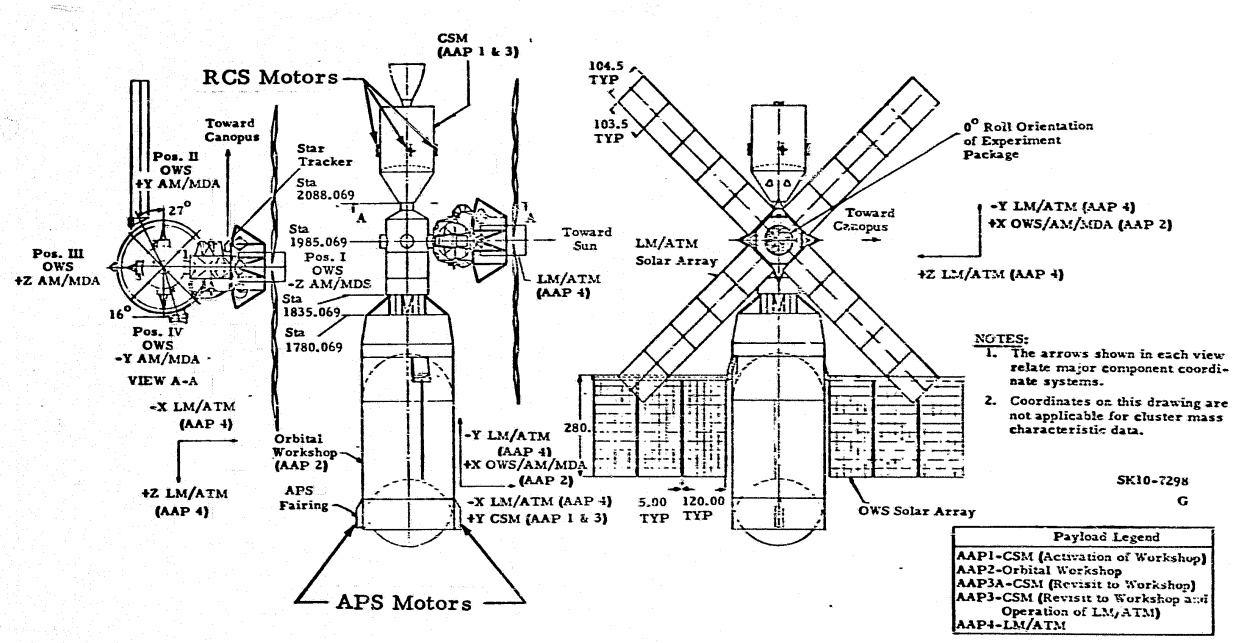


Figure 6-1 – Typical AAP Configuration Showing Possible Location for Impingement Instrumentation

SOURCE FACSIMILE — Figure 6-1 — Typical AAP Configuration Showing Possible Location for Impingement Instrumentation. Complete original configuration drawing, notes, abbreviation key and caption, rotated for reading. Image-only labels; zoom for fine detail.

7 Data Correlation

In order to confirm the analytical model developed in this study, some test and flight data correlations were attempted. The test data were obtained from R-P&VE-PT and consisted of pressures and heating rates on the surface of a model J-2 engine subjected to impingement from a simulated O_2/H_2 burner. Figure 7-1 presents a correlation of the calculated and measured impact pressures. As can be seen good agreement was obtained. Figures 7-2, 7-3 and 7-4 show the comparison of computed and measured heating rates. Figure 7-5 depicts the geometrical relationship between the 72 lb ullage motor exhaust plume and the J-2 engine on Saturn V flight 501. A comparison of the measured and analytical heating rates is presented in Figure 7-6 for this flight.

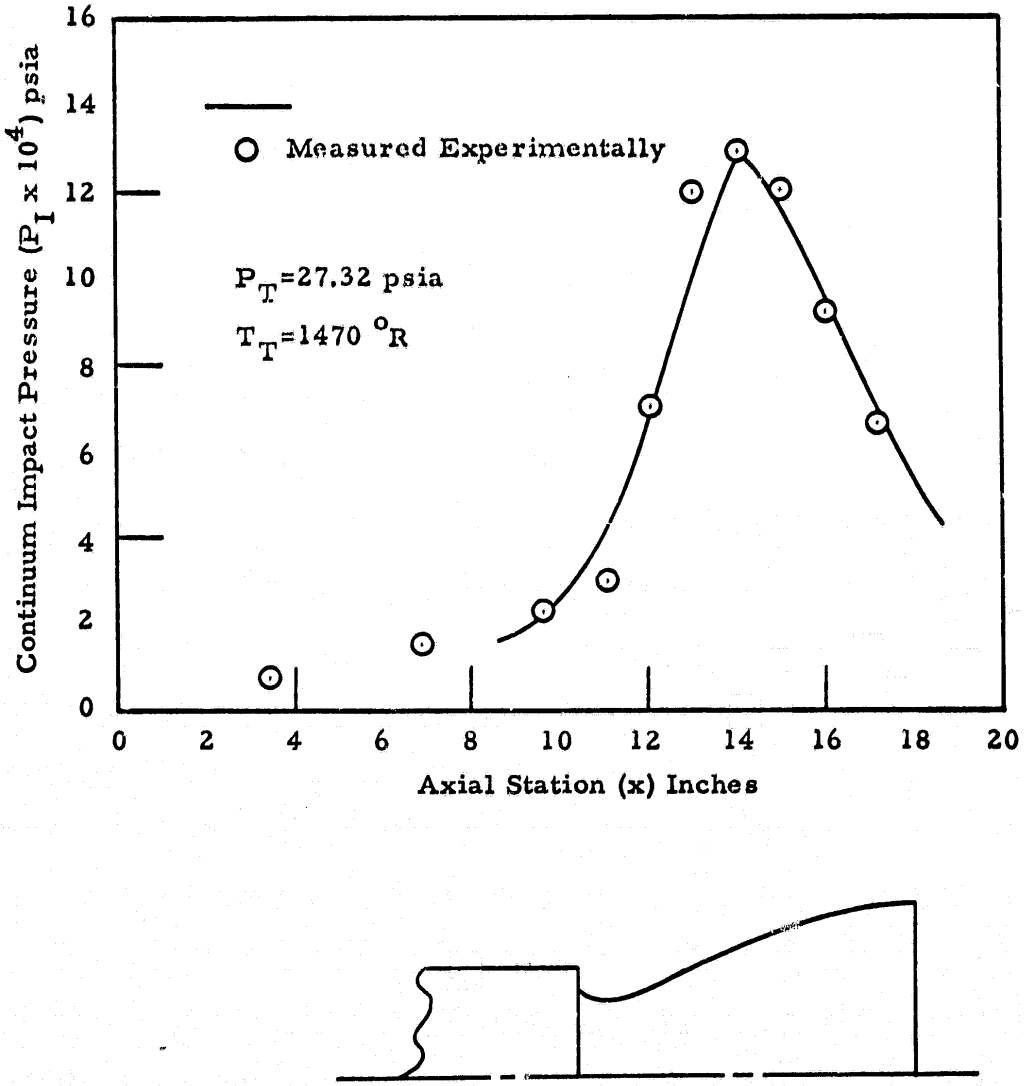


Figure 7-1 – Correlation of Surface Impact Pressure on Stagnation Line of Model J-2 Engine from O_2/H_2 Burner Impingement

SOURCE FACSIMILE — Figure 7-1 — Correlation of Surface Impact Pressure on Stagnation Line of Model J-2 Engine from O_2/H_2 Burner Impingement. Complete original graph, model profile and caption; image-only labels.

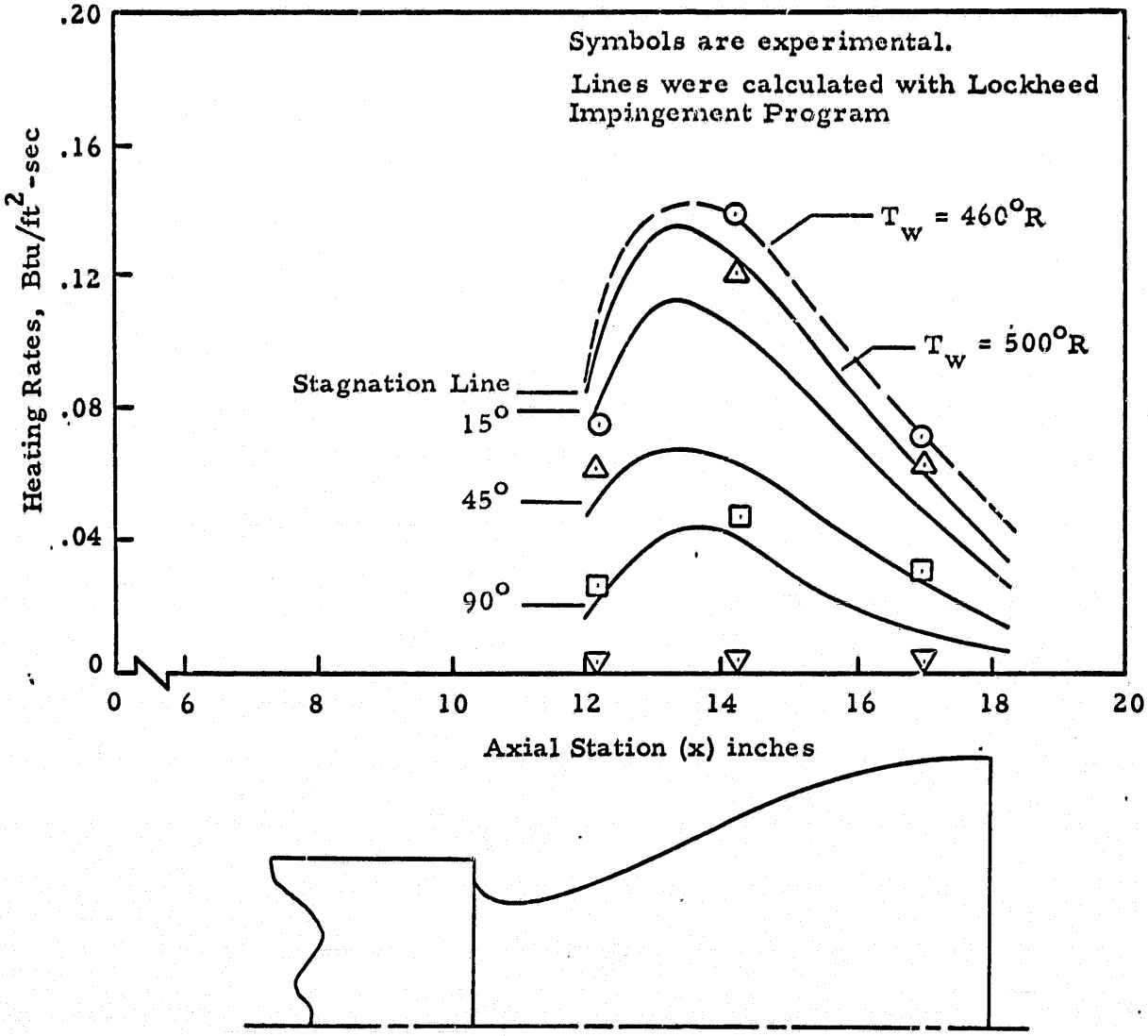


Figure 7-2 – Correlation of Heating Rates on Surface of Model J-2 Engine from O_2/H_2 Burner Impingement

SOURCE FACSIMILE — Figure 7-2 — Correlation of Heating Rates on Surface of Model J-2 Engine from O_2/H_2 Burner Impingement. Complete graph, model profile and caption; image-only labels.

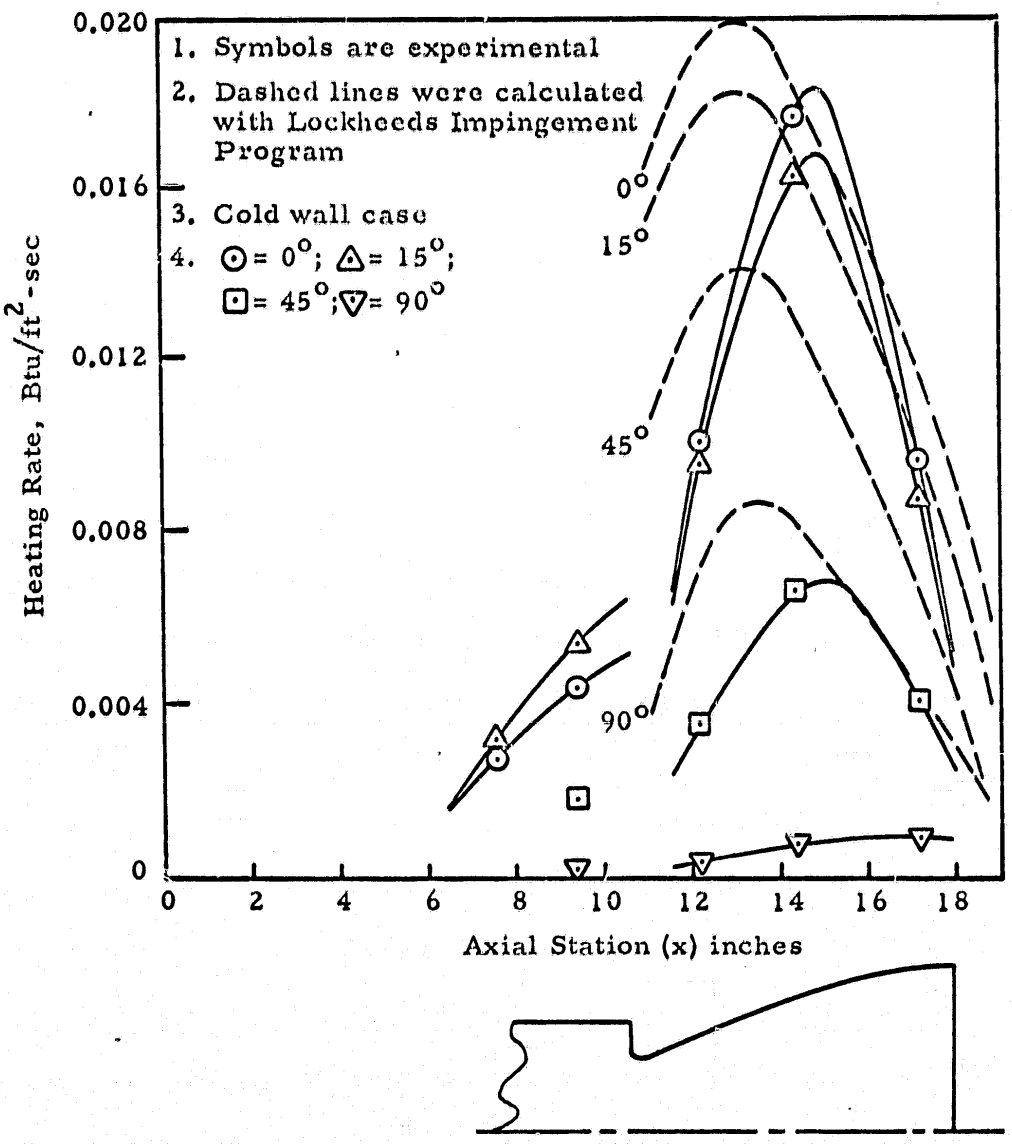


Figure 7-3 - Correlation of Heating Rates on Surface of Model J-2 Engine from O_2/H_2 Burner Impingement

SOURCE FACSIMILE — Figure 7-3 — Correlation of Heating Rates on Surface of Model J-2 Engine from O_2/H_2 Burner Impingement. Complete graph, model profile and caption; image-only labels.

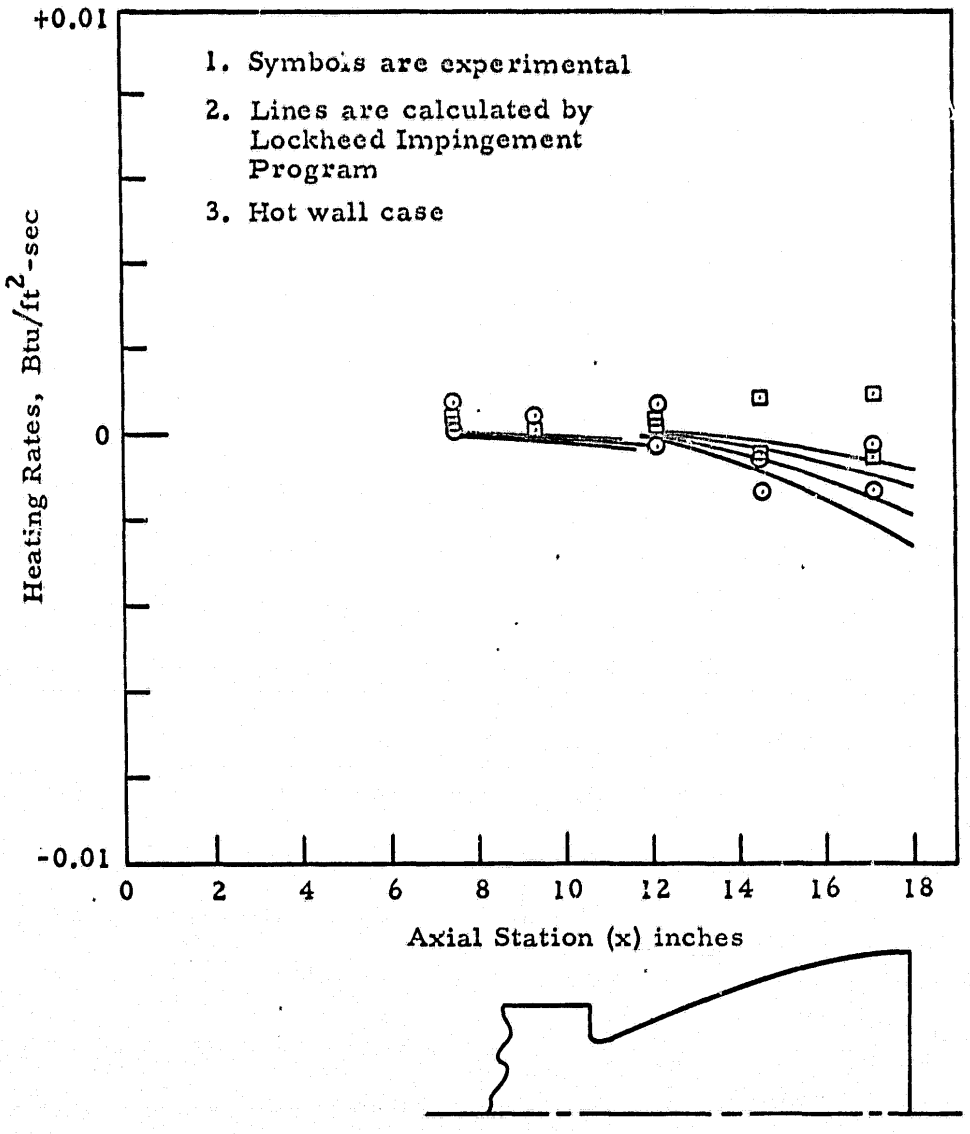


Figure 7-4 – Correlation of Heating Rates on Surface of Model J-2 Engine from O_2/H_2 Burner Impingement

SOURCE FACSIMILE — Figure 7-4 — Correlation of Heating Rates on Surface of Model J-2 Engine from O_2/H_2 Burner Impingement. Complete graph, model profile and caption; image-only labels.

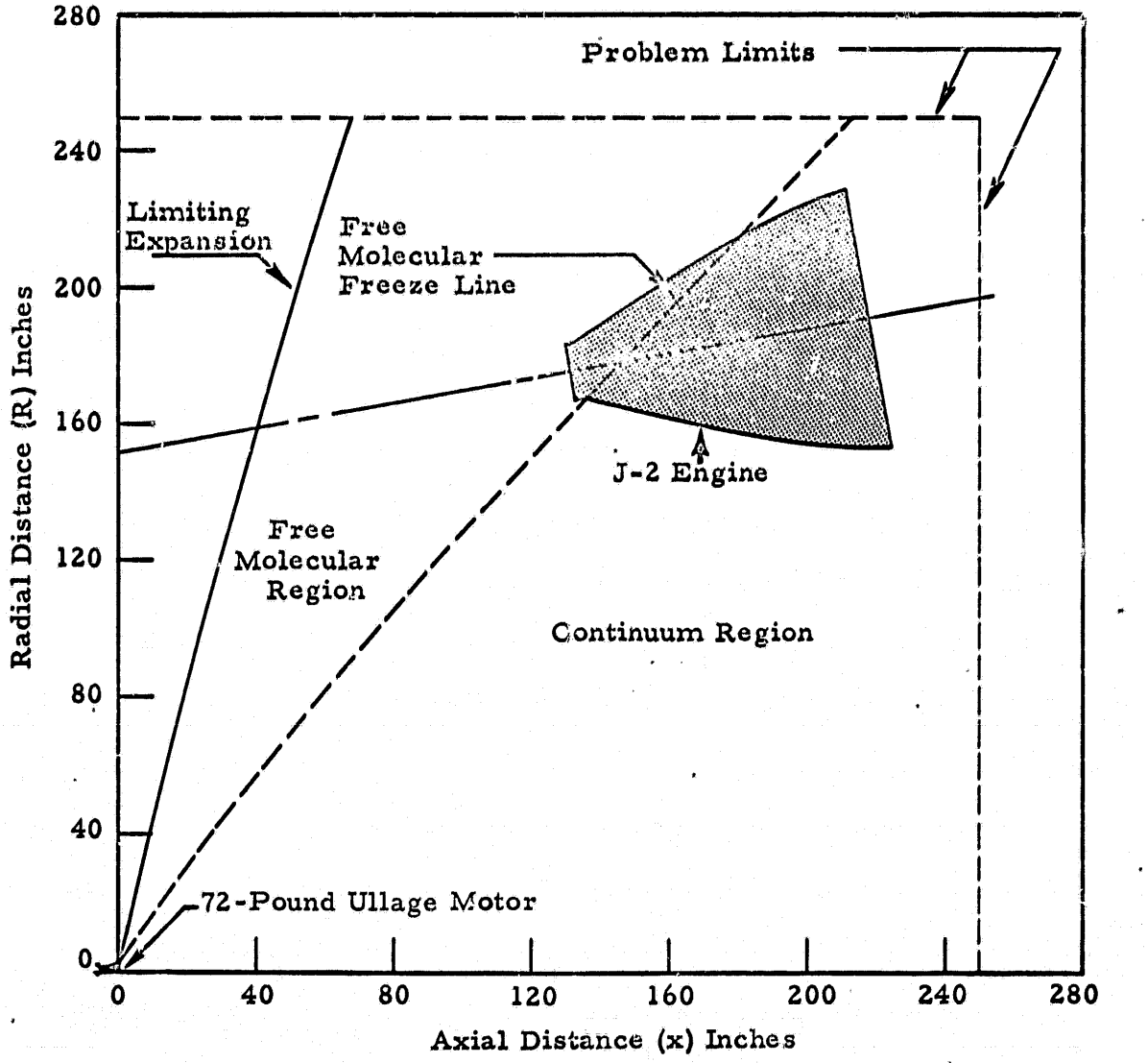


Figure 7-5 — Orientation of Full Scale J-2 Engine with Respect to the 72-Pound Ullage Motor Showing the Region of Plume Impingement

SOURCE FACSIMILE — Figure 7-5 — Orientation of Full Scale J-2 Engine with Respect to the 72-Pound Ullage Motor Showing the Region of Plume Impingement. Complete graph and caption; image-only labels.

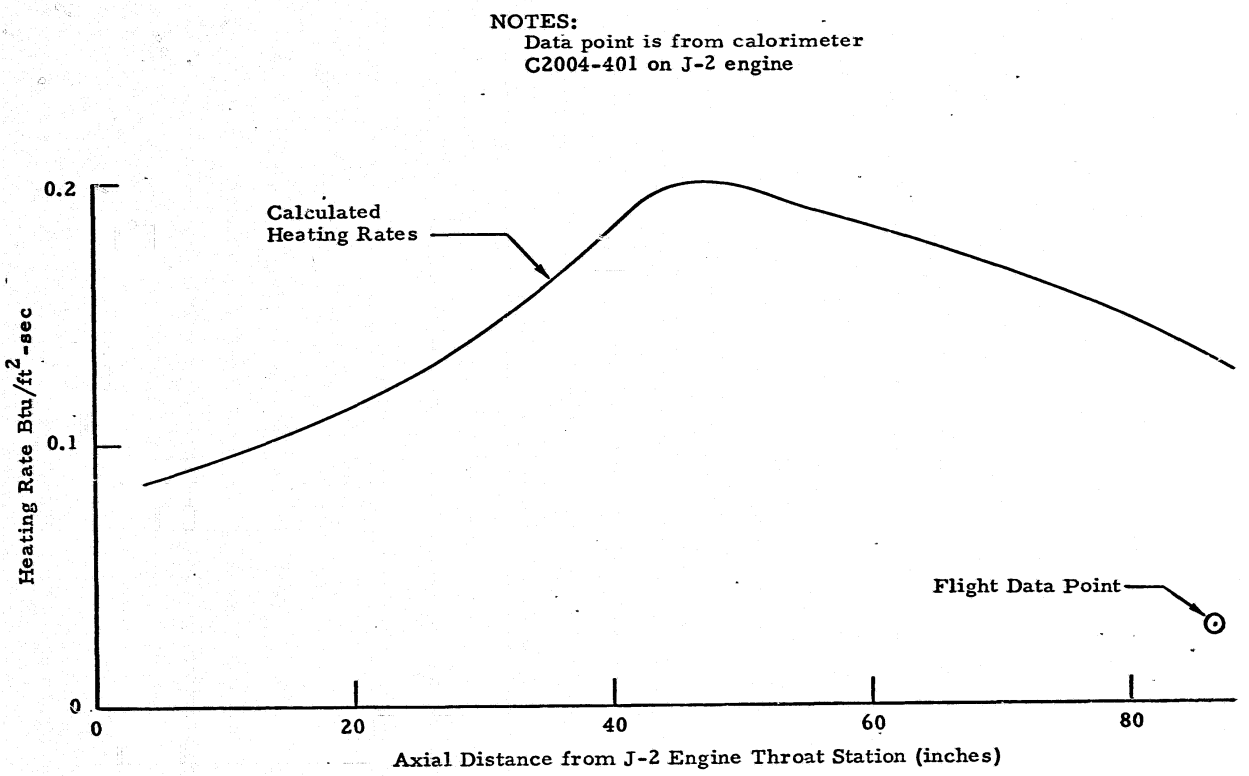


Figure 7-6 – Correlation of Analytical and Measured Data from Saturn Flight 501

SOURCE FACSIMILE — Figure 7-6 — Correlation of Analytical and Measured Data from Saturn Flight 501. Complete graph, calorimeter note and caption, rotated for reading; image-only labels.

8 Conclusions

This study has resulted in the development and/or improvement of sophisticated engineering methods and computer programs for the prediction of heating rates and pressures on objects subjected to rocket plume impingement.

The use of this group of methods and programs will permit a designer to evaluate the effects of the potentially hostile rocket exhaust plume environment on an arbitrary immersed body. Each method and program has been discussed and the limitations and assumptions of each were pointed out. These programs represent the current state-of-the-art in methods of predicting plume impingement effects.

The basic product from this study is a set of experimentally verified computer programs for the prediction of heating rates and pressures in jet exhaust impingement regions. The scope of this study covered continuum, transitional and free molecular flow regimes. Although much work was accomplished during this study toward the development of techniques and computer programs, there are areas where the models developed could be improved.

Part of the effort during this contract was expended to try to improve the capability for noncontinuum plume predictions. During this part of the study, an extensive literature search revealed a large amount of information concerning the aerodynamics of free jets expanding into a vacuum. A method was selected from the literature and implemented into the flow field program so that one could calculate exhaust plumes from their continuum state through the free molecular region. During implementation and checkout of this program, it was determined that the method selected was somewhat restrictive

in nature due to the numerical problems associated with the method of characteristics at high Mach numbers.

To obtain the complete exhaust plume flow field, it is necessary to change from a continuum analysis to a free molecular flow model. This “transition” region is a function of several flow variables and gradients which are used to determine when transition occurs. The basic problem encountered is that the continuum flow Mach number gets too large, such that the method of characteristics theory “breaks down,” before the “transition” region is attained. Thus, the calculations must be terminated. This problem is a function of the type of gas, its properties and the chamber temperature and pressure of the nozzle under analysis. More work should be done in this area in order to remove the present model limitations.

In light of the preceding discussion, additional work should be done to improve the calculational capability in the regions where characteristic theory no longer applies, but the flow is not yet free molecular. Studies have shown that the flow becomes “source like” at large distances from the nozzle when high Mach numbers exist. Making use of this fact, the calculations could be continued from the point where the characteristic theory degenerated by using a continuum source flow model. This model would permit the calculations to be continued until translational freezing occurs, indicating the onset of free molecular flow.

The continuum heat transfer methods provided under this study are considered adequate for the types of calculations desired. Emphasis was placed on generality and ease of operation by way of computer tape communication between the flow field and the general impingement analysis program. The heating rate models could be improved somewhat by adopting a more exact boundary layer analysis along the streamlines in the Streamline Divergence Technique. This would sacrifice the automation and generality now provided by requiring more handwork and more computer runs to map out the heating rates on a given configuration. Instead of trying to improve the heat transfer

model by making it more sophisticated, at the sacrifice of user convenience and generality, it is suggested that a heating rate correlation study be carried out in order to further verify the model. These correlations could be used as guidelines indicating when certain parameters in the heating rate equations should be modified in order to match test data better. In addition, the program could be used to analyze and correlate flight data and make predictions for future flights. There also exist many problem areas on existing and proposed vehicles which should and can be analyzed with the tools provided under this contract.

The noncontinuum heat transfer methods could be improved in two general areas. First, the assumption of a constant gamma should be removed from the shock layer calculation. This could be done by deriving a model based on a Lighthill-type dissociating gas which would realistically approximate the effects of dissociation in the shock layer. The basic blunt body low density equations would remain unaltered, but the new chemistry model would replace the ideal gas assumption. In the current model, the viscosity must vary linearly with temperature in the shock layer. A more realistic viscosity model could easily be incorporated into the overall solution if the dissociated chemistry model were also added.

In conclusion, the following specific items merit further investigation in order to improve the calculational capability in the area of plume impingement.

- Provide a model for the flow field description where the characteristic theory no longer applies but the flow has not become free molecular
- Make studies of such heat transfer and flow field data as can be obtained, in order to improve heating rate data correlations
- Analyze and correlate flight data and make predictions for future flights
- Improve noncontinuum heat transfer method by removing some of the limitations now imposed.

References

1. Zeleznik, F. J. and S. Gordon, “A General IBM 704 or 7090 Computer Program for Computation of Chemical Equilibrium Compositions, Rocket Performance and Chapman-Jouget Detonation,” NASA TN D 454, Lewis Research Center, Cleveland, Ohio, October 1962.

2. Prozan, R. J., “Development of a Method-of-Characteristics Solution for Supersonic Flow of an Ideal, Frozen or Equilibrium Reacting Gas Mixture,” Lockheed Missiles & Space Company, Huntsville, Ala., HREC-0082-8, LMSC/HREC A782535, April 1966.

3. Robertson, S. J., “A Method for Calculating Flow Field Properties in Low Density Plumes,” Lockheed Missiles & Space Company, Huntsville, Ala., TM 54/20-154, LMSC/HREC A784697, October 1967.

4. Butler, H. W., “Description and User’s Manual for a Program to Calculate the Loads and Heating Experienced by a Body in a Supersonic Flow Field,” Lockheed Missiles & Space Company, Huntsville, Ala., TM 54/20-184, LMSC/HREC A791251, March 1968.

5. Sentman, Lee H., “Free Molecule Flow Theory and Its Application to the Determination of Aerodynamic Forces,” Lockheed Missiles & Space Company, Sunnyvale, Calif., LMSC-F48514, 1 October 1961.

6. Patterson, G. N., *Molecular Flow of Gases*, Wiley, New York, 1956.

7. Vaglio-Laurin, Roberto, “Turbulent Heat Transfer on Blunt-Nosed Bodies in Two-Dimensional and General Three-Dimensional Hypersonic Flow,” *J. Aerospace Sci.*, January 1960.

8. Vaglio-Laurin, Roberto, “Laminar Heat Transfer on Blunt Nosed Bodies in Three-Dimensional Hypersonic Flow,” WADC Technical Note 58-147, May 1958.

9. Lockheed Missiles & Space Division, “Study of Heat Shielding Requirements for Manned Mars Landing and Return Missions,” Final Report, Contract NAS2-1798, Ames Research Center, Moffett Field, Calif., December 1964.

10. Maslen, S. H., “Second Approximation to Laminar Compressible Boundary Layer on a Flat Plate in Slip Flow,” NACA TN 2818, 1952.

11. Marvin, Joseph G. and George S. Deiwert, “Convective Heat Transfer in Planetary Gases,” Ames Research Center, Moffett Field, Calif., NASA TR R-224, July 1965.

12. Lees, L., “Laminar Heat Transfer over Blunt Nosed Bodies at Hypersonic Speeds,” *J. Propulsion*, No. 26, Vol. 4, (1956), p. 259.

13. Gibson, J. G. and D. V. Hale, “A Technique for Predicting Rocket Exhaust Impingement Pressure on a Flat Plate,” LMSC/HREC A782534, Lockheed Missiles & Space Company, Huntsville, Ala., April 1966.

14. Hoenig, R. J., “LMSC/HREC Boundary Layer Computer Program – User’s Manual,” LMSC/HREC A782404, Lockheed Missiles & Space Company, Huntsville, Ala., August 1966.

15. Hirschfelder, J. O., C. F. Curtiss and R. B. Bird, *Molecular Theory of Gases and Liquids*, New York, John Wiley & Sons, Inc., 1964.

16. Svehla, Roger A., “Estimated Viscosities and Thermal Conductivities of Gases at High Temperatures,” NASA TR R-132, 1962.

17. Araue, R. J., "A Method for Estimating the Viscosity and Thermal Conductivity of High Temperature Gas Mixtures," Chrysler Corp., Advanced Engineering Branch, TB-AE-64-56.

SOURCE FACSIMILE — Reference 17, retained exactly from the source because the author surname is uncertain in the scan. Image-only text.

18. Butler, J. M. and R. S. Brokaw, “Thermal Conductivity of Gas Mixtures in Chemical Equilibrium,” *J. Chem. Phys.*, Vol. 26, No. 6, June 1957, pp. 1936-1943.

19. Sherwood, T. K. and R. C. Reid, *Properties of Gases and Liquids*, McGraw-Hill, New York, 1958.

20. Cheng, H. K., “The Blunt-Body Problem in Hypersonic Flow at Low Reynolds Number,” CAL Report AF-1285-A-10, June 1963.

21. Cheng, H. K., “Hypersonic Shock-Layer Theory of the Stagnation Region at Low Reynolds Number,” Proceedings of the 1961 Heat Transfer and Fluid Mechanics Institute, June 1961, pp. 161-175.

22. Probstein, R. F., “Shock-Wave and Flow Field Development in Hypersonic Reentry,” *ARS J.*, Vol. 31, No. 2, February 1961, p. 185.

23. Huffaker, Robert M. and Marcus J. Dash, “A General Program for the Calculation of Radiation from an Inhomogeneous, Nonisobaric, Nonisothermal Rocket Exhaust Plume,” NASA TM X-53622, Marshall Space Flight Center, Huntsville, Alabama, 19 June 1967.

24. Laderman, A. J., et al., “Study of Thermal Radiation, Particle Impingement Heating and Flow Field Analysis of Solid Propellant Rocket Exhausts,” Publication No. U-4045, Aeronutronic Division of Philco Ford, Newport Beach, Calif., 19 April 1967.

Appendix A — Low Density Stagnation Region Blunt Body Solution

Original appendix divider. The appendix text begins on the following source page.

Appendix A — Low Density Stagnation Region Blunt Body Solution

For the purpose of the present analysis, the flow field around the body will be divided into an outer region, called the shock-transition zone, and an inner region, called the shock layer (see Figure A-1). For convenience, the surface separating the two regions will be referred to as the shock interface. The compression ratio, ρ/ρ_∞, across the shock transition zone is assumed to be large, and therefore both regions can be assumed to be thin in comparison to the local nose radius; these two assumptions are consistent with a hypersonic low density approach flow. The solution derived here treats the steady uniform flow of an ideal gas over an axisymmetric smooth blunt body for the case of a highly cooled surface, i.e., the ratio of wall temperature to freestream stagnation temperature is small. It is also postulated that a linear viscosity-temperature relation adequately describes the flow medium.

Referring to Figure A-1, let x denote the distance along the body surface and y the distance along the outward normal from the surface. Since both the shock layer and the shock-transition zone are thin, it is reasonable to assume that $\partial/\partial x << \partial/\partial y$. The Navier-Stokes equations governing the compressible, viscous, heat conducting flow can then be reduced to the following form:

(a) $$\frac{\partial}{\partial x}(\rho u Z) + \frac{\partial}{\partial y}(\rho v Z) = 0$$ (conservation of mass)

(b) $$\frac{\partial p}{\partial x} - \rho K_c u v + \rho \left(u \frac{\partial}{\partial x} + v \frac{\partial}{\partial y}\right) u = \frac{\partial}{\partial y}\left(\mu \frac{\partial u}{\partial y}\right)$$ (conservation of tangential component of momentum)

(c) $$\frac{\partial p}{\partial y} + \rho K_c u^2 + \rho \left(u \frac{\partial}{\partial x} + v \frac{\partial}{\partial y}\right) v = \frac{4}{3} \frac{\partial}{\partial y}\left(\mu \frac{\partial v}{\partial y}\right)$$ (conservation of normal component of momentum)

SOURCE FACSIMILE — Equation (1), parts (a)–(c), with all original conservation labels. Part (d) continues on original p. A-3, following Figure A-1. Image-only mathematical notation.

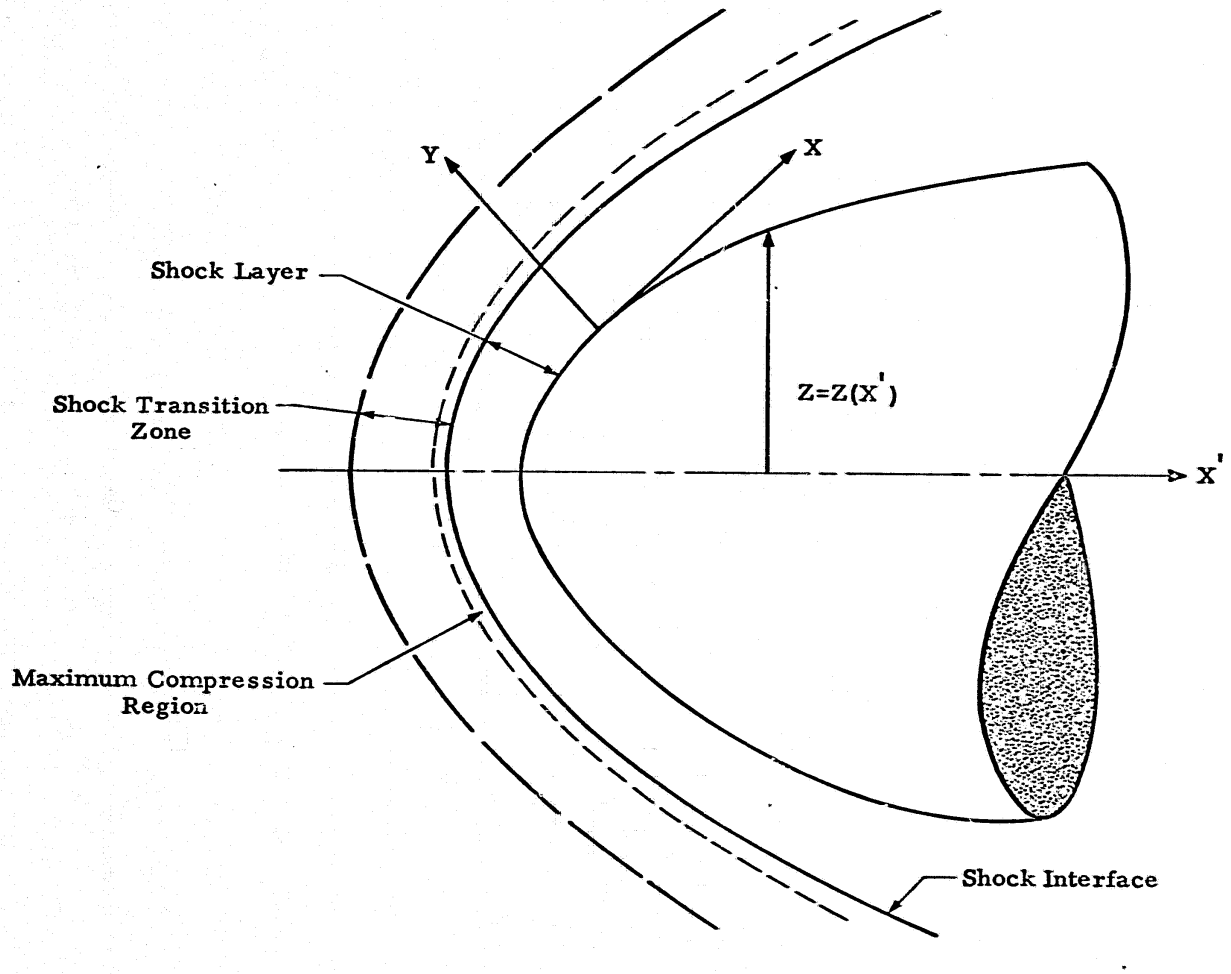


Figure A-1 – Description of Blunt Body Problem (Not to Scale)

SOURCE FACSIMILE — Figure A-1 — Description of Blunt Body Problem (Not to Scale). Complete original diagram and caption, rotated for reading; image-only labels.

$$\text{(d)} \qquad \rho\left(u\frac{\partial}{\partial x}+v\frac{\partial}{\partial y}\right)\left(h+\frac{u^2+v^2}{2}\right)=\frac{\partial}{\partial y}\left\{\mu\frac{\partial}{\partial y}\left[\frac{h}{Pr}+\frac{u^2}{2}+\frac{2}{3}v^2\right]\right\} \quad \text{(conservation of energy)} \qquad (1)$$

SOURCE FACSIMILE — Equation (1), part (d), conservation of energy and original equation number. Image-only mathematical notation.

These general equations are the basic conservation laws and are applied to both the shock-transition zone and the shock layer.

Analysis of the Shock-Transition Zone

Although the shock-transition zone contains all of the effects of the shock wave, it is hypothesized that a major portion of the compression is confined to a narrow region of the shock transition zone adjacent to the shock interface. Excluding this narrow region, it is then reasonable that,

$$\frac{v}{u} \geq O(1) \qquad \text{and} \qquad \frac{\rho}{\rho_\infty} \cong O(1)$$

SOURCE FACSIMILE — Original order-of-magnitude inequalities. Image-only mathematical notation.

Applying Equation (1) to the shock transition zone, where now the surface y=0 coincides with the shock interface, reduces to

$$\text{(a)} \qquad \frac{\partial}{\partial y}(\rho v) = 0$$

$$\text{(b)} \qquad \rho v \frac{\partial u}{\partial y} = \frac{\partial}{\partial y}\left(\mu \frac{\partial u}{\partial y}\right)$$

$$\text{(c)} \qquad \frac{\partial p}{\partial y} + \rho v \frac{\partial v}{\partial y} = \frac{4}{3} \frac{\partial}{\partial y}\left(\mu \frac{\partial v}{\partial y}\right)$$

$$\text{(d)} \qquad \rho v \frac{\partial}{\partial y}\left(h + \frac{u^2 + v^2}{2}\right) = \frac{\partial}{\partial y}\left\{ \mu \frac{\partial}{\partial y}\left[\frac{h}{Pr} + \frac{u^2}{2} + \frac{2}{3} v^2\right]\right\} \qquad (2)$$

SOURCE FACSIMILE — Equation (2), parts (a)–(d). Image-only mathematical notation.

These equations can be integrated once with respect to y, and the constant of integration can be evaluated at the shock interface or, in other words, the

downstream side of the narrow compression region. Since the component of velocity, v, at the shock interface is very much smaller than the v component of the freestream flow, terms of order v at the shock interface are neglected. Hence, the integrated form of Equation (2) becomes

$$\text{(a)} \qquad \rho_2 v_2 = \rho_1 v_1$$

$$\text{(b)} \qquad \rho_1 v_1 (u_2 - u_1) = \left(\mu \frac{\partial u}{\partial y}\right)_2$$

$$\text{(c)} \qquad p_2 = \rho_1 v_1^2$$

$$\text{(d)} \qquad \rho_1 v_1 (H_2 - H_1) = \left\{ \frac{\mu}{Pr} \frac{\partial}{\partial y} \left[H + (Pr - 1) \frac{u^2}{2} \right] \right\}_2 \qquad (3)$$

where

$(\ )_1$ = value in the freestream

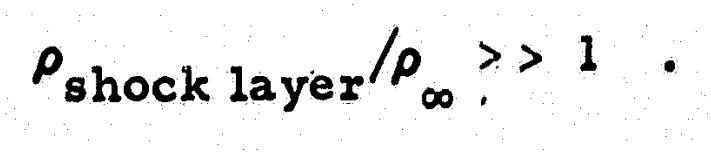
$(\ )_2$ = value at the shock interface

SOURCE FACSIMILE — Equation (3), parts (a)–(d), and complete original subscript definitions. Image-only mathematical notation.

Equations (3b) and (3d) show explicitly the importance of viscous effects across the shock wave because of the fact that tangential momentum and total enthalpy are no longer conserved. Equation (3), called the modified Rankine-Hugoniot relations, define certain values of the flow variables at the shock interface which become the boundary conditions for the governing equations in the shock layer.

Analysis of the Shock Layer

The general conservation laws of Equation (1) applied in the viscous shock layer can be simplified somewhat by observing two order of magnitude relationships. Because of the high compression ratio assumed in the shock-transition zone, the density in the shock layer must necessarily be



SOURCE FACSIMILE — Original shock-layer density inequality. Image-only mathematical notation.

Also, the normal component of velocity, v, in the shock layer will be very much less than the freestream value

$$v_{\text{shock layer}}/v_{\infty} << 1 \quad .$$

SOURCE FACSIMILE — Original shock-layer velocity inequality. Image-only mathematical notation.

Then, the conservation equations simplify to

$$\text{(a)} \qquad \frac{\partial}{\partial x}(\rho u Z) + \frac{\partial}{\partial y}(\rho v Z) = 0$$

$$\text{(b)} \qquad \frac{\partial p}{\partial x} + \rho\left(u\frac{\partial}{\partial x} + v\frac{\partial}{\partial y}\right)u = \frac{\partial}{\partial y}\left(\mu\frac{\partial u}{\partial y}\right)$$

$$\text{(c)} \qquad \frac{\partial p}{\partial y} + K_c \rho u^2 = 0$$

$$\text{(d)} \qquad \rho\left(u\frac{\partial}{\partial x} + v\frac{\partial}{\partial y}\right)H = \frac{\partial}{\partial y}\left\{\frac{\mu}{Pr}\frac{\partial}{\partial y}\left[H + (Pr - 1)\frac{u^2}{2}\right]\right\} \qquad (4)$$

SOURCE FACSIMILE — Equation (4), parts (a)–(d). Image-only mathematical notation.

In solving problems of this type, it is very advantageous to use von Mises coordinates (x,ψ) not only because it simplifies the coordinate system, but also because it eliminates the need for one equation – the conservation of mass. Thus, if the compressible stream function, ψ(x,y), is defined such that

$$\frac{\partial \psi}{\partial x} = -2\pi Z \rho v$$

$$\frac{\partial \psi}{\partial y} = 2\pi Z \rho u$$

SOURCE FACSIMILE — Original two stream-function derivative definitions. Image-only mathematical notation.

then Equation (4a) is identically satisfied. The remaining three equations readily transform to

$$\text{(b)} \qquad u \frac{\partial u}{\partial x} = 2\pi Z u \frac{\partial}{\partial \psi} \left(\mu \rho u \frac{\partial u}{\partial \psi} \right) - \frac{1}{\rho} \frac{\partial p}{\partial x}$$

SOURCE FACSIMILE — Equation (5), part (b), continuing on original p. A-6. Image-only mathematical notation.

$$\text{(c)} \qquad \frac{\partial p}{\partial \psi} = -\frac{K_c u}{2\pi Z}$$

$$\text{(d)} \qquad \frac{\partial H}{\partial x} = 2\pi Z \frac{\partial}{\partial \psi}\left\{\frac{\mu}{Pr}\rho u \frac{\partial}{\partial \psi}\left[H + (Pr - 1)\frac{u^2}{2}\right]\right\} \qquad (5)$$

SOURCE FACSIMILE — Equation (5), parts (c) and (d), and original equation number. Image-only mathematical notation.

These partial differential equations are still formidable to solve in their present form. Based on the lessons taught by experience and hindsight, another transformation is introduced for the purpose of setting up a perturbation problem.

Let

$$\lambda = 2\frac{x'}{a}$$

$$\zeta = \left[\frac{\psi}{\rho_\infty u_\infty \pi Z^2}\right]^{1/2}$$

where $(dx')^2 = (dZ)^2 - (dx)^2$ since the equations are constrained to lie on surfaces of constant ψ. The transformation to ζ in effect nondimensionalizes the stream function with respect to the body geometry. In addition to this transformation, the dependent variables are nondimensionalized as

$$\bar{u} \equiv \frac{u}{U_\infty \cos\beta}$$

$$\Theta = \frac{H - H_w}{H_\infty - H_w}$$

$$\bar{p} \equiv \frac{p}{\rho_\infty U_\infty^2 \sin^2\beta}$$

where β is the local shock angle.

SOURCE FACSIMILE — Complete original transformation definitions, associated explanatory text and nondimensional dependent variables through the local shock-angle definition. Image-only technical material.

The result of these substitutions is a new transformed set of three partial differential equations in terms of λ and ζ. However, these equations are valid throughout the complete shock layer around the body, and the

region of interest for this problem is only the stagnation region. The equations may be simplified greatly by setting up a perturbation problem about the λ=0 axis, or the stagnation streamline. All of the dependent flow variables are expanded in a geometric series in the chosen independent variable λ, e.g.

$$\bar{u} = \bar{u}_o + \lambda \bar{u}_1 + \lambda^2 \bar{u}_2 + \cdots$$

$$\bar{p} = \bar{p}_o + \lambda \bar{p}_1 + \lambda^2 \bar{p}_2 + \cdots$$

$$\Theta = \Theta_o + \lambda \Theta_1 + \lambda^2 \Theta_2 + \cdots$$

SOURCE FACSIMILE — Original three perturbation series, preserving overbars, subscripts and powers. Image-only mathematical notation.

These series expansions are substituted into the equations and coefficients of like powers of λ are equated. The equations in the set for the λ^0 order have become ordinary differential equations in ζ with only an implicit dependence on λ in the tangential pressure gradient term. These equations, which are valid in the stagnation region, are given by

$$\text{(a)} \qquad \bar{u}_o^2 - \zeta \bar{u}_o \bar{u}_o' = \frac{\bar{u}_o}{K^2 \zeta} \left[N \frac{\bar{u}_o \bar{u}_o'}{\zeta} \right]' + 2\epsilon (1 - \bar{p}_1) \left[\frac{H_w}{H_\infty} + \left(1 - \frac{H_w}{H_\infty}\right) \Theta_o \right]$$

$$\text{(b)} \qquad \frac{1}{Pr K^2} \left(N \frac{\bar{u}_o \Theta_o'}{\zeta} \right)' + \zeta^2 \Theta_o' = 0$$

$$\text{(c)} \qquad \bar{p}_o' = 0$$

$$\bar{p}_1' = \bar{u}_o \zeta \qquad (6)$$

SOURCE FACSIMILE — Equation (6), parts (a)–(c), including both pressure relations. Image-only mathematical notation.

where

$$(\quad)' = \text{differentiation with respect to } \zeta$$

$$K^2 = \text{low density Reynolds number}$$

$$= \epsilon \frac{\rho_\infty U_\infty a}{\mu_o} \left(\frac{\mu_o T^*}{\mu^* T_o} \right)$$

$$\epsilon = \frac{\gamma - 1}{2\gamma}$$

SOURCE FACSIMILE — Complete original definitions following Equation (6), including differentiation variable, K² and ε. Image-only mathematical notation.

These are the equations to be solved for a stagnation region solution.

Boundary Conditions

Because of the transformations used to obtain Equation (6), the boundary conditions at the body surface are to be applied at ζ=0 and the boundary conditions at the shock interface are to be applied at ζ=1. If the identical transformations performed on the shock layer equations are applied to the shock-transition zone Equation (3), the following boundary conditions result:

$$\bar{u}_o(1) = 1 - \frac{N}{K^2} \bar{u}_o(1) \bar{u}_o'(1)$$

$$\Theta_o(1) = 1 - \frac{N}{Pr\, K^2} \bar{u}_o(1) \Theta_o'(1)$$

$$\bar{p}_o(1) = 1 \text{ and } \bar{p}_1(1) = 0 \qquad (7)$$

SOURCE FACSIMILE — Equation (7), complete original shock-interface conditions. Image-only mathematical notation.

These are to be applied at ζ=1.

The accepted theory about conditions next to a surface in low density flow is to postulate a slip velocity and a temperature jump. However, close examination of these two quantities for this problem reveals that

$$\frac{T - T_w}{T_o} \sim \sqrt{\epsilon \frac{T_w}{T_o}} \left(1 - \frac{T_w}{T_o}\right) C_H$$

$$\frac{U_{slip}}{U} \sim \sqrt{\epsilon \frac{T_w}{T_o}} C_f$$

SOURCE FACSIMILE — Original temperature-jump and slip-velocity relationships. Image-only mathematical notation.

where C_H is the heat transfer coefficient and C_f is the skin friction coefficient. For the hypersonic blunt body problem, $\varepsilon << 1$ due to a high compression ratio across the shock wave, T_w/T_o is usually very much less than 1, and C_H and C_f can never exceed unity even in free molecular flow. Thus, by order of magnitude considerations, neither of the two surface effects are important to the hypersonic blunt body problem. This would justify the use of conventional no-slip conditions, i.e.

$$\bar{u}_o(0) = 0$$

$$\Theta_o(0) = 0$$

SOURCE FACSIMILE — Original two no-slip boundary conditions. Image-only mathematical notation.

at the body surface, $\zeta=0$.

Method of Solution

The stagnation region theory derived up to this point is valid for the low density flow regimes between continuum flow and full transition flow. This range encompasses the vorticity-interaction regime, the viscous-layer regime, the incipient-merged layer regime and the fully-merged layer regime. All of the low density effects incorporated into the theory are not of equal importance

in each of these regimes. In order to derive maximum use of this characteristic, the low density regimes are divided into two regions based on the order of magnitude of the product of ε and K^2,

$$\text{Regime I:} \qquad 0(1) \leq \epsilon K^2 < \infty$$

$$\text{Regime II:} \qquad 0(\epsilon) \leq \epsilon K^2 \leq 0(1)$$

SOURCE FACSIMILE — Original Regime I and Regime II inequalities. Image-only mathematical notation.

By this mathematical division, Regime I includes the vorticity-interaction regime and part of the viscous-layer regime, while Regime II contains the remaining lower density flow regimes.

Regime I

This regime is closest to continuum flow and hence exhibits many of the characteristic relationships found in a continuum shock layer. The solution to Equation (6) in Regime I can be described adequately with a local similarity solution found in conventional boundary layer theory. In reference to boundary conditions, however, the viscous effects across the shock transition zone in the stagnation region are not significant enough to be included. Hence, the solution can be found by applying a local similarity transformation to the low density viscous shock layer equations using essentially continuum boundary conditions. Vorticity generated by the shock curvature will still affect the boundary layer solution. Introducing the familiar variables of boundary layer theory

$$\eta \equiv \sqrt{2\bar{u}^*}\, K \int_0^y \left(\frac{\rho}{\rho_\infty}\right) \frac{dy}{a}$$

$$f \equiv K\zeta^2/\sqrt{2\bar{u}^*}$$

SOURCE FACSIMILE — Original similarity-variable definitions. Image-only mathematical notation.

then Equation (6) transforms to

$$f''' + ff'' - \frac{1}{2} f'^2 = -\frac{1}{2} \left[\frac{H_w}{H_\infty} + \left(1 - \frac{H_w}{H_\infty}\right) \Theta \right] \left(\frac{\phi}{\phi_i}\right)$$

$$\Theta'' + Prf\Theta' = 0$$

with boundary conditions

$$f(0) = f'(0) = \Theta(0) = 0$$

$$f(\eta_s) = K/\sqrt{2\bar{u}^*}$$

$$f'(\eta_s) = \frac{1}{\bar{u}^*}$$

$$\Theta(\eta_s) = 1$$

where

$$\bar{u}^* = \left[\frac{8}{3}\epsilon\right]^{1/2}$$

$(\ )'$ = differentiation with respect to η

$$\phi \equiv 2\left\{1 + \int_{\zeta}^{1} \bar{u}\,\zeta\, d\zeta\right\}$$

= function of the tangential pressure gradient

SOURCE FACSIMILE — Original transformed equations, all six boundary conditions and complete following definitions of the velocity parameter, differentiation and tangential pressure-gradient function. No new equation numbers supplied. Image-only mathematical notation.

As in boundary layer theory, the velocity is proportional to f′. A question arises immediately as to why six boundary conditions are needed to solve two coupled equations requiring only five. The answer lies in the fact that in the original formulation, the value ζ=1 defined the shock interface; the extra boundary condition is then needed to define this value in terms of the

new independent variable η, i.e., $\eta_s = \eta/\text{shock interface}$ ($\zeta = 1$). Equation (9) was solved on a computer with a numerical integration method utilizing a rapid convergence scheme. The heat transfer coefficient is determined from the relation

$$C_{H_{\text{Regime I}}} = \sqrt{2\bar{u}^*} \quad \frac{\bar{p}_o}{Pr\,K} \; \Theta'/\eta=0$$

SOURCE FACSIMILE — Continuation of the independent-variable explanation, original reference to Equation (9), and Regime I heat-transfer coefficient expression. Image-only technical notation.

Regime II

Due to the lower density flow contained in Regime II, viscous effects across the shock wave are definitely important and the equations cannot be solved with a local similarity transformation. However, a unique method suggests itself from an order of magnitude analysis of each term in Equation (6a). For the conditions defined in Regime II, the second term on the right-hand side will always be an order of magnitude smaller than the remaining terms. It would, therefore, be possible to expand both dependent variables $\bar{u}$ and Θ as

$$\bar{u} = \bar{u}_{11} + \bar{u}_{22} + \cdots$$

$$\Theta = \Theta_{11} + \Theta_{22} + \cdots$$

SOURCE FACSIMILE — Original Regime II dependent-variable series. Image-only mathematical notation.

where the $(\,)_{22}$ order is assumed to be an order of magnitude smaller than the $(\,)_{11}$ order, etc. By substituting these series into Equation (6) and equating terms of equal order of magnitude, a set of equations will result for each order. The important point here, is that the equations for the $(\,)_{11}$ order are uncoupled since the second term on the right-hand side of Equation (6a) will drop out. This solution, which is easily found, can then be substituted into the set of equations involving the $(\,)_{22}$ order, which will contain the dropped term, to find the second order or correction solution, $(\,)_{22}$.

For the $(\ )_{11}$ order:

$$\text{(a)} \qquad \bar{u}_{11}^{\,2} - \zeta\, \bar{u}_{11}\, \bar{u}_{11}' = \frac{1}{K^2}\, \frac{\bar{u}_{11}}{\zeta} \left(\frac{\bar{u}_{11}\, \bar{u}_{11}'}{\zeta} \right)'$$

$$\text{(b)} \qquad N \left(\frac{\bar{u}_{11}\, \Theta_{11}'}{\zeta} \right)' + \mathrm{Pr} K^2 \zeta^2 \Theta_{11}' = 0 \qquad (10)$$

It should be noted that although Equation (10b) contains the term $\bar{u}_{11}$, the equation can be solved in its general form for Θ_{11} with an integrated dependence on $\bar{u}_{11}$.

SOURCE FACSIMILE — The $(\ )_{11}$-order heading, Equation (10), parts (a) and (b), and the complete following explanation. Image-only mathematical notation.

For the $(\ )_{22}$ order:

$$\frac{1}{K^2} \left\{ \frac{(\bar{u}_{11}\, \bar{u}_{22})'}{\zeta} \right\}' + \zeta^2\, \frac{(\bar{u}_{11}\, \bar{u}_{22})'}{\bar{u}_{11}} - 2\zeta \bar{u}_{22}$$

$$= - \frac{\epsilon \phi \zeta}{\bar{u}_{11}} \left(\frac{T_w}{T_\infty} \right) - \frac{\epsilon \phi \zeta}{\bar{u}_{11}} \left(1 - \frac{T_w}{T_\infty} \right) \Theta_{11} \qquad (11)$$

SOURCE FACSIMILE — The $(\ )_{22}$-order heading and Equation (11). Image-only mathematical notation.

The equation for Θ_{22} is the same as Equation (10b) with $\bar{u}_{11}$ replaced by $(\bar{u}_{11} + \bar{u}_{22})$. The details of the solution of these two sets of equations are too long and involved to be included here. The final solution for $\bar{u}$ and Θ is an algebraic expression in terms of exponentials and incomplete gamma functions. This solution is used to find the heat transfer coefficient from the expression

$$C_{H_{\text{Regime II}}} = \frac{\bar{p}_o}{\mathrm{Pr} K^2} \left[\bar{u}_\zeta \cdot \Theta_\zeta \right]_{\zeta = 0}$$

SOURCE FACSIMILE — Complete original following explanation and final Regime II heat-transfer coefficient expression. Overbars/subscripts retained without conjecture; image-only technical content.

Appendix A — Nomenclature

a	local body nose radius
h	static enthalpy
H	total enthalpy
K^2	low density Reynolds number $\left[\epsilon \frac{\rho_\infty U_\infty a}{\mu_o} \left(\frac{\mu_o T^*}{\mu^* T_o} \right) \right]$
K_c	longitudinal curvature
N	constant = $\frac{\mu T^*}{\mu^* T}$
p	pressure
$\bar{p}$	$p/(\rho_\infty U_\infty^2 \sin^2\beta)$ = nondimensional pressure
Pr	Prandtl number
T	temperature
u	velocity component in the x-direction
U_∞	freestream total velocity
$\bar{u}$	$u/(U_\infty \cos\beta)$
v	velocity component in the y-direction
x	direction tangential to surface

SOURCE FACSIMILE — Complete original nomenclature from a through x, including every expression and definition. Image-only mathematical symbols and text.

x'	direction along axis of symmetry of body
y	direction along outward normal from surface
Z	distance of a give body surface point from the axis of symmetry

Greek

β	local shock angle
γ	ratio of specific heats
ϵ	γ-1/2γ
η	transformed boundary layer coordinate
Θ	enthalpy function = $\frac{H - H_w}{H_\infty - H_w}$
μ	coefficient of viscosity
ψ	stream function
ρ	density

Subscripts

$(\ )_\infty$	evaluated at freestream conditions
$(\ )_w$	evaluated at surface temperature
$(\ )_o$	evaluated at freestream stagnation conditions (not to be confused with series expansion terms)

Superscripts

$(\ )^*$	evaluated at reference temperature

SOURCE FACSIMILE — Complete continuation of Appendix A nomenclature: x′, y, Z; Greek symbols; all subscripts and superscripts. Image-only mathematical symbols and text.

Appendix B — Free Molecular Heating

Original appendix divider. The appendix text begins on the following source page.

B.1 General Discussion

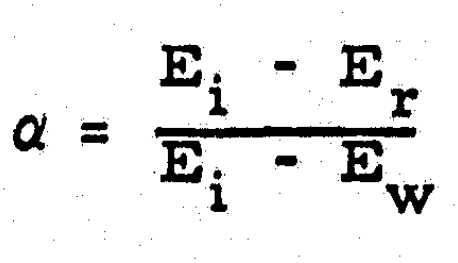
In the free molecular flow regime, the aerodynamic heating rate to an element of surface area can be calculated from an energy balance.

$$q = E_i - E_r \quad \text{(B.1)}$$

where

q = heat transfer rate
E_i = rate at which total energy is incident on the surface area
E_r = rate at which total energy is reflected from the surface area

Because of the assumption in free molecular flow that the molecules have a Maxwellian velocity distribution, then there is a temperature associated with each of the energy rates, E_i and E_r. Although the temperature of the incoming or incident molecules is usually a well-defined quantity, the temperature of the reflected molecules is a function of the particular gas-surface interaction and is not known. It is common practice in all free molecular theory to combine this uncertainty into a parameter called the accommodation coefficient, α, defined by



SOURCE FACSIMILE — Original accommodation-coefficient definition. Image-only mathematical notation.

where

E_w = rate at which total energy is reflected from the surface area assuming that the velocity distribution of the reflected molecules is characterized by the wall or surface temperature, T_w.

Note the type of gas-surface interaction under consideration here. It is hypothesized that the incoming molecules can be described with a Maxwellian velocity distribution characterized by a temperature, T_i. All of the molecules striking the surface are “captured” by the surface and give up all their energy to the surface. At some later time (the length of time is not important to this analysis), the molecules are diffusely emitted or “reflected” from the surface as if they originated from an infinite reservoir with zero mean velocity. Again, their velocity distribution is considered to be Maxwellian, characterized by a temperature T_r. This gas-surface interaction must conserve mass. The parameter α is considered to be a measure of how well the surface accommodates the incident energy. Thus, Equation (B.1) can be written

$$q = \alpha(E_i - E_w) \quad \text{(B.2)}$$

The maximum heat transfer occurs when α has a value of unity.

The total energy associated with each one of the molecules striking the surface consists of kinetic energy and internal energy. It is convenient to define

$$E_i = e_{ik} + e_{ii} \quad \text{(B.3)}$$

where

e_{ik} = rate at which kinetic energy is transferred to the surface by the incident molecules assuming their velocity distribution is characterized by the temperature T_i
e_{ii} = rate at which internal energy is transferred to the surface by the incident molecules assuming their velocity distribution is characterized by the temperature T_i

Similarly, the total energy carried away from the surface by the reflected or emitted molecules can be written as

$$E_w = e_{wk} + e_{wi} \quad (B.4)$$

where

e_{wk} = rate at which kinetic energy is carried away from the surface by the emitted molecules, assuming that the velocity distribution of the emitted molecules is characterized by the temperature, T_w

e_{wi} = rate at which internal energy is carried away from the surface by the emitted molecules, assuming that the velocity distribution of the emitted molecules is characterized by the temperature, T_w

T_w = temperature of the wall

Thus, Equation (B.2) can be written

$$q = \alpha[(e_{ik} - e_{wk}) + (e_{ii} - e_{wi})] \quad (B.5)$$

It is desired to calculate the heat transfer to a flat plate of unit area at an angle of attack, θ, to the incoming flow.

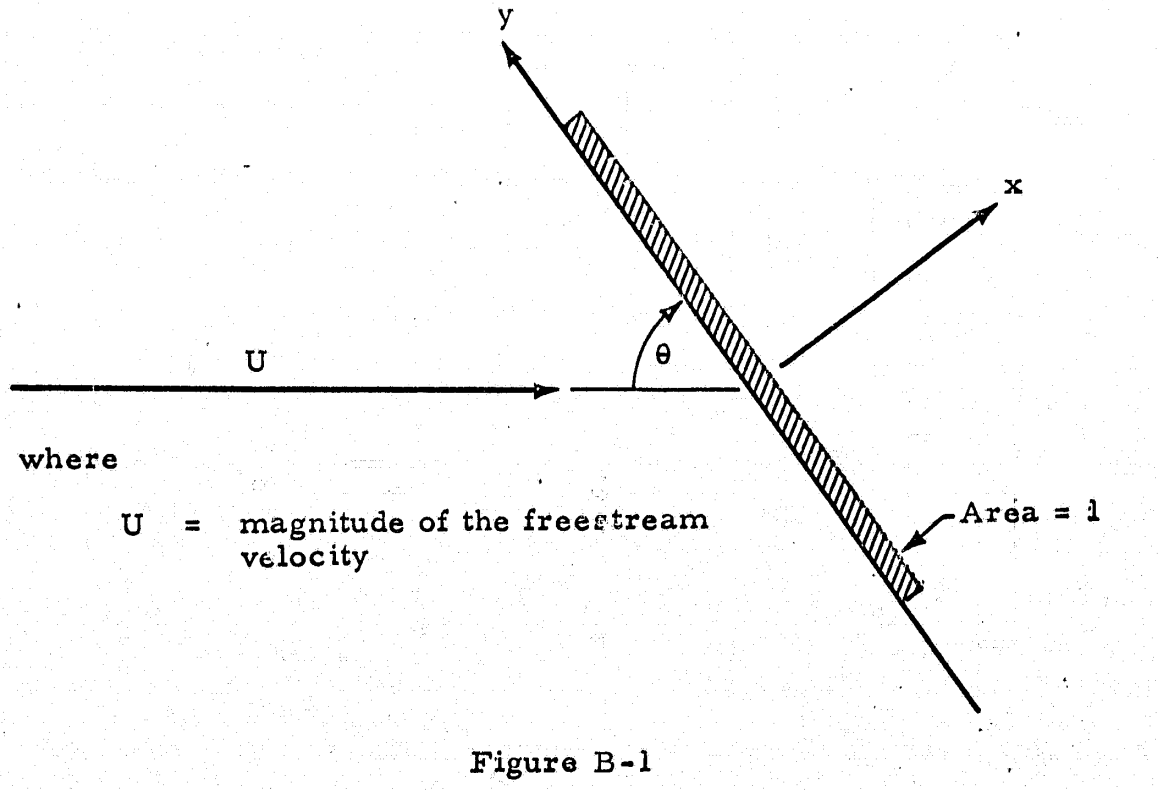


Figure B-1

SOURCE FACSIMILE — Figure B-1. Complete original flat-plate geometry, velocity definition, unit-area label and caption; image-only labels.

By definition, the front side of the plate is the negative x side and the back side is the positive x side. Both sides of the plate experience heating.

B.2 Front Side Heating

To find an expression for the front side heating, all the terms in Equation (B.5) must be evaluated. If $\vec{C}$ is the velocity vector of a molecule, and m_i is the mass of one molecule, then the molecule possesses $\frac{1}{2} m_i |\vec{C}|^2$ kinetic energy. Total kinetic energy transferred to any point is found by integrating the product of f and $\frac{1}{2} m_i |\vec{C}|^2$ over the appropriate region of velocity space. Thus, for the quantity e_{ik},

$$e_{ik} = \iiint \tfrac{1}{2} m_i (C_x^2 + C_y^2 + C_z^2) f \, dV \qquad \text{(B.6)}$$

where

C_x, C_y, C_z = Cartesian components of the molecular velocity $\vec{C}$

f = Maxwell-Boltzmann distribution function

$$= n_i \left(\frac{m_i}{2\pi k T_i} \right)^{3/2} e^{-\frac{m_i}{2kT_i} \left[(C_x - U_x)^2 + (C_y - U_y)^2 + (C_z - U_z)^2 \right]}$$

n_i = number density of incident flow

T_i = temperature of the incident flow

U_x, U_y, U_z = components of freestream velocity vector

dV = differential element of velocity flux space

SOURCE FACSIMILE — Complete molecular-velocity/kinetic-energy lead-in, Equation (B.6), Maxwell-Boltzmann distribution function and every following variable definition. Image-only technical content.

Since only those molecules striking the front surface will transfer energy to the front surface, the integration over velocity space must include only those molecules having velocity components in the positive C_x direction. Thus, the differential element of velocity flux space will be

$$dV = C_x\, dC_x\, dC_y\, dC_z$$

and the integral for e_{ik} becomes

$$e_{ik} = \int_{-\infty}^{+\infty}\int_{0}^{+\infty} \frac{m_i n_i}{2}\left(\frac{m_i}{2\pi k T_i}\right)^{3/2} (C_x^2 + C_y^2 + C_z^2)$$

$$e^{-\frac{m_i}{2kT_i}\left[(C_x-U_x)^2+(C_y-U_y)^2+(C_z-U_z)^2\right]}$$

$$C_x\, dC_x\, dC_y\, dC_z \qquad \text{(B.7)}$$

SOURCE FACSIMILE — Original differential velocity-flux element and integral lead-in, and complete Equation (B.7). Image-only mathematical notation.

From Figure B-1, it is clear that the components of the freestream velocity are

$$U_x = U \sin\theta$$
$$U_y = -U \cos\theta$$
$$U_z = 0$$

Completing the integration in Equation (D.7),

$$e_{ik} = \frac{\rho_i R_i T_i}{J}\left(\frac{R_i T_i g}{2\pi}\right)^{1/2}\left\{(2 + S^2)\, e^{-S^2 \sin^2\theta} + \pi^{1/2} S \sin\theta\,(1 + \operatorname{erf} S\sin\theta)\left(\frac{5}{2} + S^2\right)\right\} \qquad \text{(B.8)}$$

where

$\rho_i = m_i n_i$ = density of the incident flow

$R_i = k/m_i$ = gas constant of the incident flow

SOURCE FACSIMILE — Equation (B.8) and complete following density and gas-constant definitions. Original reference to (D.7) above is retained as printed. Image-only mathematical notation.

$$S = \text{molecular speed ratio}$$

$$= \frac{U}{\sqrt{2R_i g T_i}}$$

SOURCE FACSIMILE — Original molecular speed-ratio definition. Image-only mathematical notation.

To find an expression for e_{wk}, the boundary conditions of the gas-surface interaction process must be imposed on the system. First, the number of molecules which reach the front side of the unit area per unit time must be computed. From the geometry of Figure B-1 and consideration of kinetic theory,

$$N_i = \iiint f \, dV$$

$$N_i = n_i \left(\frac{m_i}{2\pi k T_i}\right)^{3/2} \int_{-\infty}^{+\infty}\int_{0}^{+\infty}\int_{-\infty}^{+\infty} e^{-\frac{m_i}{2kT_i}\left[(C_x-U_x)^2+(C_y-U_y)^2+(C_z-U_z)^2\right]} C_x \, dC_x \, dC_y \, dC_z$$

SOURCE FACSIMILE — Original incident molecular-number flux integrals. Image-only mathematical notation.

Completing the integration,

$$N_i = n_i \left(\frac{R_i T_i g}{2\pi}\right)^{1/2} \left[e^{-S^2 \sin^2\theta} + \pi^{1/2} S \sin\theta (1 + \operatorname{erf} S \sin\theta)\right] \qquad (B.9)$$

SOURCE FACSIMILE — Equation (B.9). Image-only mathematical notation.

The quantity N_i represents the number of incident molecules striking the unit surface in a unit time. These molecules are “captured” by the surface and later emitted or reflected from the surface as if they came from an infinite reservoir held at temperature T_w with zero mean velocity. However, the number of molecules reflected from the surface per unit time, N_r, must be equal to the number of molecules striking the surface per unit time evaluated at “reservoir conditions.” Thus

$$N_r = N_i \Big|_{\substack{n = n_w \\ T = T_w \\ R = R_w \\ U = 0}}$$

SOURCE FACSIMILE — Original reflected molecular-number flux boundary-condition substitution. Image-only mathematical notation.

Applying this condition to Equation (D.9),

$$N_r = n_w \left(\frac{R_w T_w g}{2\pi} \right)^{1/2} \qquad \text{(B.10)}$$

SOURCE FACSIMILE — Equation (B.10). Image-only mathematical notation.

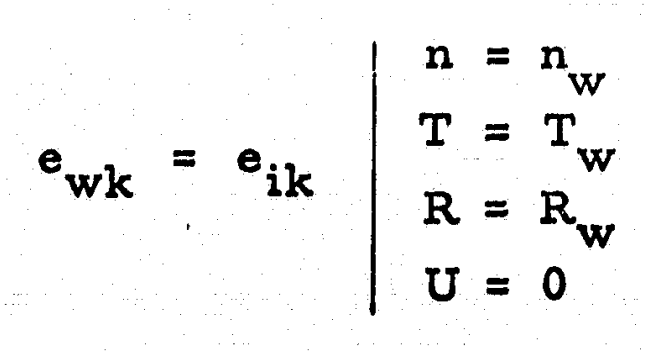
But since at the surface, $N_i = N_r$ at all times, then from Equations (B.9) and (B.10).

$$n_w = n_i \left(\frac{R_i T_i}{R_w T_w} \right)^{1/2} \left[e^{-S^2 \sin^2\theta} + \pi^{1/2} S \sin\theta (1 + \operatorname{erf} S \sin\theta) \right] \qquad \text{(B.11)}$$

SOURCE FACSIMILE — Equation (B.11). Image-only mathematical notation.

Equation (B.11) gives the necessary expression for the number density of the reflected molecules in terms of the number density of the incident molecules and the temperature of the wall.

The amount of kinetic energy stored in the reservoir, which is emitted from the surface, can be found by imposing the boundary conditions on the incident kinetic energy, viz.,



$$e_{wk} = e_{ik} \Big| \begin{array}{l} n = n_w \\ T = T_w \\ R = R_w \\ U = 0 \end{array}$$

SOURCE FACSIMILE — Original emitted kinetic-energy boundary-condition substitution. Image-only mathematical notation.

Thus, from Equation (B.8)

$$e_{wk} = \frac{2 n_w k T_w}{J} \left(\frac{R_w T_w g}{2\pi} \right)^{1/2}$$

SOURCE FACSIMILE — Original unnumbered emitted kinetic-energy expression. Image-only mathematical notation.

Substituting the expression from Equation (B.11) for n_w,

$$e_{wk} = \frac{2 \rho_i R_i T_w}{J} \left(\frac{R_i T_i}{2\pi} \right)^{1/2} \left\{ e^{-S^2 \sin^2\theta} + \pi^{1/2} S \sin\theta \cdot (1 + \operatorname{erf} S \sin\theta) \right\} \quad \text{(B.12)}$$

SOURCE FACSIMILE — Equation (B.12). Image-only mathematical notation.

In addition to the heating caused by transfer of kinetic energy, the surface also experiences heating due to the transfer of internal energy by the incident molecules. Because of the way in which the energy balance at the surface is formulated, the amount of internal energy which contributes to the heating is the total internal energy minus that part of the internal energy due to translational degrees of freedom – which has already been accounted for. In the conventional free molecular heating theory for cold air (Reference B-1), the molecules under consideration are, at most, diatomic. Thus, there exists a simple relationship between γ and the number of degrees of freedom, i.e.,

$$\gamma = 1 + 2/j \quad \text{(B.13)}$$

where

γ = ratio of specific heats
j = number of degrees of freedom

Using the principle of equipartition of energy and the above relationship, the amount of internal energy due to j - 3 degrees of freedom can be readily calculated. Now, if the problem is changed such that the incident flow may be composed of high temperature gases from a rocket engine exhaust, then this theory is no longer adequate.

In the search for a new solution, a digression into kinetic theory will be helpful. It is well known that the total internal energy stored by N molecules of a gas in thermodynamic equilibrium at a temperature T is given by

$$U_{TOT} = NkT^2 \left(\frac{\partial \ell n f}{\partial T}\right)_v \qquad \text{(B.14)}$$

SOURCE FACSIMILE — Equation (B.14), preserving the original partition-function derivative and subscript. Image-only mathematical notation.

where

f = total partition function

Depending upon the complexity of the molecules and the level of excitation, f could be an extremely complicated function. However, it will always be given in the form,

$$f = (f_{trans})(f_{rot})(f_{vib})(\ldots)(\ldots \qquad \text{(B.15)}$$

where

f_{trans} = translational partition function

f_{rot} = rotational partition function

f_{vib} = vibrational partition function

and so on.

SOURCE FACSIMILE — Equation (B.15), including its printed open-ended factors, and all original component partition-function definitions. Image-only technical content.

Hence, if we know f for any complex molecule, we can find an expression for the total internal energy of each of the N molecules using Expression (B.1).

$$U_{TOT} = NkT^2 \frac{\partial}{\partial T}\left\{\ell n f_{trans} + \ell n f_{rot} + \ell n f_{vib} + \ldots + \ldots\right\}\Big|_v \qquad \text{(B.16)}$$

SOURCE FACSIMILE — Equation (B.16). Image-only mathematical notation.

From this expression, it is clear that the total internal energy is composed of contributions from each “type” of freedom in the complex molecule.

$$U_{TOT} = U\Big|_{\text{due to translation}} + U\Big|_{\text{due to rotation}} + U\Big|_{\text{due to vibration}} + \cdots$$

SOURCE FACSIMILE — Original decomposition of total internal energy into translational, rotational and vibrational contributions. Image-only mathematical notation.

As has been mentioned, the quantity of interest is the total internal energy minus the contribution of the translational degrees of freedom. Thus,

$$U_S = U_{TOT} - NkT^2 \frac{\partial}{\partial T} (\ell n f_{trans})_v \qquad (B.17)$$

SOURCE FACSIMILE — Equation (B.17). Image-only mathematical notation.

is a direct method to calculate this quantity. If the velocity of a molecule is given by

$$\vec{C} = C_x \vec{i} + C_y \vec{j} + C_z \vec{k}$$

SOURCE FACSIMILE — Original molecular velocity vector in Cartesian components. Image-only mathematical notation.

then the translational partition function is

$$f_{trans} = \exp\left[-\frac{m}{2kT}(C_x^2 + C_y^2 + C_z^2)\right] \qquad (B.18)$$

SOURCE FACSIMILE — Equation (B.18). Image-only mathematical notation.

Substituting Equation (B.18) into Equation (B.17).

$$U_S = U_{TOT} - N\left(\frac{mC^2}{2}\right)$$

where

$$C^2 = C_x^2 + C_y^2 + C_z^2$$

or on the basis of one molecule,

$$u_S = u_{TOT} - \frac{mC^2}{2} \qquad \text{(B.19)}$$

SOURCE FACSIMILE — Original resulting internal-energy expression, squared-speed definition, one-molecule lead-in and Equation (B.19). Image-only technical notation.

Although the total internal energy of a complicated molecule of gas, U_{TOT}, is usually very difficult to describe by use of partition functions, it can be determined from thermodynamic relations if the assumption is made that the gas is in equilibrium at a temperature T, i.e.,

$$h = \text{total internal energy} + p/\rho J$$

where

h = static enthalpy per unit mass

p = static pressure

ρ = density

SOURCE FACSIMILE — Original static-enthalpy/internal-energy relation and complete h, p and ρ definitions. Image-only technical notation.

In terms of internal energy per molecule

$$u_{TOT} = \left(h - \frac{p}{\rho J}\right)\frac{\rho}{n} \quad \left(\frac{\text{energy}}{\text{molecule}}\right) \qquad \text{(B.20)}$$

SOURCE FACSIMILE — Equation (B.20), with original energy-per-molecule units. Image-only mathematical notation.

Since it was assumed that h, p, ρ are thermodynamic properties of the gas at equilibrium, they are steady state values. Thus, it would seem reasonable to use the average or “steady state” value of C^2 in Equation (B.19). This average value is called a most probable value defined by

$$\overline{C^2} = \iiint_{-\infty}^{+\infty} C^2 f \, dV$$

$$\overline{C^2} = \frac{3kT}{m} \qquad \text{(B.21)}$$

SOURCE FACSIMILE — Original squared-speed integral and Equation (B.21). Image-only mathematical notation.

Thus, Equation (B.19) becomes

$$u_S = u_{TOT} - \frac{3}{2} kT \qquad (B.22)$$

$$u_S = \left(h - \frac{p}{\rho J}\right) \frac{\rho}{n} - \frac{3}{2} kT \qquad (B.23)$$

SOURCE FACSIMILE — Equations (B.22) and (B.23). Image-only mathematical notation.

Since the thermodynamic equation of state relates the equilibrium properties of the gas, Equation (B.23) can be re-written as

$$u_S = \left(h - \frac{RT}{2J}\right) \frac{\rho}{n} \quad \left(\frac{\text{energy}}{\text{molecule}}\right) \tag{B.24}$$

SOURCE FACSIMILE — Equation (B.24), with original energy-per-molecule units. Image-only mathematical notation.

where again, R = k/m

By using the method-of-characteristics plume which gives an accurate description of the local properties of the gas at every point in the flow field, the quantity u_S can easily be determined. Assuming that this accurate description of the properties exists, then no approximate relationship between γ and the number of degrees of freedom in the molecule is needed.

Now, the amount of internal energy incident on the surface can be calculated by multiplying the number of molecules incident on the surface per unit time, N_i, by the internal energy contribution of one molecule, u_S, i.e.,

$$e_{ii} = (N_i)(u_S)$$

Using Equation (B.9),

$$e_{ii} = \rho_i \left(\frac{R_i T_i g}{2\pi}\right)^{1/2} \left[h_i - \frac{R_i T_i}{2J}\right] \left\{e^{-S^2 \sin^2\theta} + \pi^{1/2} S \sin\theta (1 + \operatorname{erf} S \sin\theta)\right\} \tag{B.25}$$

SOURCE FACSIMILE — Equation (B.25). Image-only mathematical notation.

Using a similar analysis for the reflected molecules, the internal energy is given by

$$u_{Sw} = \left(h_w - \frac{R_w T_w}{2J}\right) \frac{\rho_w}{n_w}$$

$$= \text{reflected internal energy/molecule}$$

SOURCE FACSIMILE — Original reflected internal-energy expression and energy-per-molecule definition. Image-only mathematical notation.

and the amount of internal energy carried away from the surface by the reflected molecules is

$$e_{wi} = (N_r)(u_{Sw})$$

$$e_{wi} = \rho_i \left(\frac{R_i}{R_w}\right)\left(\frac{R_i T_i g}{2}\right)^{1/2} \left[h_w - \frac{R_w T_w}{2J}\right] \left\{e^{-S^2 \sin^2\theta} + \pi^{1/2} S \sin\theta (1 + \operatorname{erf} S \sin\theta)\right\} \qquad \text{(B.26)}$$

SOURCE FACSIMILE — Original emitted internal-energy product and Equation (B.26), retaining the printed denominator. Image-only mathematical notation.

The heat transfer rate to the front side of the unit surface is found by substitution of Equations (B.8), (B.12), (B.25) and (B.26) into Equation (B.5). Thus,

$$\frac{q_f}{\alpha} = \frac{\rho_i R_i T_i}{J} \left(\frac{R_i T_i g}{2\pi}\right)^{1/2} \left\{e^{-S^2 \sin^2\theta} \left[2\left(1 - \frac{T_w}{T_i}\right) + S^2\right] + \pi^{1/2} S \sin\theta (1 + \operatorname{erf} S \sin\theta) \left[S^2 + \frac{5}{2} - 2\left(\frac{T_w}{T_i}\right)\right]\right\}$$

$$+ \rho_i \left(\frac{R_i T_i g}{2\pi}\right)^{1/2} \left\{\left[h_i - \frac{R_i T_i}{2J}\right] - \frac{R_i}{R_w}\left[h_w - \frac{R_w T_w}{2J}\right]\right\}$$

$$\left[e^{-S^2 \sin^2\theta} + \pi^{1/2} S \sin\theta (1 + \operatorname{erf} S \sin\theta)\right] \qquad \text{(B.27)}$$

SOURCE FACSIMILE — Equation (B.27), complete four-line front-side heat-transfer expression. Image-only mathematical notation.

B.3 Back Side Heating

The heat transfer to the back side of the flat plate shown in Figure is also found from an energy balance at the surface.

$$\frac{q_b}{\alpha} = (e_{ikb} - e_{wkb}) + (e_{iib} - e_{wib}) \qquad (B.28)$$

SOURCE FACSIMILE — Equation (B.28). Image-only mathematical notation.

where

e_{ikb} = rate at which kinetic energy is transferred to the backside surface by the incident molecules, assuming that their velocity distribution is characterized by the temperature, T_i

e_{wkb} = rate at which kinetic energy is carried away from the backside surface by the reflected molecules, assuming that their velocity distribution is characterized by the temperature, T_w.

e_{iib} = rate at which internal energy is transferred to the backside surface by the incident molecules, assuming that their velocity distribution is characterized by the temperature, T_w.

e_{wib} = rate at which internal energy is carried away from the backside surface by the reflected molecules, assuming that their velocity distribution is characterized by the temperature, T_w.

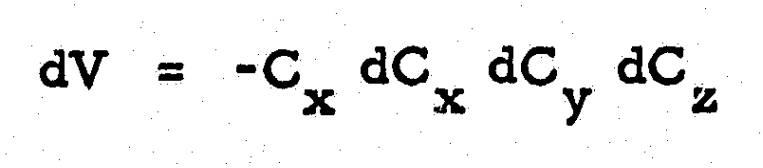
SOURCE FACSIMILE — Complete original definitions following Equation (B.28), including the printed wall-temperature subscript in the incident internal-energy definition. Image-only technical notation.

The rate at which kinetic energy is transferred to the backside of the surface is found in a similar manner to that for the front side, i.e.,

$$e_{ikb} = \iiint \frac{1}{2} m_i (C_x^2 + C_y^2 + C_z^2) f \, dV$$

SOURCE FACSIMILE — Original backside incident kinetic-energy integral. Image-only mathematical notation.

Since only those molecules striking the backside surface will transfer energy to the surface, the integration over velocity space must include only those molecules having velocity components in the negative C_x direction. For this region of velocity space, the differential velocity flux element becomes



$$dV = -C_x\, dC_x\, dC_y\, dC_z$$

SOURCE FACSIMILE — Original negative-direction differential velocity-flux element. Image-only mathematical notation.

and

$$e_{ikb} = \int_{-\infty}^{+\infty}\int_{-\infty}^{+\infty}\int_{-\infty}^{0} \frac{m_i n_i}{2}\left(\frac{m_i}{2\pi k T_i}\right)^{3/2} (C_x^2 + C_y^2 + C_z^2)$$

$$e^{-\frac{m_i}{2kT_i}\left[(C_x-U_x)^2+(C_y-U_y)^2+(C_z-U_z)^2\right]}$$

$$(-C_x)\, dC_x\, dC_y\, dC_z \qquad \text{(B.29)}$$

SOURCE FACSIMILE — Equation (B.29), complete original integral and bounds. Image-only mathematical notation.

Again, the velocity components of the freestream flow are

$$U_x = U \sin\theta$$
$$U_y = -U \cos\theta$$
$$U_z = 0$$

Completing the integration,

$$e_{ikb} = \frac{\rho_i R_i T_i}{J}\left(\frac{R_i T_i g}{2\pi}\right)^{1/2}\left\{e^{-S^2\sin^2\theta}\,(2 + S^2) - \pi^{1/2} S \sin\theta \left(\frac{5}{2} + S^2\right)(1 - \operatorname{erf} S\sin\theta)\right\} \qquad \text{(B.30)}$$

SOURCE FACSIMILE — Equation (B.30). Image-only mathematical notation.

The three other terms in Equation (B.28) are generated in the same manner as they were in the front side heating calculations. The only difference being the different region of velocity space which governs the limits of the integration. The results of the computations are

$$e_{wkb} = 2 \frac{\rho_i R_i T_w}{J} \left(\frac{R_i T_i g}{2}\right)^{1/2} \left[e^{-S^2 \sin^2\theta} - \pi^{1/2} S \sin\theta \, (1 - \operatorname{erf} S \sin\theta)\right] \qquad \text{(B.31)}$$

SOURCE FACSIMILE — Equation (B.31), retaining the printed denominator. Image-only mathematical notation.

$$e_{iib} = \rho_i \left(\frac{R_i T_i g}{2}\right)^{1/2} \left[h_i - \frac{R_i T_i}{2J}\right] \left\{e^{-S^2 \sin^2\theta} - \pi^{1/2} S \sin\theta (1 - \operatorname{erf} S \sin\theta)\right\} \quad \text{(B.32)}$$

$$e_{wib} = \rho_i \left(\frac{R_i}{R_w}\right) \left(\frac{R_i T_i g}{2\pi}\right)^{1/2} \left[h_w - \frac{R_w T_w}{2J}\right] \left\{e^{-S^2 \sin^2\theta} - \pi^{1/2} S \sin\theta (1 - \operatorname{erf} S \sin\theta)\right\} \quad \text{(B.33)}$$

SOURCE FACSIMILE — Equations (B.32) and (B.33), complete original expressions. Image-only mathematical notation.

Thus, the heat transfer rate to the backside surface is given by Equation (B.28)

$$\frac{q_b}{\alpha} = \frac{\rho_i R_i T_i}{J} \left(\frac{R_i T_i g}{2\pi}\right)^{1/2} \left\{e^{-S^2 \sin^2\theta} \left[S^2 + 2\left(1 - \frac{T_w}{T_i}\right)\right] - \pi^{1/2} S \sin\theta (1 - \operatorname{erf} S \sin\theta)\left(S^2 + \frac{5}{2} - 2\frac{T_w}{T_i}\right)\right\}$$

$$+ \rho_i \left(\frac{R_i T_i g}{2\pi}\right)^{1/2} \left\{\left[h_i - \frac{R_i T_i}{2J}\right] - \frac{R_i}{R_w}\left[h_w - \frac{R_w T_w}{2J}\right]\right\}$$

$$\left[e^{-S^2 \sin^2\theta} - \pi^{1/2} S \sin\theta (1 - \operatorname{erf} S \sin\theta)\right] \quad \text{(B.34)}$$

SOURCE FACSIMILE — Equation (B.34), complete four-line backside heat-transfer expression. Image-only mathematical notation.

In determining the heating rate to a large body or vehicle, the surface area is visualized as a great number of differential areas which are considered to be flat plates at an angle of attack to the freestream flow. Equations (B.27) and (B.33) are used to calculate the heating rates, depending on whether the element of surface area is exposed to the freestream velocity (front side) or not (backside). This is possible because the mechanism for energy transfer

to an element of surface area is not influenced by any preceding or adjacent phenomena.

The theory of free molecular heat transfer presented here is an extension of the existing theory in that it includes an accurate method of determining heat transfer to surfaces exposed to gases with arbitrary composition and temperature. This is necessary for any problems where the gas surrounding the vehicle is not composed of diatomic molecules at low temperatures. However, the accuracy of the new method depends on how accurately the local thermodynamic properties of the gas can be determined.

Appendix B — Nomenclature

$\vec{C}$	molecular velocity (ft/sec)
E	rate at which total energy strikes a surface (Btu/ft^2-sec)
e_{ij}	rate at which a specific type of energy strikes a surface (Btu/ft^2-sec)
erf(x)	error function of x
f	Maxwell-Boltzmann distribution function
g	gravitational constant = $32.2 \frac{ft\text{-}lbf}{lbm\text{-}sec^2}$
h	static enthalpy (Btu/lbm)
J	mechanical equivalent of heat = $778 \frac{ft\text{-}lbf}{Btu}$
j	number of degrees of freedom
k	Boltzmann's constant = $5.66 \times 10^{-24} \frac{ft\text{-}lbf}{molecule\,^oR}$
m	mass of a molecule (lbm)
N	rate at which molecules strike a unit surface per unit time $\left(\frac{molecules}{ft^2\text{-}sec}\right)$
n	number density $\left(\frac{molecules}{ft^3}\right)$
p	static pressure (lbf/ft^2)
q	heat transfer rate (Btu/ft^2-sec)
R	gas constant $\left(\frac{ft\text{-}lbf}{lbm\,^oR}\right)$

SOURCE FACSIMILE — Complete original Appendix B nomenclature from molecular velocity through gas constant, including all units and numerical constants. Image-only mathematical symbols and text.

Nomenclature (Continued)

S	molecular speed ratio
T	temperature (^{o}R)
$\vec{U}$	freestream velocity (ft/sec)
U_{TOT}	total internal energy (Btu/lbm)
u	internal energy (Btu/molecule)
α	accommodation coefficient
γ	ratio of specific heats
θ	angle between freestream direction and positive y direction of plate
ρ	density (lbm/ft^3)

Subscripts

$(\quad)_b$	pertaining to back-side conditions
$(\quad)_i$	property evaluated at freestream temperature
$(\quad)_i$	due to internal energy
$(\quad)_k$	due to kinetic energy
$(\quad)_w$	property evaluated at temperature of wall

SOURCE FACSIMILE — Complete continuation of Appendix B nomenclature: S through ρ and every subscript definition. Image-only mathematical symbols and text.

Appendix B — Reference

Oppenheim, A. K., “Generalized Theory of Convective Heat Transfer in a Free-Molecule Flow,” *J. Aeron. Sci.*, January 1963, p. 49.

Editorial verification notes

These notes are new editorial material, not part of the original report.

The title-page author initials are partly obscured by a blemish. The supplied author information supplies A. W. Ratliff and the full author list, in original order. The approval signature is retained as an image.

Original p.5 (source PDF p.12) reads “about 100 different propellant systems,” not the OCR reading “144.” The printed value 100 is retained.

The original contents places Section 3.2 on p.12, but its heading is already present on p.11. The contents reference is retained unchanged.

Original p.12 gives two coordinate definitions with “cos” as printed. They are preserved in the source image without scientific correction. The surface-shading test on p.14 retains its printed inequality signs, rather than the less precise OCR rendering.

Original p.36 reads “500°K,” not the OCR reading “5000K.” Equation (4.15) was visually verified and re-typeset.

Figure 4-5 contains a legend line ending “Windshie.” in the supplied scan. That source wording is retained in the image; no missing letters are conjectured.

Original wording such as “nozzle exist plane” on p.32 and “amount of effect” on p.53 is retained without correction.

Reference 17 on original p.68 is retained as a source crop because the author surname cannot be confidently read from the supplied scan.

Appendix A retains the source equation numbering, including the reference to Equation (9) on A-12 where the preceding displayed expressions have no visible equation numbers. No numbers have been invented.

Appendix B retains cross-references as printed: (D.7) on B-5, (D.9) on B-7, Expression (B.1) on B-9, and (B.33) in the concluding paragraph on B-16. The displayed labels are not silently reconciled with these prose references.

On B-13, the original phrase “shown in Figure” has no following figure number; it is retained. On B-14, the incident internal-energy definition prints a wall-temperature subscript; the source crop retains it without correction.

Technical crops deliberately preserve vectors, direction-cosine symbols, matrix layouts, primes and inequalities where a confident reconstructed transcription has not been made. Their labeling does not imply that the original material is erroneous.

The report is complete in this edition.